Tgfbr3 regulates alveolarisation in late lung development

Inaugural Dissertation submitted to the
Faculty of Medicine
in partial fulfillment of the requirements
for the PhD-Degree
of the Faculties of Veterinary Medicine and Medicine
of the Justus Liebig University Giessen

by
Pożarska, Agnieszka Ewa
Born in
Olsztyn, Poland

Giessen (2020)

From the Max Planck Institute for Heart and Lung Research

Director: Prof. Dr. Werner Seeger

of the Faculty of Medicine of the Justus Liebig University Giessen

First Supervisor and Committee Member: Prof. Dr. Werner Seeger

Second Supervisor: Prof. Dr. David Warburton

Committee Member (Chair): Prof. Dr. Ralph Schermuly

Committee Member: Prof. Dr. Reinhard Dammann

Date of Doctoral Defence: 21.02.2020

Contents

i) List of Figures

ii) List of Tables

iii) List of Abbreviations

Acvrl1	Activin receptor-like kinase 1
ADRP	Adipose differentiation-related protein
alv air	Alveolar airspaces
APS	Ammonium persulfate
ATII	Alveolar epithelial type II
B	Bridge
bp	Base pair(s)
BSA	Bovine serum albumin
BrdU	5-bromo-2'-deoxyuridine
CE	Coefficient of error
Ct	Cycle threshold
CD	Cytosolic domain
COPD	Chronic obstructive pulmonary disease
CS	Chondroitin sulfate
Ctrl	Control
CV	Coefficient of variation
DAPI	4',6-diamidino-2-phenylindole
DMEM	Dulbecco’s modified Eagle’s medium
E	Embryonic day
ECM	Extracellular matrix
ECD	Extracellular domain
EMT	Epithelial-to-mesenchymal transition

FACS	Fluorescence-activated cell sorting
FBM	Foetal breathing movements
FCS	Foetal calf serum
FEV_1	Forced expiratory volume in 1 second
FGF	Fibroblast growth factor
GAG	Glycosaminoglycan
GDF	Growth and differentiation factor
GFP	Green fluorescent protein
GIPC	GAIP-interacting protein C terminus
GPCR	G protein-coupled receptor
HBSS	Hank's balanced salt solution
Het	Heterozygous
Hh	Hedgehog
HS	Heparan sulfate
hs	*Homo sapiens*
HYX	Hyperoxia
I	Number of intersections with the vessel wall
IGF	Insulin growth factor
i.p.	Intraperitoneal
KO	Knockout
LAP	Latency associated peptide
Lp	Length per point
Lbh	Limb bud and heart

M	Number of points falling on the vessel wall
MAPK	Mitogen-activated protein kinase
MFS	Marfan syndrome
MLI	Mean linear intercept
mm	*Mus musculus*
MMP	Matrix metalloproteinase
MPI	Max Planck Institute
NOX	Normoxia
NGS	Next generation sequencing
NFκB	Nuclear factor κ-light-chain-enhancer of activated B cells
Nkx2.1	NK2 Homeobox 1
P	Post-natal
PAEC	Pulmonary artery endothelial cell
PASMC	Pulmonary artery smooth muscle cell
PCNA	Proliferating cell nuclear antigen
PBS	Phosphate buffered saline
PCR	Polymerase chain reaction
PDGFRα	Platelet-derived growth factor receptor α
PDZ	Postsynaptic density-95/disc large protein/Zonula occludens-1
PECAM1	Platelet endothelial cell adhesion molecule
P/S	Penicillin/streptomycin
RNAi	RNA interference

RNA-seq	RNA sequencing
RT	Room temperature
S	Surface area
SD	Standard deviation
siRNA	Small interfering RNA
Sox2	Sex determining region Y box 2
SMMHC	Smooth muscle myosin heavy chain
SNP	Single nucleotide polymorphism
Tgf-β	Transforming growth factor β
Tgfbr1	Transforming growth factor β receptor 1
Tgfbr2	Transforming growth factor β receptor 2
Tgfbr3	Transforming growth factor β receptor 3
Tie2	TEK receptor tyrosine kinase
TMD	Transmembrane domain
V	Valine
VEGF	Vascular endothelial growth factor
VEGFR2	Vascular endothelial growth factor receptor 2
Wt	Wild-type
ZP	Zona pellucida

1 Summary

The Transforming growth factor (Tgf)-β signalling pathway is a key regulator of lung homeostasis as it is involved in organ development, as well as in pathological conditions of stunted lung growth such as bronchopulmonary dysplasia (BPD). The accessory Tgf-β receptor 3 (Tgfbr3), also known as betaglycan, is a key ancillary molecule in the Tgf-β pathway that has been documented to be essential for the development of the mouse embryo. The siRNA-mediated knockdown of Tgfbr3 resulted in an increase in the proliferation and migration of primary mouse lung fibroblasts, independently of Tgf-β ligand stimulation. To study the role of Tgfbr3 in post-natal lung development, a mouse strain carrying a floxed Tgfbr3 allele was created. The Tgfbr3 floxed mouse strain was crossed to mice expressing Cre recombinase specific to cells with smooth muscle properties, such as smooth muscle myosin heavy chain $(SMMHC)^+$ cells, and platelet-derived growth factor receptor $(PDGFR)\alpha^+$ cells. Temporal conditional knockout of Tgfbr3 was induced in mouse pups at post-natal day (P)1 and P2, by administration of tamoxifen. Stereological analysis of lung structure at P7 revealed significantly decreased alveolarisation of the lung in both knockout mouse lines. It was demonstrated that genetic changes following *in vivo* knockout of Tgfbr3 from fibroblasts with smooth muscle cell properties include a pronounced increase in the expression of fibronectin, proliferating cell nuclear antigen and β-catenin protein. A Tgfbr3-specific knockout in $Tie2^+$ cells led to impaired lung development, with a decreased septal thickness and decreased vessel wall thickness. The potential downstream signalling mechanisms were investigated by whole-transcriptome microarray analysis following *in vitro* knockdown of Tgfbr3. Limb bud and heart (Lbh) was selected as a candidate gene that was demonstrated to have a significant impact on the migration and proliferation of primary mouse lung fibroblasts. This led to the study of the lung phenotype of the global Lbh knockout (KO) mice, which exhibited an increase in septal thickness. Data taken together data suggest novel role for Tgfbr3 in lung development and underscore it as a central regulator of late lung development.

2 Zusammenfassung

Der *Transforming growth factor* (Tgf)-β-Signalweg ist, sowohl in verschiedenen Entwicklungsprozessen, als auch in Krankheitsverläufen bei denen vermindertes Wachstum auftritt, wie zum Beispiel bei der Bronchonpulmonale Dysplasie, entscheident involviert. Somit stellt dieser Signalweg einen Schlüsselregulator in der Organmorphogenese und –homöostase dar. Der Tgf-β Rezeptor III (Tgfbr3), auch Betaglykan genannt, ist ein entscheidender Bestandteil des Tgf-β-Signalwegs und auch für diesen Rezeptor konnte eine essentielle Rolle in der embryonalen Entwicklung der Maus und der Homöostase des vaskulären Systems nachgewiesen werden. Ein Knockout des Tgfbr3 mittels siRNA in Mausexperimenten, resultierte, unabhängig einer Stimulation des Tgf-β-Liganden, in einer Erhöhung der Proliferation und Migration von primären Fibroblasten der Lunge.

Zur Untersuchung der Rolle von Tgfbr3 in der postnatalen Lungenentwicklung wurden Tgfbr3 gefloxte Mäuse kreiert und mit zwei Cre Rekombinase exprimierenden Mauslinien gekreuzt. Diese Cre Rekombinase wird in den Mauslinien entweder in Zellen exprimiert, die schwere Myosinketten der glatten Muskelzellen (*smooth muscle myosin heavy chain*; SMMHC) positiv oder Thrombozyten-Wachstumsfaktor-Rezeptor α (*platelet derived-growth factor receptor α*; PDGFRα) positiv sind.

Ein temporaler konditioneller Knockout von Tgfbr3 wurde mit Hilfe zweier Injektionen von Tamoxifen zum postnatalen Tag (P) 1 und P2 herbeigeführt. Stereologische Untersuchungen zum Zeitpunkt P7 zeigten eine signifikante Verringerung der Alveolarisierung in der Lunge beider Knockout-Mauslinien. Zudem konnte deutlich gemacht werden, dass genetische Veränderungen, durch *in vivo* hervorgerufene Knockdowns von Tgfbr3, bei primären Lungenfibroblasten zu einer signifikanten Erhöhung der Proteinexpression von Fibronektin, Proliferating-Cell-Nuclear-Antigen (PCNA) und β-Catenin führte. Ein Tgfbr3 spezifischer Knockout in $Tie2^{+}$-Zellen zeigten eine ähnliche Lungenentwicklung mit einer verminderten Septumsdicke und einer verminderte Gefäßwanddicke. Mit Hilfe von *whole transcriptome microarray* Analysen wurden die Auswirkungen auf potentielle Herunterregulierungen von Signalwegen und –mechanismen untersucht. Im Rahmen dieser Analysen wurde das *limb bud and heart* (Lbh-Gen) näher betrachtet und es konnte ein Zusammenhang und signifikanter Einfluss auf die Migration und Proliferation von primären Lungenfibroblasten in der Maus aufgezeigt werden. Aufgrund dieses Zusammenhangs zwischen Lbh und primären Fibroblasten

der Lunge wurden zusätzliche Versuche mit Lbh-Knockout-Mäusen durchgeführt. Dabei wurde bei stereologischen Auswertungen der Lunge eine Erhöhung der Septumsdicke deutlich.

Die in dieser Arbeit aufgeführten Ergebnisse geben Hinweise auf eine neue Rolle von Tgfbr3 bei der Lungenentwicklung über die bereits bekannte Funktion als zentraler Signalwegsregulator hinaus.

3 Declaration

I declare that I have completed this dissertation single-handedly without the unauthorised help of a second party and only with the assistance acknowledged therein. I have appropriately acknowledged and referenced all text passages that are derived literally from or are based on the content of published or unpublished work of others, and all information that relates to verbal communications. I have abided by the principles of good scientific conduct laid down in the charter of the Justus Liebig University of Giessen in carrying out the investigations described in the dissertation.

4 Introduction

4.1 Lung morphogenesis

The respiratory system optimally facilitates the process of respiration, i.e. the transport of atmospheric oxygen (O_2) from the inspired air to the mitochondria and removal of carbon dioxide (CO_2) from the mitochondria to the atmosphere during ventilation. The physiology of the respiratory system ensures safe and efficient passage of O_2 from the outside environment into the respiratory unit of the lungs; the alveolus. O_2 molecules transit via nose or throat, trachea, conducting airways (bronchi and bronchioles), reaching the respiratory airways composed of alveolar ducts, and alveolar sacs, which are comprised of alveoli. In the alveolus, a rapid passive diffusion of O_2 occurs down the O_2 concentration gradient, through the thin barrier of the alveolar wall into the capillary. The pulmonary structures allow mammals to achieve a high volume-to-surface ratio facilitating an optimal rate of O_2-CO_2 exchange. This highly organised system evolved after the establishment of the foregut in both vertebrates and invertebrates; and many of the developmental signalling pathways in the lungs are thought to have been adopted from the foregut (Wu and Hill 2009). The five distinct developmental stages of the human lung are presented in Fig. 1 where the schematic airway structure becomes more complex as lung development progresses.

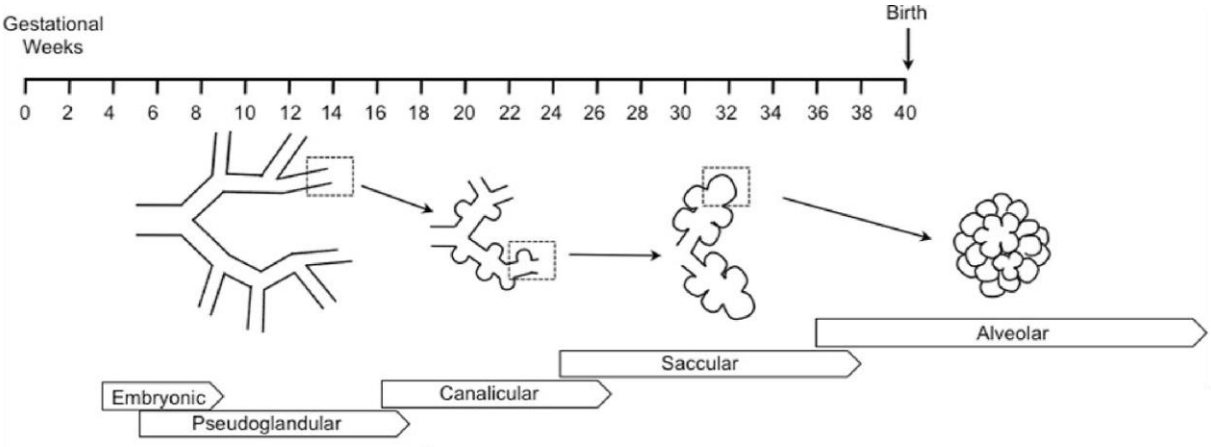

Figure 1 | Stages of human lung development.

Progress of the lung development throughout foetal and post-natal life results in the formation of the highly complex gas-exchange surface area. The stages of human lung development include the embryonic, pseudoglandular, canalicular, saccular and alveolar. Figure modified from Baker and Alvira (2015).

During the embryonic stage (4-8 weeks of gestation) the process of lung organogenesis begins with the primitive lung bud formation from the anterior foregut endoderm. Division of the primitive lung bud results in the establishment of two individual lung buds, which is accompanied by endodermal specification and grounding of the left-right symmetry axis along the future oesophagus (Copland and Post 2004). In the pseudoglandular stage (8-17 weeks of gestation) the primitive lungs buds undergo repetitive evagination during branching morphogenesis and pre-acinar, tree-like airways are formed. The first episodes of foetal breathing movements (FBM) are detected, which facilitate lung branching (Hooper and Harding 1995) and generate small tidal volumes of amniotic fluid that promote cellular proliferation and differentiation (Liu, Tanswell, and Post 1999). In the canalicular stage (17-25 weeks of gestation) differentiation of epithelium results in the formation of terminal bronchioles, and the bronchioalveolar duct junctions (Schittny 2017). In the saccular stage of the lung development (24-36 weeks of gestation), terminal bronchioles narrow resulting in the formation of the immature terminal airspaces, saccules, which consist of thick septa with a double pulmonary capillary layer (Copland and Post 2004). During saccular stage of lung development first alveoli are formed as concave indentation from saccules walls (Hislop 2002). In the alveolarisation stage (36 weeks of gestation-post-natal), 90 % of lung gas exchange surface area is created when saccules partition into alveolar sacs and pulmonary capillaries concomitantly protrude into newly created airspaces to create gas exchange surface area (Schittny 2017). Lungs transition promptly from foetal to neonatal life at the moment of birth when the aeration of the lungs and onset of ventilation trigger an increase in pulmonary blood flow that provides oxygenated pre-load for left ventricle (Hooper, Polglase, and Roehr 2015). Lungs continue to develop and re-model throughout post-natal and early adulthood period.

The formation of the pulmonary vascular system occurs by the process of vasculogenesis when mesodermal angioblasts and haemangioblasts differentiate in previously avascular regions (Risau 1997). Vasculogenesis is regulated by growth factors present in the distal lung buds: vascular endothelial growth factor (VEGF), ephrins, and angiopoietins (Gao and Raj 2010). Concentration levels of VEGF determine the fate of endothelial cells, where high VEGF concentration directs differentiation towards arterial specification and low VEGF concentration promotes venous specification (Sriram et al. 2015). New capillaries develop during the process of angiogenesis, through the proliferation of endothelial cells from the pre-existing capillaries. The TEK receptor tyrosine kinase (Tie2) is an angiopoietin surface

receptor that co-localises to the endothelium during early development and its expression emerges in large vessels associated with central airways (Grzenda et al. 2013). $Tie2^{+}$ endothelial cells are employed during the processes of sprouting and non-sprouting angiogenesis, where the latter is a dominant mechanism occurring in the lungs (Risau 1997).

Lung development in mouse

The molecular mechanisms of lung development have been closely explored in the mouse, since it is the most commonly-employed species in experimental animal models, and the availability of human tissues is limited. The murine lung, together with oesophagus, begins formation from the anterior foregut endoderm at embryonic day (E)9. At this timepoint, the expression of the early marker of the respiratory epithelium, NK2 Homeobox 1 (Nkx2.1) emerges on the anterior side of the foregut endoderm in respiratory endoderm progenitor cells (Herriges and Morrisey 2014). Trachea starts to separate from the foregut endoderm and the crosstalk between Transforming growth factor (Tgf)-β and Wnt pathways, specifically involving bone morphogenetic protein (BMP) and Wnt molecules, establishes a morphogen gradient along the ventral-dorsal axis of the anterior foregut endoderm. Pulmonary epithelial cell differentiation is regulated by the sex determining region Y box 2 (Sox2) transcription factor, resulting in the formation of the trachea and two lung buds.

Branching morphogenesis in the mouse lungs occurs during the embryonic and subsequent pseudoglandular stages between E12.5 and E16.5. Generation of the tree-like structure of new branch tips from the two lung buds is driven by the signalling interplay between the endoderm and mesoderm (Herriges and Morrisey 2014). During the canalicular (E16.5-E17.5) and saccular stages (E18.5-P5), terminal buds form clusters of epithelial sacs, resulting in formation of saccules (Herriges and Morrisey 2014). Mouse pups are born in the saccular stage of lung development, which corresponds to the developmental stage at which human preterm infants are born; however, the lungs of mice are competent for gas exchange. Post-natal alveolarisation in the mouse is an entirely post-natal process and it starts at post-natal day (P)4 when the secondary septa project from the saccules, and divide the saccules into pre-alveolar sacs. The mouse lung at P14 reaches alveoli density that remains constant until late adulthood (Pozarska et al. 2017). Post-natal alveolarisation has been described to commence in two phases: classical and

continued and the schematic diagram of the two modes of alveolarisation is presented on Fig. 2 (Schittny, Mund, and Stampanoni 2008). In the classical (bulk) alveolarisation phase alveoli are formed at the high rate during secondary septation of immature septa that contain double capillary layer, whereas in continued alveolarisation stage new septa are created from the mature septa lined with a single capillary layer, and capillary network expands via angiogenesis (Schittny, Mund, and Stampanoni 2008). Molecular signalling pathways that were demonstrated to regulate post-natal alveolarisation include fibroblast growth factor (FGF) (Jones et al. 2018) and hedgehog (Hh) signalling (Kugler et al. 2015), as well as microRNAs signalling (Nardiello and Morty 2016).

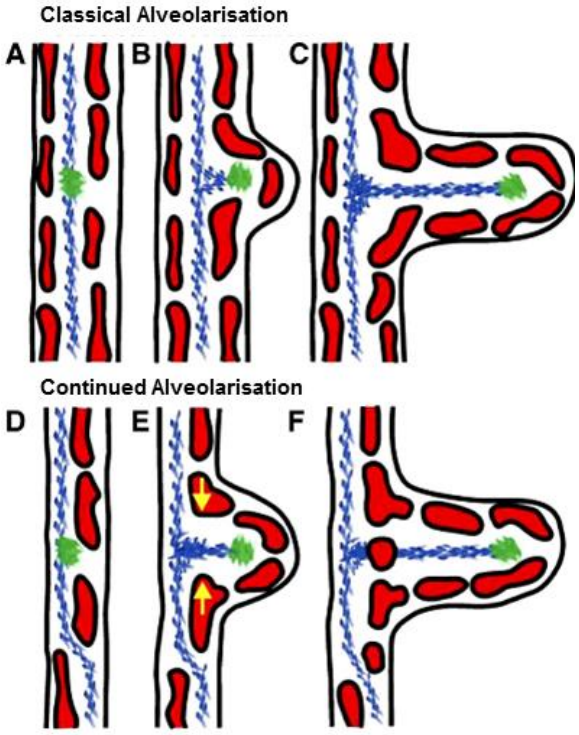

Figure 2 | Stages of post-natal lung alveolarisation.

During classical alveolarisation (A-C), new septa are created from saccules containing double-capillary layer (red). In the continued alveolarisation stage (D-F), new septa are lifted off from the mature septa accompanied with angiogenesis from pre-existing capillaries (yellow arrows). Green, smooth muscle cell precursors; blue, connective tissue. Figure modified from (Schittny, Mund, and Stampanoni 2008).

Lung development is a process that requires paracrine signalling between various cell-types such as fibroblasts, as well as epithelial and endothelial cells, to achieve developmental hallmarks (Silva et al. 2015). Cell-types that have been documented to be essential for the process of post-natal secondary septation is

platelet-derived growth factor receptor (PDGFR)α^+ fibroblasts, which were reside in the tips of the secondary septal crests, forming alveolar ring muscles and secreting elastin and ECM components. The inhibition of PDGFRα^+ cellular signalling led to the inhibition of post-natal secondary septation, and a steep reduction in myofibroblasts numbers (Bostrom et al. 1996). The application of PDGFRα antagonist, imatinib mesylate, during the post-natal period P1-P7 was demonstrated to impair long-term lung alveolarisation, possibly through disturbed formation of the elastin scaffold (Lau et al. 2011). A study performed with a Pdgfra-CreER^{T2} BAC mouse strain has revealed that PDGFRα^+ cells labelled at P1 traced to myofibroblasts and lipofibroblasts at P7 (Ntokou et al. 2015). It was observed that at P3 PDGFRα^+ cells were present within primary septa and at P5 PDGFRα^+ cells were placed at the tip of secondary septa, co-expressing αSMA, indicating trans-differentiation of PDGFRα^+ cells to myofibroblasts (Ntokou et al. 2015). Another study employed Pdgfra^{rtTA} knock-in mouse strain and concluded that 95% of PDGFRα^+ cells labelled at P1 give rise to myofibroblasts and 5% to lipofibroblasts assessed in the lungs at P7 (Li et al. 2018). It was documented in a mouse model of developmental disease of impaired alveolarisation, bronchopulmonary dysplasia (BPD) that correction of aberrant abundance of PDGFRα^+ cell-types with antimiR-34a treatment partially corrected lung alveolarisation (Ruiz-Camp et al. 2019).

The emergence of the smooth muscle myosin heavy chain (SMMMH)$^+$ cells, encoded by the *Myh11* gene, was first noted at E13.5-E14.5 in developing lung buds and peripheral vessels (Miano et al. 1994). The spontaneous phasic contraction of smooth muscle in foetal lung maintains the positive intraluminal pressure and propels the amniotic luminal fluid (Nakamura and McCray 2000). In the post-natal lung, the smooth muscle contraction occurs in the tonic mode facilitating lung growth by mechanical distortion of mesenchyme. As presented in Table 1, at P7 PDGFRα^+ cells acquire smooth muscle cell properties evidenced by the expression of both *Acta2* and *Myh11* genes, which by P15 are downregulated by respectively log fold change of 1.79 and 0.84 (Li et al. 2018).

Table 1 | PDGFRα$^+$ fibroblasts acquire a contractile phenotype at post-natal day 7.

Gene	Avg. UMIs. P7	Avg. UMIs. P15	Avg. logFc
Acta2	2.32	0.51	1.79
Actg2	0.89	0.04	1.36
Tagln	1.69	0.53	1.26
Myh11	1.18	0.4	0.84
Dcn	3.28	3.7	-0.14
Col1a1	4.9	4.97	-0.02

Abbreviations: Avg. logFc, average log fold change; P, post-natal day; Avg. UMI, average unique molecular identifier. Data for table adapted from Li et al. (2018).

This finding was reproduced in another study presented in Fig. 3 where PDGFRα$^+$ cells were revealed to co-express αSMA at P7, and lose αSMA expression by P15 (Branchfield et al. 2016). This suggests that PDGFRα$^+$ cells are able to acquire a transient contractile phenotype at the critical for secondary septation timeframe to facilitate the development of new septa.

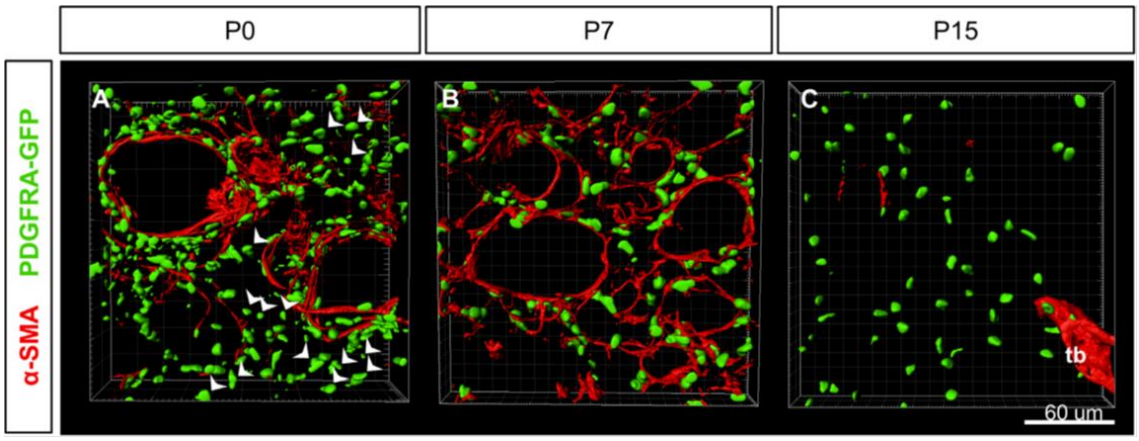

Figure 3 | PDGFRα$^+$ cells co-express αSMA during post-natal lung alveolarisation.

PDGFRα$^+$ lung fibroblasts acquire αSMA expression at post-natal day 7 (P7). Figure adapted from (Branchfield et al. 2016). Abbreviations: GFP, green fluorescent protein; P, post-natal day; PDGFRα, platelet-derived growth factor α; αSMA, α smooth muscle actin.

By P40 all PDGFRα$^+$ cells lose lipo- and myo-fibroblast phenotype and they are speculated to differentiate into resting mesenchymal cells, underscoring key functions of PDGFRα$^+$ cells during late post-natal lung development (Li et al. 2018).

4.2 Tgf-β pathway

Expression of components of the Tgf-β superfamily are dynamically-controlled throughout the stages of lung morphogenesis, and are continually required for the maintenance of homeostasis in the mature organ (Wu and Hill 2009). The Tgf-β pathway is present in all cell-types of the lung, regulating functions such as proliferation, migration and apoptosis. Some members of the Tgf-β pathway are presented on the Fig. 4 including the signalling serine/threonine kinase receptors, including transforming growth factor β receptor type 1 (Tgfbr1), and transforming growth factor β receptor type 2 (Tgfbr2), activin receptor-like kinase 1 (Acvrl1), and the accessory Tgf-β receptor 3 (Tgfbr3), also known as betaglycan. Endoglin is another accessory type 3 receptor that regulates lung development (Pozarska and Morty 2017) and shares some morphological motifs with Tgfbr3 (Somashekar et al. 2017). The Tgf-β family include ligands such as Tgf-β ligands, inhibinis, growth and differentiation factors (GDFs), BMPs and Nodal. Ligands homo- or hetero-dimerise intracellularly, and are secreted as precursors to the extracellular space where they are cleaved by furin-like enzymes into mature polypeptide ligands (Wu and Hill 2009).

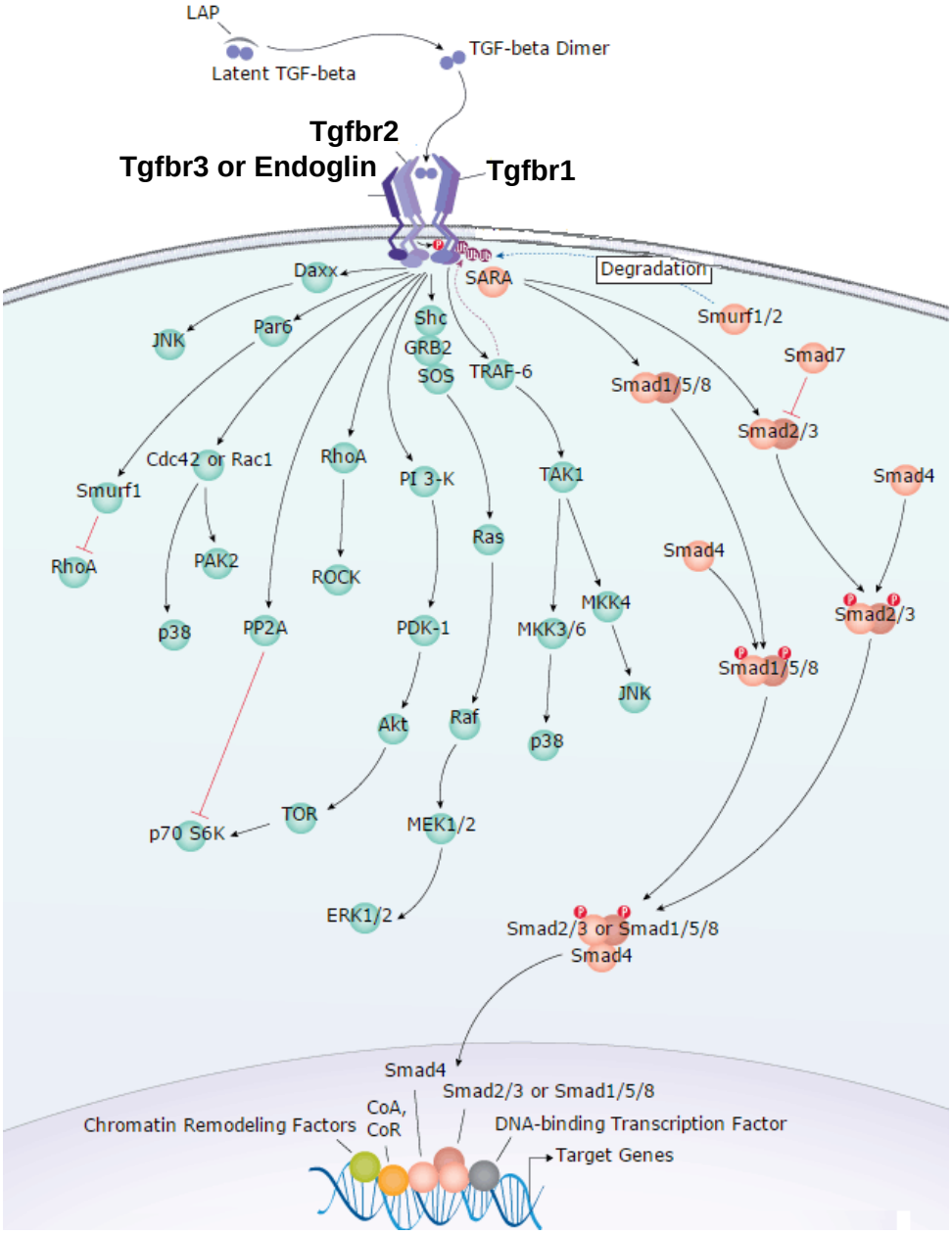

Figure 4 | Schematic diagram of the Tgf-β signalling pathway.

The actions of Tgf-β signalling pathway result in the regulation of cellular processes such as proliferation and migration. Image adapted from https://www.rndsystems.com/pathways/tgf-beta-signaling-pathways.

Abbreviations: Daxx, Death-associated protein; 6JNK, c-Jun N-terminal kinases; LAP, latency associated peptide; MEK, Mitogen-activated protein kinase kinase; PDK-1, Phosphoinositide-dependent protein kinase-1; PI 3-K, Phosphoinositide 3-kinase; PP2a, Protein Phosphatase 2A; RhoA, Ras homolog gene family, member A; ROCK, Rho-associated protein kinase; TAK1, Transforming growth factor beta-activated kinase 1; TRAF, TNF receptor associated factor.

The actions of ligands are regulated by latent Tgf-β-binding proteins that control the establishment of signalling gradients and regulate the availability of the ligands. Tgf-β ligands bind to the receptors at the extracellular side of the cell resulting in the formation of dynamic intracellular signalling cascades. For example, the binding of Tgf-β1/2/3 ligands to Tgfbr1 and Tgfbr2 triggers heterotetrameric complex formation that induces the phosphorylation and activation of Tgfbr1 by Tgfbr2. The accessory Tgf-β receptors are also involved in signalling heterotetrameric complex formation (Lopez-Casillas, Wrana, and Massague 1993; Ray et al. 2010). Activated receptor complexes act via intracellular serine kinase enzyme that leads to the phosphorylation of the downstream Smad molecules that further regulate gene transcription. Activated molecules within the pathway undergo negative regulation via dephosporylation by phosphatases (Liu and Feng 2010). Tgf-β signalling is also regulated by the receptor internalisation and trafficking by clathrin-dependent endosomes and caveolin-positive lipid rafts. It was demonstrated that these different endocytic pathways can converge revealing novel mechanisms for Tgf-β receptor recycling and degradation (He et al. 2015). Tgf-β ligands have varied affinities for different receptor combinations that results in the fine-tuned, cell- and dose-dependent responses to Tgf-β signalling that may range from growth induction to growth inhibition (Wu and Hill 2009).

4.3 Tgfbr3: structure and modes of signalling

Expression and structure of Tgfbr3

Tgfbr3 is the most abundantly expressed receptor of the Tgf-β pathway, reaching expression of 200,000 particles per cell whereas Tgfbr1 and Tgfbr2 achieve expression of 5,000 – 10,000 receptors per cell (Gatza, Oh, and Blobe 2010). The mRNA of Tgfbr3 consists of 18 exons and Tgfbr3 can be expressed from two alternative active promoters, proximal and distal. The mRNA transcripts of Tgfbr3 are mostly expressed from the proximal promoter and the expression can be negatively regulated by Tgfbr1 and Tgf-β1 ligand, mechanisms demonstrated in ovarian and breast cancer cell-lines (Hempel et al. 2008). Figure 5 presents the structure of Tgfbr3, which is expressed as a non-covalently linked homodimer, and consists of a 766 amino acids-long extracellular domain (ECD) with variable glycosaminoglycans (GAG) chains, transmembrane domain (TMD) and 42 amino acids-long cytosolic domain (CD).

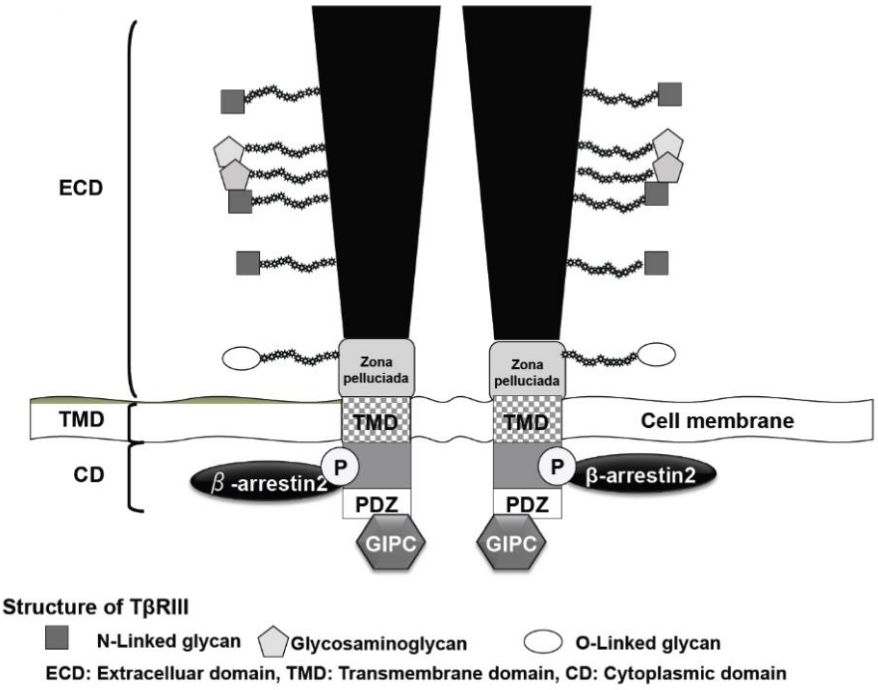

Figure 5 | Schematic structure of Tgfbr3.

Tgfbr3 contains glycosaminoglycan side chained-linked extracellular domain, short transmembrane and intracellular domain. Diagram adapted from Gatza (2010). Abbreviation: GIPC, GAIP-interacting protein C terminus; PDZ, class I postsynaptic density 95/disc large protein/zonula occludens-1.

Heterotetrameric complex formation and regulation of Tgfbr3

There are two ligand binding sites on ECD of Tgfbr3: a membrane-distal site (E region or orphan region), which is highly homologous to the binding site on endoglin, and the membrane-proximal zona pellucida (ZP) site, of which the crystal structure has been resolved revealing immunoglobulin-like folding (Lin et al. 2011). The two binding sites on Tgfbr3 differ in specificity for ligands, which is exemplified by inhibin A that is capable of binding only at the ZP region, whereas Tgf-β1/2/3, bone morphogenetic protein (BMP)-2/4/7 and GDF-5 can bind at both sites (Kirkbride et al. 2008). It has been demonstrated that Tgf-β2 binds the ZP region via extended finger region using residues Ile92, Lys97, Glu99, which are specific to Tgf-β isoforms and inhibin A (Henen et al. 2018). Tgfbr3 is an essential accessory for cells to respond to Tgf-β2 signal, due to the ability of Tgfbr3 to bind and concentrate Tgf-β2 in a 1:1 stoichiometric ratio to establish a signalling complex with Tgfbr2 (Lopez-Casillas, Wrana, and Massague 1993), which can be followed by Tgfbr1 replacing Tgfbr3 in the complex. The ancillary actions of Tgfbr3 within Tgf-β pathway can be both potentiating as well as inhibitory, where the latter function is exemplified by Tgfbr3 binding to inhibin A, establishing an inactive complex with Acvrl2, which renders Acvrl2 unable to respond to activin signalling (Wiater et al. 2006).

Enzymatic activity of matrix metalloproteinase (MMP)-1 and MMP-3 cleave the ECD of Tgfbr3 regulating the release of ECD into the extracellular space, sequestering binding partners away from signalling receptors, and resulting in a signal inhibition. Following the ECD cleavage, the TMD and CD were demonstrated to be stable and available as substrates for γ secretase to be cleaved and released intracellularly (Blair, Stone, and Wells 2011). Mutant construct of Tgfbr3 that displayed enhanced shedding of ECD was overexpressed in A549 cells to increase the concentration of soluble form of Tgfbr3, and as a result A549 cells displayed increased epithelial-to-mesenchymal transition (EMT), and a decrease in migration and invasion capabilities (Huang et al. 2019).

Tgfbr3/β-arrestin 2 signalling complex

β-arrestin 2 is a multifunctional adaptor, scaffold and signal-transducing protein that acts as a phosphoprotein sensor (Lefkowitz and Shenoy 2005). β-arrestin 2 promotes desensitisation and internalisation of G protein-coupled receptors (GPCR) and acts as signalling molecule in non-GPCR pathways such as smoothened, frizzled and wingless, insulin-like growth factor (IGF), and Notch (Kovacs et al. 2009;

Lefkowitz and Shenoy 2005). The structure of β-arrestin 2 is flexible and it is thought to be able to undergo multiple global conformational changes and post-translational modifications upon binding to the activated binding partners (Lefkowitz and Shenoy 2005). Within the structure of Tgfbr3, β-arrestin 2 binds to the serine/threonine-rich class I postsynaptic density 95/disc large protein/zonula occludens-1 (PDZ) domain at the C terminus (Chen et al. 2003). Phosphorylation of Tgfbr3 by Tgfbr2 at Thr841 caused recruitment of β-arrestin 2 to Tgfbr3 and the internalisation of Tgfbr3 via clathrin-independent/lipid raft-dependent pathway. (Finger et al. 2008; Chen et al. 2003). Tgfbr2 co-localised in the endocytic vesicles together with GFP-tagged Tgfbr3/β-arrestin 2 complexes, demonstrating β-arrestin 2 can cause internalisation of complete heterotetrameric complexes via interaction with Tgfbr3. Tgfbr3/β-arrestin 2 signalling was also documented to activate Cdc42 to suppress cellular migration through actin reorganisation (Mythreye and Blobe 2009), regulate mitogen-activated protein kinase (MAPK) signalling (Zhang 2017), inhibit nuclear factor κ-light-chain-enhancer of activated B cells (NFκB) pathway-dependent migration (You, How, and Blobe 2009), trigger internalisation of α5β1 and promote epithelial cell adhesion to fibronectin (Mythreye et al. 2013).

Post-translational modifications of Tgfbr3

Biochemically, Tgfbr3 belongs to the heparan sulfate proteoglycan family. The distinct morphological feature of Tgfbr3 among all human transmembrane proteoglycans is that the protein core can be post-translationally modified with covalent attachments of both highly-negatively charged heparan sulfate (HS) and chondroitin sulfate (CS) GAG chains. Ligands such as FGF, Tgf-β, Wnt proteins, chemokines, interleukins and BMPs can be stored attached to GAG chains (Bishop, Schuksz, and Esko 2007). Other properties of Tgfbr3 including interaction with ECM, control of diffusion rate of signalling gradients and cell migration are also facilitated by GAG chains (Kicheva and Gonzalez-Gaitan 2008), whereas it was demonstrated that GAG chains were not required for the intracellular binding of Tgfbr3 to β-arrestin 2 (Chen et al. 2003).

4.4 Tgfbr3 in homeostasis and disease

Tgfbr3 is a key regulator of mouse embryonic development since global Tgfbr3 knockout (KO) mice die at E13.5 due to lethal proliferative defects in the heart, and apoptosis occurring in liver. Embryonic fibroblasts from global Tgfbr3 KO mice displayed reduced responsiveness to the Tgf-β2 ligand, assessed by a reduction in Smad2 nuclear localisation (Stenvers et al. 2003).

The *Tgfbr3* expression profile in different cell-types of adult mouse lung blood vessels has been made available in a RNA sequencing (RNA-seq) study, which reveals a high *Tgfbr3* expression in all vessel cell-types, particularly cartilage perichondrial cells, vascular fibroblast-like cells and endothelial cells (Fig. 6) (Vanlandewijck et al. 2018; He et al. 2018; 'http://betsholtzlab.org/VascularSingleCells/database.html').

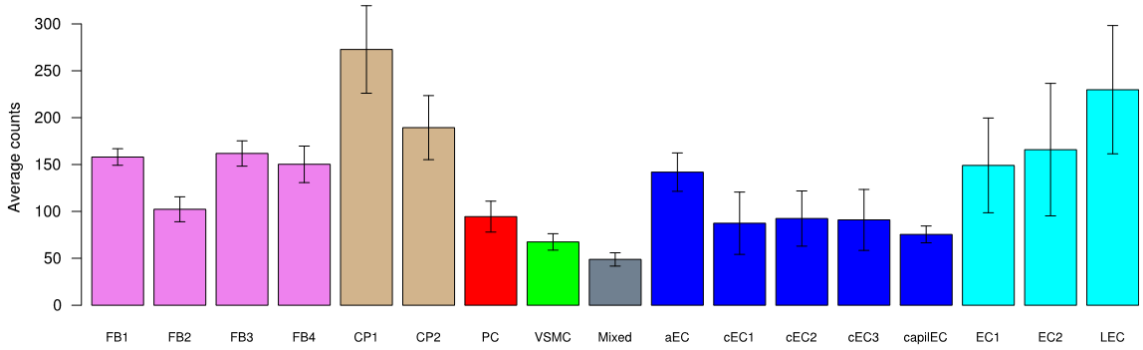

Figure 6 | Tgfbr3 expression in mouse lung vascular cells-types.

Abbreviations: FB, Vascular fibroblast-like cells (purple); CP, Cartilage perichondrium (beige); PC, Pericytes (red); VSMC, Vascular smooth muscle cells (green); EC, Endothelial cells (dark blue); capil, capillary; a, arterial; c, continuum; L, Lymphatic; 1,2,3,4, subtypes. Data taken from Vanlandewijck et al. 2018.

The next generation sequencing (NGS) analysis of over 60,000 individuals displayed the genetic diversity of *TGFBR3* including 246 observed missense *TGFBR3* gene variants and 9 observed loss of function gene variants present within individuals from various ancestry, indicating the prevalence of the human *TGFBR3* 'KO' genotype (Lek et al. 2016). The analysis of genetic variations with NGS in individuals with bicuspid aortic valve demonstrated that pArg423Trp mutation of *TGFBR3*, present within the ECD of the Tgfbr3 protein, contributes to the bicuspid aortic valve formation and can be linked alone to the aortic root dilation (Sticchi et al. 2018).

TGFBR3 is a well-described tumour suppressor gene, with expression of *TGFBR3* demonstrated to be downregulated in solid tumours of the breast, lung, ovary, renal, prostate, and pancreas tumours (Gatza, Oh, and Blobe 2010), as well as in haematological malignancies (Kubiczkova et al. 2012).

Tgfbr3 in pulmonary physiology

In an effort to identify genetic polymorphisms that regulate pulmonary function including lung volumes and compliance, a genome-wide linkage analysis employed C3H/HeJ and JF1/Msf inbred mice strains, that characterise with divergent phenotypes, and revealed correlation between lung function of both mice strains and murine chromosome 15 region, with *Tgfbr3* as a main candidate gene in the peak region (Reinhard et al. 2005). *Tgfbr3* gene was found to be downregulated in a mouse model of BPD, a condition that characterises with stunted lung alveolarisation (Alejandre-Alcazar et al. 2007). Genome-wide linkage analysis stratified by CT emphysema of 949 probands from 127 early-onset emphysema-predominant chronic obstructive pulmonary disease (COPD) patients revealed an intronic single nucleotide polymorphism (SNP) in *TGFBR3* i.e. rs2296621, as the only susceptibility gene with significant linkage to COPD affection status, forced expiratory volume in 1 second (FEV_1), and CT emphysema (Hersh et al. 2009). Interestingly, same SNP s2296621 variant of *TGFBR3* was found to have higher expression frequency in patients with intracranial aneurysm (Santiago-Sim et al. 2009). *TGFBR3* was further documented to be downregulated in lung samples from five patients with emphysema compared to normal lung tissue, assessed by RT-qPCR (Golpon et al. 2004). Patients with sporadic primary pulmonary hypertension displayed downregulated expression of *TGFBR3* when compared to patients with familial primary pulmonary hypertension assessed by microarray analysis (Geraci et al. 2001).

Tgfbr3 in fibrotic disorders

The role of Tgfbr3 in the maintenance of ECM is exemplified by Marfan syndrome (MFS), where Tgfbr3 protein expression is upregulated in fibroblasts from MFS patients. The ectopic expression of Tgfbr3 correlated with the increased Tgf-β pathway signalling and could contribute to connective tissue pathogenesis (Groeneveld et al. 2018). Upregulation of *TGFBR3* expression together with other pro-fibrotic genes such as *THBS1*, *TGFBR2*, *CTGF*, and *PAI*-1, was validated in

skeletal muscle samples from patients from pancreatic ductal adenocarcinoma cachexia characterised by debilitating skeletal muscle wasting (Judge et al. 2018).

Taken together, Tgfbr3 emerges as a key component of homeostasis and plays roles in progression of different pathological conditions through not fully understood disease mechanisms. The published reports highlight the importance of Tgfbr3 as a key molecule involved in the maintenance of the structure of alveolus, regulation of the physiological lung development, homeostasis and respiratory function.

5 Hypothesis

Tgfbr3 is the most ubiquitously expressed Tgf-β receptor of the Tgf-β signalling pathway, but the role of Tgfbr3 is not well-described in lung development, since most of the mechanistic studies have been executed in *in vitro* set-up. It is therefore important to better understand the role of Tgfbr3 during the progression of normal lung development, to provide a perspective on the pathological phenotypes that result from disruptions to the Tgfbr3 gene function and to explore the idea of potential therapeutic intervention.

Aims of the project:

(1) To determine the expression levels of receptors of the Tgf-β pathway in different lung cell-types.
(2) To determine the effects of knockdown of Tgfbr3 in primary mouse lung fibroblasts on functional properties such as proliferation and migration.
(3) To delineate the role of Tgfbr3 in the key cell-types involved in alveolarisation, and late lung development, such as PDGFRα^{+} cells and SMMHC^{+} cells.
(4) To study the role of Tgfbr3 in Tie2^{+} cells in late lung development.
(5) To delineate the role of the potential downstream signalling pathways of Tgfbr3, to which end, limb bud and heart (Lbh) global knockout mouse was employed.

6 Materials and Methods

6.1 Materials

Equipment used in the study is listed in Table 2.

Table 2│Technical equipment.

Item	***Supplier***
Immunoblotting	
LAS-4000 luminescent image analyser	GE Healthcare, USA
Nanoquant Tecan Infinite® 200 Pro	Tecan Group Ltd., Switzerland
Transfer-blot® Turbo™ Transfer System	Bio-Rad, USA
FACS	
GentleMACS™ Dissociator, 130-093-235	Miltenyi biotec, Germany
BD FACSARIA III	BD Biosciences, USA
Stereology	
NanoZoomer-XR C12000	Hamamatsu, Japan
Feather Trimming Blade, No. 130, Type (S)	Medical AG, Germany
PCR	
Thermocycler	PeqLab, VWR, UK

Abbreviations: FACS, fluorescence-activated cell sorting; PCR, polymerase chain reaction.

Reagents used in the study are listed in Table 3.

Table 3│Chemicals and reagents.

Item	***Catalogue number and supplier***
Immunoblotting	
2-mercaptoethanol	M6250-100ML, Merck, Germany
4x Laemmli Sample Buffer	1610747, Bio-Rad, USA
β-actin antibody	4967, Cell Signaling Technology, USA
Acetone	T906.1, Carl Roth, Germany
Complete™ protease inhibitor cocktail	11697498001 Merck, Germany
HRP-conjugated anti-rabbit IgG	31460, ThermoFisher Scientific, Germany
Milk powder	T145.1, Carl Roth, Austria
Mini-PROTEAN® TGX™ Gels	456-1083, Bio-Rad, USA
Precision Plus Protein™ Dual Color Standard	161-0374, Bio-Rad, USA
Quick StartTM Bradford dye reagent	5000205, Bio-Rad, USA
RIPA Buffer	R0278-500ml, Merck, Germany
Sodium orthovanadate	S6508, Merck, Germany
SuperSignal® West Femto Chemiluminescent substrate	34095, ThermoFisher Scientific, Germany
Transfer-blot® Turbo™ Transfer Pack	1704158, Bio-Rad, USA
TGF-β Receptor III antibody	2519, Cell Signaling Technology, USA
LBH antibody	ab173737, Abcam, USA
Cellular fibronectin antibody	F6140, Sigma, USA
β-catenin antibody	9587S, Cell Signaling Technology, USA
Smad2/3 antibody	5678S, Cell Signaling Technology, USA
PDGFRα antibody	2992, Cell Signaling Technology, USA
PCNA antibody	sc7907, Santa Cruz Biotechnology, USA
Tween 20	8170722500, Merck, Germany
RNA Inteference	
Control siRNA-A	sc-37007, Santa Cruz Biotechnology, USA
Immunoblotting	
Opti-MeM™ I Reduced Serum Media	31985062, ThermoFisher Scientific, Germany
TGFβ RIII siRNA (m)	sc-40225, Santa Cruz Biotechnology, USA
TGF-β ligand	240-B, R&D Systems, USA
X-tremeGENE™ HP DNA Transfection Reagent	06366236001, Merck, Germany
Proliferation	
Cell Proliferation ELISA, BrdU	11647229001, Merck, Germany
Wound Healing – Cell Migration Assay	
Culture-Insert, 2 µ-Dish 35 mm	81176, Ibidi, Germany

Table 3 - continued

Item	*Catalogue number and supplier*
Cell Culture	
Ultrapure Agarose	16500500, ThermoFisher Scientific, Germany
Collagenase type I	17100017, ThermoFisher Scientific, Germany
Dulbecco's modified Eagle's medium	D6421, Merck, Germany
Dulbecco's phosphate buffered saline	D8537-500ML, Merck, Germany
Fetal calf serum	A3160802, ThermoFisher Scientific, Germany
Hank's balanced salt solution	14025092, ThermoFisher Scientific, Germany
Iron (II,III) oxide	310069-25G, Merck, Germany
Media 199	BE12-117F, Lonza, USA
Penicillin/Streptomycin (10,000 U/mL)	15140122, ThermoFisher Scientific, Germany
Smooth muscle cell medium	C-22162, PromoCell, UK
Genotyping	
Agarose NEEO Ultra-Qualität	2267.4, Carl Roth, Austria
Ethanol	5054.3, Carl Roth, Austria
Ethidium bromide	H5041, Promega, USA
GoTaq® Flexi DNA Polymerase	M829, Promega, USA
Isopropanol	0733.1, Carl Roth, Austria
Proteinase K	AM2542, ThermoFisher Scientific, Germany
***In vivo* experiments**	
Migloyol 812	Cäesar & Lorentz, Germany
NarcoreN	Boehringer Ingelheim Vetmedica GmbH, Germany
Tamoxifen	T5648-1G, Merck, Germany
Immunofluorescence	
2-methylbutane	277258-1L, Merck, Germany
Anti-smooth muscle myosin heavy chain antibody	Ab53219, Abcam, UK
Dako Pen	S2002, Agilent, USA
Goat anti-rabbit AF647	A21244, Invitrogen, Carlsbad, USA
IgG Rabbit	2729, Cell Signaling Technology, USA
Mowiol®	81381-50G, Merck, Germany
Normal goat serum	50062Z, ThermoFisher Scientific, Germany
O.C.T.™ Compound Containing	4583, Sakura Finetek Europe, Netherlands
Triton X-100	H5141, Promega, Germany
FACS	
CD16/CD32-biotin antibody	101303, Biolegend, USA
CD45-biotin antibody	103104, Biolegend, USA
CD140a-APC antibody	135908, Biolegend, USA
CD326-biotin antibody	118204, Biolegend, USA
CD202b-PE antibody	124008, Biolegend, USA

Table 3 - continued

Item	*Catalogue number and supplier*
CD45-APC antibody	103112, Biolegend, USA
CD31-PE antibody	102508, Biolegend, USA
FACS	
CD326-FITC antibody	118208, Biolegend, USA
Corning® Dispase	354235, Corning, USA
PE Streptavidin	405204, Biolegend, USA
FACS buffer	00-4222-26, eBioscience, USA
FACS tubes	352054, Corning, USA
DNase I	9003-98-9 Serva, Germany
gentleMACS™ C tubes	130-096-334 Miltenyi Biotec, Germany
HEPES (1 M)	15630080, ThermoFisher Scientific, Germany
Real-time RT-qPCR	
10x PCR buffer II	4376212, Applied Biosystems, USA
25 mM $MgCl_2$	A351H, Promega, USA
dNTPs Mix	U1511, Promega, USA
MuLV reverse transcriptase	4311235, Applied Biosystems, USA
Total RNA Kit, PeqGOLD	732-2868, VWR, UK
Platinum™ SYBR™ Green qPCR SuperMix-UDG	11733038, ThermoFisher Scientific
Random hexamers	100026484, Applied Biosystems, USA
RNase inhibitor	N8080119, Applied Biosystems, USA
Stereology	
Paraformaldehyde	P6148-1KG, Merck, Germany
Glutaraldehyde 50% solution in water	23116.02, Serva, Germany
HEPES (1 M)	15630080, ThermoFisher Scientific, Germany
PBS	D8537-500ML, Merck, Germany
Agar-agar	05040-1KG, Merck, Germany
Sodium cacodylate	15540.03, Serva, Germany
Uranyl acetate	77870, Serva, Germany
Technovit 7100	64709003, Kulzer Technik, Germany
MTT Cell Proliferation Kit	
Cell Proliferation Kit I (MTT)	11 465 007 001, Roche, Germany

Abbreviations: FACS, fluorescence-activated cell sorting; RT-qPCR, reverse transcription quantitative polymerase chain reaction.

The primers employed for the real-time RT-qPCR assays are listed in Table 4.

Table 4│Oligonucleotide sequences

Gene	Species	Primer	Sequence: 5'-3'
Acta2	*mm*	forward	AGAGCAAGAGAGGGATCCTGA
	mm	reverse	GTCGTCCCAGTTGGTGATGAT
Acvrl1	*mm*	forward	CGATATCCAGGTAATCGCTG
	mm	reverse	CCAAGATGCCCATTGTTCACA
Ctnnb1	*mm*	forward	TGACACCTCCCAAGTCCTTT
	mm	reverse	TTGCATACTGCCCGTCAAT
Ctr9	*mm*	forward	CCAACCCGAGACCGAGAAAA
	mm	reverse	CTTTGCAAGACCAAGGCCAC
Eng	*mm*	forward	CGTGCTACTCATGTCCCTGAT
	mm	reverse	CAGGACAAGATGGTCGTCAGT
Epcam	*mm*	forward	GAGTCCCTGTTCCATTCTT
	mm	reverse	TCTCCTTTATCTCAGCCTTC
Fn1	*mm*	forward	CGAGGTGACAGAGACCACAA
	mm	reverse	CTGGAGTCAAGCCAGAC
ITGAD	*hs*	forward	CCTACAATGTTGGTCTCCCAGA
	hs	reverse	AGTAACCAGTTGCCTTTTGGATT
Klhl28	*mm*	forward	CTACCTGGTTTCGAGCAGGG
	mm	reverse	GACGACCAGAAGTGCCTTGA
Lbh	*mm*	forward	CTGCTCTGACTATCTGAGATCGG
	mm	reverse	CGGTCAAAGTCTGATGGGTCC
LBH	*hs*	forward	GCCCCGACTATCTGAGATCG
	hs	reverse	GCGGTCAAAATCTGACGGGT
Lsm14a	*mm*	forward	CAGTGAAGGGAATGCTGATGAGG
	mm	reverse	TCTTCAGCCCAAGTTGGTCTCC
MT1X	*hs*	forward	CTTCTTGCAGGAGGTGCATT
	hs	reverse	AGTCCAGTCTCTCCTCGGCT
Myh11	*mm*	forward	GCAATGCGAAAACCGTCAA
	mm	reverse	GATGCGAATGAACTTGCCAAA
Nfkb1	*mm*	forward	GAAATTCCTGATCCAGACAAAAAC
	mm	reverse	ATCACTTCAATGGCCTCTGTGTAG
Nhlrc3	*mm*	forward	CCAGCTGAACCTCAGTAGGC
	mm	reverse	CCAGGGCCACCAGAAAGAAA
Pecam	*mm*	forward	ACGCTGGTGCTCTATGCAAG
	mm	reverse	TCAGTTGCTGCCCATTCATCA
Polr2a	*mm*	forward	CTAAGGGGCAGCCAAAGAAAC
	mm	reverse	CCATTCAGCATACAACTCTAGGC
Ptprc	*mm*	forward	GAGGTGTCTGATGGTGCAAG
	mm	reverse	TGTATTCCACTAAAGCCTGATGAA
Sar1b	*mm*	forward	TGTGCTAAAAAGGCAGGGCT
	mm	reverse	GCATGTTGGGGGATGGATCT
Smad2	*mm*	forward	AAGCCATCACCACTCAGAATT
	mm	reverse	CACTGATCTACCGTATTTGCT
Smad3	*mm*	forward	AGGGGCTCCCTCACGTTAT
	mm	reverse	CATGGCCCGTAATTCATGGT
Tgfbr1	*mm*	forward	CAGAGGGCACCACCTTAAA
	mm	reverse	AATGGTCCTGGAAGTTC
Tgfbr2	*mm*	forward	CCAAGATGCCCATTGTTCACA
	mm	reverse	CATCCTGGATTCTAGAACTTC

Table 4 - continued

Gene	*Species*	Primer	Sequence: 5'-3'
Tgfbr3 exon 2	*mm*	forward	GGTGTGAACTGTCACCGATCA
	mm	reverse	GTTTAGGATGTGAACCTCCCTTG
Tgfbr3 exon 5	*mm*	forward	GGTTCTGTGGTCCAGTTTTC
	mm	reverse	TATTCCTTTTGGGCCCAGTGTA
Vegfc	*mm*	forward	CCAGCACAGGTTACCTCAGCAA
	mm	reverse	TAGACATGCACCGGCAGGAA
Yhwah	*mm*	forward	CTTAGCCAAACAAGCCTTCG
	mm	reverse	ATCTGAATAGCTGTGCTGCC
Genotype	**Species**	**Annealing T (°C)**	**Sequence: 5'-3'**
Tgfbr3 floxed	*mm*	56	GCACACTTAGTAACACTTCCT CTCTTGACAAACATGGACTTT
Tie2-CreER^{T2}	*mm*	58	GAAGTCGCAAAGTTGTGAGTTG TGGCTTGCAGGTACAGGA GAGAATGGCGAGAAGTCACTG
SMMHC-CreER^{T2}	*mm*	58	TGACCCCATCTCTTCACTCC AACTCCACGACCACCTCATC AGTCCCTCACATCCTCAGGTT
PDGFRα-CreER^{T2}	*mm*	61	CAGGTCTCAGGAGCTATGTCCAATTTACTGAA CGTA GGTGTTATAAGCAATCCCCAGAA
Lbh floxed	*mm*	58	GAGATGGCGCAACGCAATTAATG AGTTTCTCTAAAGCCTACCCCTGCC
Flippase	*mm*	58	GTCCACTCCCAGGTCCAACTGCAGCCCAAG CGCTAAAGAAGTATATGTGCCTACTAACGC
Neomycin cassette	*mm*	61	AGGATCTCCTGTCATCTCACCTTGCTCCTG AAGAACTCGTCAAGAAGGCGATAGAAGGCG
LacZ	*mm*	58	GTTGCAGTGCACGGCAGATACACTTGCTGA GCCACTGGTGTGGGCCATAATTCAATTCGC

Abbreviations: *hs*, *homo sapiens*; *mm*, *mus musculus*; PDGFRα, platelet-derived growth factor α; SMMHC, smooth muscle myosin heavy chain; T, temperature.

6.2 Methods

6.2.1 Mouse transgenic experiments

Tgfbr3$^{tm1a(EUCOMM)Hmgu}$ embryonic stem cells on a C57BL/6N-A/a background were purchased from European Mouse Mutant Cell Repository. Stem cells were injected into a C57Bl/6J blastocyst at the transgenic facility of Max Planck Institute (MPI) for Heart and Lung Research, Bad Nauheim. After injection, blastocysts were transferred into NMRI foster mother, which gave birth to chimeric pups. Chimeric mice were bred to C57BL/6J wild-type (Wt) mice and germline transmission of Tgfbr3$^{tm1a(EUCOMM)Hmgu}$ construct was achieved. The Tgfbr3$^{tm1a(EUCOMM)Hmgu}$ mouse carries a lacZ-tagged insertion with one loxP site inserted upstream of exon 5 of Tgfbr3, and the other loxP site is located downstream of the exon 5 to create a knock out first allele (Skarnes et al. 2011). The heterozygous for the construct mouse was back-crossed to C57BL/6J mouse for eight generations. As presented in Fig. 7 *A*, heterozygous mice for the insert were crossed to the FLPeR mouse to excise neomycin and LacZ genes and create floxed Tgfbr3 conditional allele. A Tgfbr3$^{fl/fl}$ strain was crossed to Cre recombinase cell-specific driver lines to induce temporal and cell-specific Tgfbr3 deletion by application of 16 mg.ml^{-1} tamoxifen dissolved in Migloyol 812. Tamoxifen was injected intraperitoneally (i.p.) on P1 and P2 (0.4 mg) to new-born transgenic pups. Lungs were harvested at the P7.

Limb bud and heart (Lbh) global KO mice were generated from Lbh$^{tm1a(KOMP)Wtsi}$ embryonic stem cells at the University of California, Davis, Mouse Biology Program facility. Lbh KO mice carry a lacZ-tagged insertion between exons 1 and 2 of the *Lbh* gene to create a knockout-first allele (Fig. 7 *B*) (Skarnes et al. 2011).

Tg(Myh11-cre/ERT2)1Soff (SMMHC-CreER^{T2}) and Tg(Tek-cre/ERT2)1Soff (Tie2-CreER^{T2}) driver mouse lines were provided by Prof. Stefan Offermanns (MPI for Heart and Lung Research, Bad Nauheim) and generation of mice strains was described previously (Wirth et al. 2008) and (Rautureau et al. 2015), respectively. Male mouse pups were employed in the study of SMMHC cell-specific genetic deletion, since SMMHC-CreER^{T2} has been inserted on Y chromosome (Wirth et al. 2008). Pdgfra-cre/ERT21Wdr (Pdgfrα-CreER^{T2}) mouse strain was generated formerly (Rivers et al. 2008) and was a gift of Prof. Dr. William Richardson (UCL, London).

A

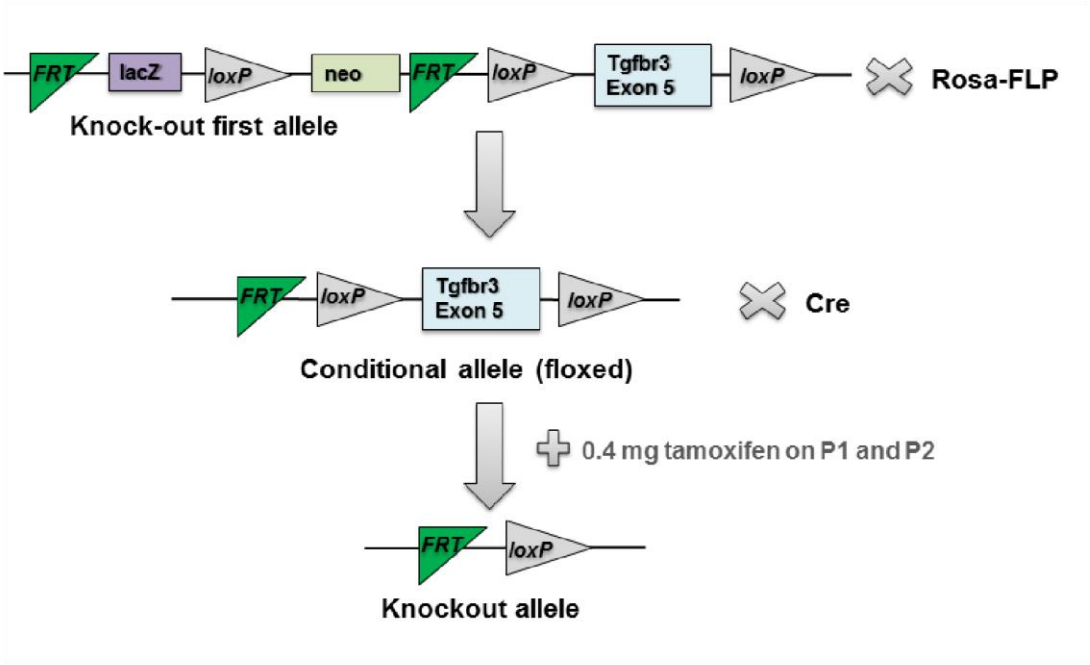

B

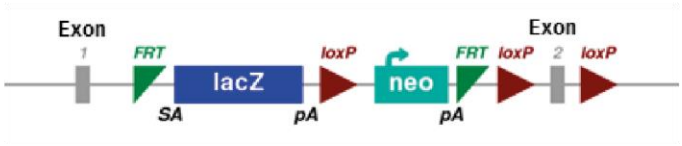

Figure 7 | Generation of a mouse with a floxed *Tgfbr3* exon 5.

(*A*) Breeding strategy of mouse carrying knock-out first Tgfbr3 allele crossed with germline delete Rosa-FLP mouse to excise lacZ and neo genes and create floxed allele functionally equivalent to wild-type allele. Floxed mouse can be crossed with a mouse carrying conditional cell-specific Cre recomobinase enzyme. (*B*) Lbh targeted knockout allele schematic. Adapted from https://www.komp.org.

6.2.2 Primary mouse lung fibroblast isolation

Mice were sacrificed with a 500 $mg.kg^{-1}$ (i.p.) overdose of pentobarbital. The chest cavity underwent sternotomy and lungs were cannulated through the right atrium with ice-cold PBS. Lungs were excised from the chest cavity and the heart was separated from the lungs. Under a sterile hood, lungs were minced with scalpel, and the resulting tissue homogenate was transferred to a 2 $mg.ml^{-1}$ collagenase type I dissolved in Hank's balanced salt solution (HBSS). The cell suspension was incubated for 30 min with agitation in an incubator at 37 °C, in a humidified atmosphere containing 5 % CO_2. The cell suspension was filtered through a 40 µm filter, centrifuged at 1,100 rpm for 5 min and re-suspended in 5 ml of DMEM

supplemented with 10% (v/v) foetal calf serum (FCS), and 100 $U.ml^{-1}$ penicillin and 100 $\mu g.ml^{-1}$ streptomycin. Cells were transferred to cell culture flasks and allowed to grow to confluence in an incubator at 37 °C, in a humidified atmosphere containing 5 % CO_2. Primary adult mouse lung fibroblasts were passaged at least three times before use in the *in vitro* experiments. Primary mouse lung fibroblasts isolated from tamoxifen-treated $Tgfbr3^{fl/fl}$ Pdgfrα-$CreER^{T2}$ and Pdgfrα-$CreER^{T2}$ mice at P7 were harvested without passaging for mRNA and protein expression analysis.

6.2.3 RNA interference

Primary mouse lung fibroblasts were seeded into 6-well plates at 200,000 cells per well. The RNA interference transfection mixture was prepared by adding X-treme gene siRNA transfection reagent to pre-heated to 37 °C Opti-MeM™, followed by either siRNA to Tgfbr3 (Santa Cruz Biotechnology) or a negative scrambled controls (Santa Cruz Biotechnology). Final transfection concentration was 100 nM in a 1 ml volume for Tgfbr3 knockdown, and 200 nM for Lbh knockdown. The media was aspirated from the cells and replaced with the transfection mixture. After 6 h, the transfection mixture was replaced with DMEM supplemented with 10 % (v/v) FCS, 100 $U.ml^{-1}$ penicillin and 100 $\mu g.ml^{-1}$ streptomycin, and fibroblasts were cultured for 48 h.

A549 cells were seeded into 6-well plates at 100,000 cells per well in DMEM/F12 (1:1) media supplemented with 10 % FCS and 100 $U.ml^{-1}$ penicillin and 100 $\mu g.ml^{-1}$ streptomycin. The following day, the RNA interference transfection mixture was prepared by adding X-treme gene siRNA transfection reagent to pre-heated to 37 °C Opti-MeM™, followed by either siRNA to Lbh (Santa Cruz Biotechnology) or a negative scrambled controls (Santa Cruz Biotechnology). Final transfection concentration was 200 nM in a 1 ml volume for Lbh knockdown. Cells were incubated for 48 h in a humidified atmosphere containing 5 % CO_2. Cells were re-plated into 96-well plate at 3,000 cells per well.

6.2.4 Primary pulmonary artery smooth muscle cell isolation

To isolate primary pulmonary artery smooth muscle cells (PASMC), mice were sacrificed with a 500 $mg.kg^{-1}$ (i.p.) overdose of pentobarbital. Mouse pups at P7 underwent sternotomy, and the lung was perfused with a pre-warmed mixture of Iron (II,III) oxide beads, 2 % (m/v) and agarose 2 % (m/v) in Media 199 that was supplemented with 100 $U.ml^{-1}$ penicillin and 100 $\mu g.ml^{-1}$ streptomycin. Pre-warmed agarose dissolved in Media 199 2 % (m/v) was instilled into the mouse lungs via the

trachea. Lungs were excised, and transferred to ice-cold PBS. The lungs were dissociated under a sterile hood. Lung cell containing iron beads were separated from cell suspensions with magnet holder and rinsed 3 x PBS. Iron beads were re-suspended in pre-heated collagenase and incubated for 1 h at 37 °C. Cell clusters were disrupted by pipetting with 18 G needle and washed for 3 x PBS. Cell clusters were washed with Media 199 supplemented with 10 % FCS (v/v). Media was aspirated and cell clusters were re-suspended with smooth muscle cell media supplemented 15 % FCS (v/v). Two lungs were used to grow a confluent cellular monolayer of PASMC on a 10 cm^2 Petri dish.

6.2.5 Stereological assessment of lung structure

Lung embedding

Mice were euthanized with a 500 $mg.kg^{-1}$ (i.p.) overdose of pentobarbital. The chest cavity was opened and the lungs were fixed at 20 cm H_2O pressure with a fixative containing 1.5 % (m/v) paraformaldehyde, 1.5 % glutaraldehyde (v/v), 150 mM HEPES in PBS, pH 7.4. Lungs were fixed for 24 h at 4 °C. For Cavalieri lung volume estimation, lungs were embedded in 2 % (m/v) agar-agar and cut into 3 mm slices using a custom-made sectioning cube and a feather trimming blade. Lungs slices were photographed on a millimetre paper background. All the lung pieces were washed in 0.1 M sodium cacodylate for 4 x 5 min and next for incubation with osmium tetroxide for 2 h. Lungs were washed with cacodylate for 4 x 5 min and transferred to 2.5 % (m/v) uranyl acetate in ddH_2O for overnight incubation. Lungs were washed with ddH_2O for 4 x 5 min, followed by 4 x 15 min. Lungs were dehydrated with 70 % (v/v) acetone for 2 x 1 h, 90 % acetone (v/v) for 2 x 1 h, and with 100 % acetone for 1 h. Lungs were transferred to mixture of 100 % acetone and glycol methacrylate (1:1 ratio) for overnight incubation. Next lungs were transferred to glycol methacrylate for 24 h incubation. Lungs were transferred to glycol methacrylate with Hardener II to solidify in block moulds. Lungs blocks were sectioned into 2 μm, where every 10^{th} section was taken for the analysis and 4 sections per lung were assessed. For alveoli number counting, the first and third sections were taken from a consecutive sectioning. Sections were stained using Richardson's stain, and images were scanned using a NanoZoomer-XR C12000 Digital slide scanner.

Lung morphometric assessment with design-based stereology

Design-based stereology applied for the morphometric assessment of the lung structure followed the recommendations of the American Thoracic Society/European Respiratory Society (Hsia et al. 2010), and has been described in detail before (Fehl et al. 2019). The stereological analysis was carried out with NewCast^{TM} software. The parameters assessed were alveoli density and alveoli number, the counting method applied was based on the Euler number (Knust et al. 2009). Other parameters estimated involved the arithmetic mean septal thickness, surface area (*S*), mean linear intercept (MLI), vessel wall thickness, and septal volume. The precision of the measurement for each parameter was estimated by the calculation of coefficient of error (CE), coefficient of variation (CV), and the squared ratio (CE^2/CV^2), with the quotient values below threshold of 0.5 regarded as precise measurements.

For stereological assessment of the vessel wall thickness, a grid of 12 x 12 lines at 68 % length was applied to the lung slides at 40x magnification (Fig. 8). The number of intersections (I) between test-lines and vessel walls was counted, as well as the number of line end-points falling on the area of vessel wall (M). The counted points allowed estimating the relationship between the volume of the vessel wall and the surface of the vessel wall giving the thickness according to the equation:

$$\textbf{Vessel wall thickness} = \textbf{Lp x } \frac{\sum(\boldsymbol{M\ vessel\ wall})}{\mathbf{2}\ .\sum(\boldsymbol{I\ vessel\ wall})}$$

Lp, length per point; M, number of points falling on the vessel wall; I, number of intersections with the vessel wall.

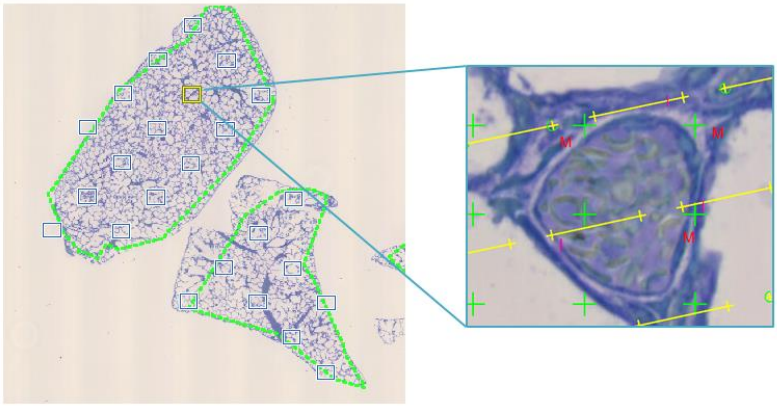

Figure 8 | Stereological counting method for vessel wall thickness.

Example field of view of Visiopharm counting tool employed for the stereological assessment showing counting with test lines intersecting vessel walls (I) and mark points falling on the vessel walls (M).

6.2.6 Fluorescence-activated cell sorting

Mouse pups were sacrificed with a 500 $mg.kg^{-1}$ (i.p.) overdose of pentobarbital. The chest cavity was opened and the right atrium was cannulated using syringe with HBSS to perfuse the lungs. Dispase I was instilled through the trachea to the lungs. The lungs were excised and transferred to Dispase I and incubated for 10 min in an incubator at 37 °C, in a humidified atmosphere containing 5 % CO_2. Under sterile hood, the heart and connective tissue were dissected from the lungs. Lungs were transferred to a gentle MACS™ C tube with 5 ml of DMEM supplemented with 1 % HEPES (v/v) and 1 % DNase I (v/v) and 100 $U.ml^{-1}$ penicillin and 100 $\mu g.ml^{-1}$ streptomycin. Lungs were dissociated using gentleMACS dissociator. Cell homogenates were filtered through 100 µm and 40 µm filters, centrifuged at 1,100 rpm for 10 min at 4 °C. Cell pellets were resuspended in FACS buffer and transferred to FACS tubes. Tubes were centrifuged for 5 min at 1,100 rpm at 4 °C.

Cell pellets were incubated with the required antibodies. Staining for PDGFRα was performed for 15 min at 4 °C with 1 µl of CD140a-APC, CD16/CD32-biotin, CD326-biotin and CD45-biotin in 100 µl of FACS buffer. Staining for Tie2 was performed with an CD202b-APC antibody. Cells were washed with 400 µl FACS buffer and resuspended in 200 µl of FACS buffer with 2 µl of secondary antibody (PE Streptavidin) for 15 min at 4 °C. Pellets were resuspended in 500 µl of FACS buffer. Cells were filtered and 1 µl of 4',6-diamidino-2-phenylindole (DAPI) was added to samples shortly before FACS analysis. Samples were sorted on BD FACSARIA III with gating settings as presented in Fig. 9.

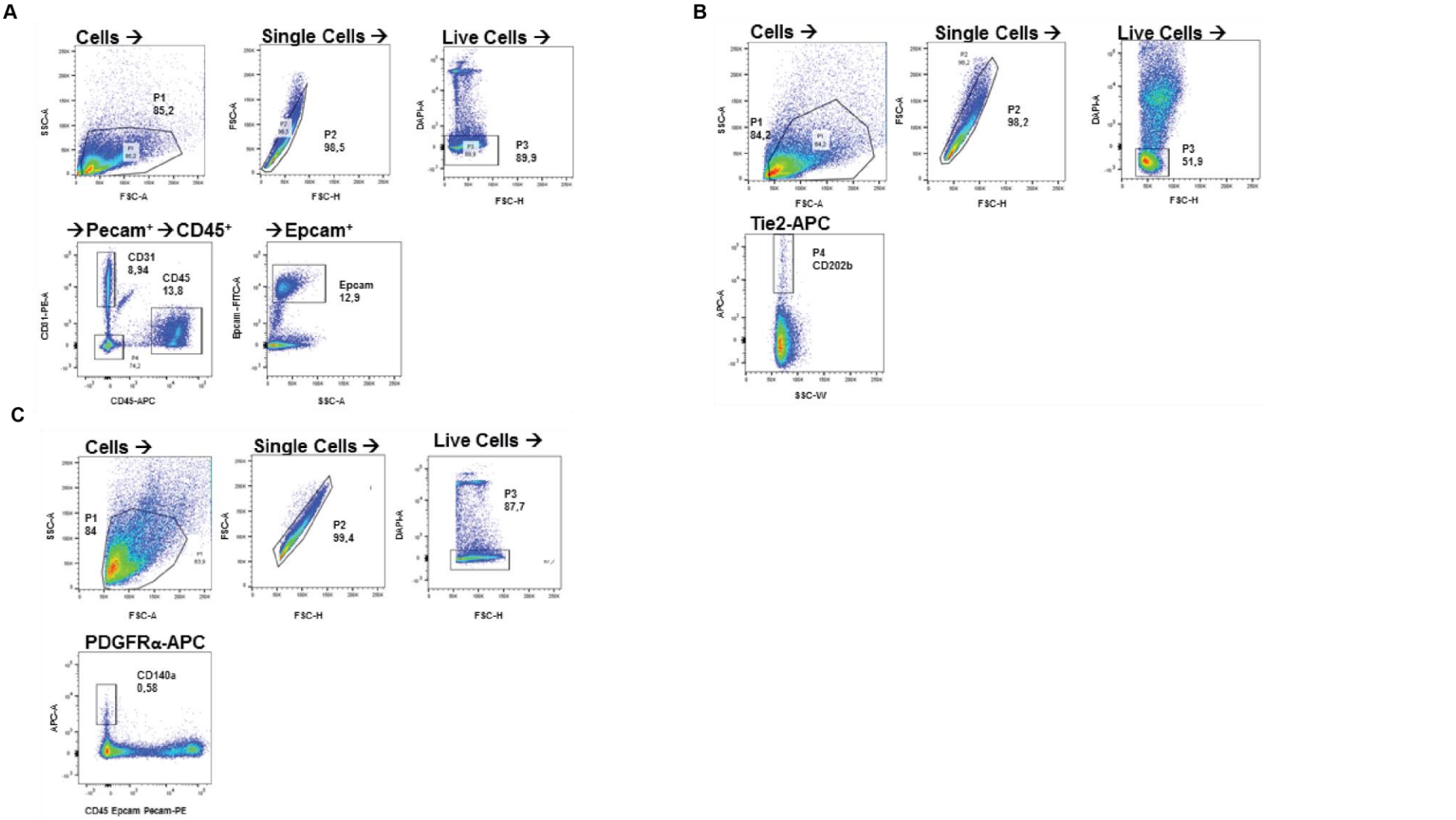

Figure 9 | Fluorescence activated cell sorting gating settings employed in the study.

Gating settings used to separate (*A*) Pecam$^+$, CD45$^+$, and Epcam$^+$ population; (*B*) Tie2$^+$ cell-types; and (*C*) PDGFRα$^+$ cell-types.

6.2.7 mRNA isolation and real-time RT-qPCR

Total mRNA was isolated using a PeqGold total RNA kit according to the manufacturer's protocol. Denaturation of 1 µg of RNA in a 20 µl-volume was performed for 10 min at 70 °C. Next, 20 µl of master mix for reverse transcription was added, which consisted of 10 x PCR buffer II, 25 mM $MgCl_2$, H_2O, random hexamers, RNase inhibitor, dNTPs and MuLV reverse transcriptase. The samples were incubated at 21 °C for 10 min, 43 °C for 1 h for cDNA synthesis, and at 99 °C for 5 min to inactivate MuLV Reverse transcriptase.

Real-time qPCR was conducted using Platinum™ SYBR™ Green qPCR SuperMix-UDG on StepOnePlus qPCR System. The differences in gene expression were given by the change (Δ) in the cycle threshold (Ct) values, obtained by the difference between mean Ct of reference gene and mean Ct of gene of interest. Reference gene employed for the study was *PolR2A*. The sequences of oligonucleotides used for the RT-qPCR analyses are listed in Table 4.

6.2.8 Western blot

Proteins were harvested using RIPA buffer supplemented with 1 mM sodium orthovanadate and Complete™ protease inhibitor cocktail. Cells or tissue samples were incubated with the RIPA buffer mixture for 5 min at 4 °C. The samples underwent disruption and homogenisation with a cell scraper for cell samples, or a Precellys Lysing Kit for tissue samples. Protein lysates were clarified by centrifugation at 8,000 x *g* for 10 min at 4 °C. The supernatants were collected and protein concentration was quantified using the Quick Start™ Bradford dye reagent. The protein concentration was assessed by measurement of the absorbance at a wavelength of 570 nm using Nanoquant Tecan Infinite m200 Pro in a 96-well plate. Samples of 25 µg of protein were precipitated with cold acetone and PBS. The samples were incubated for 1 h at -20 °C, centrifuged at 14,000 x *g* at 4 °C, and the protein pellets were air-dried for 30 min. Protein pellets were re-suspended with PBS and 4x Laemmli Sample Buffer supplemented with 2-mercaptoethanol. Samples were denatured for 10 min at 95 °C. To resolve the denatured proteins, samples and Precision Plus Protein™ standard marker were loaded into a 4-15 % gradient Mini-PROTEAN® TGX™ precast gel for the electrophoresis at 110 V for 80 min. Proteins were transferred into nitrocellulose membrane using Transfer-blot® Turbo™ Transfer Pack on Transfer-blot® Turbo™ Transfer System. Membranes were blocked with 5% (m/v) non-fat milk powder in PBS for 1 h at room temperature (RT).

Membranes were incubated with primary antibody dissolved in 5 % milk (m/v), overnight at 4 °C. The antibodies used are listed in Table 3, and were diluted accordingly: anti-Tgfbr3 (1:500, Cell Signaling Technology, 2519s), anti-β-actin (1:1000, Cell Signalling Technology, 4967), anti-Lbh (1:200, abcam, ab173737), anti-fibronectin (1:200, Sigma, F6140), anti-β-catenin (1:200, cell signalling technology, 9587S), anti-PDGFRα (1:1000, Cell Signalling Technology, 2992) and anti-PCNA (1:200, Santa Cruz Biotechnology, sc7907). Membranes were washed for 3 x PBS supplemented with Tween 20 (PBS-T) for 10 min. Membranes were transferred into 1 h-incubation with HRP-conjugated anti-rabbit IgG (1:3000) in 5 % milk in PBS (w/v). Membrane was rinsed 6 x with PBS and developed with SuperSignal® West Femto chemiluminescent substrate. Proteins were visualised using LAS-4000 luminescent image analyser.

6.2.9 Wound healing migration assay

Primary mouse lung fibroblasts were split into 6-well plates and transfected with RNAi or Scr control as described in section 6.2.3. After 24 h of transfection, cells were trypsinised, counted using a haemocytometer, and 13,000 cells were re-plated into each insert of an Ibidi 35 mm µ-Dish with a two-well insert. Cells were cultured in a humidified atmosphere containing 5 % CO_2 for 4 h, during this time fibroblasts attached to the chamber and formed a confluent monolayer. Media and the insert were removed, creating a wound. DMEM media supplemented with 10 % FCS (v/v), or DMEM media supplemented with 10 % FCS (v/v) and with 2 $ng.ml^{-1}$ of Tgf-β ligand were added to the µ-Dish. Photos of the wound were taken at 0 h, 9 h, 12 h, 20 h, and 24 h with Leica DMI3000B. The percentage of wound closure was quantified using ImageJ.

6.2.10 BrdU Cell Proliferation assay

Primary mouse lung fibroblasts were split into 6-well plates and transfected as described in section 6.2.3. After 24 h, cells were counted with a haemocytometer and re-plated into a 96-well plate, at a number of 6,000 cells per well. Cells were left for 22 h to incubate. Protocol of cell proliferation ELISA BrdU kit was employed for the assay. Briefly, BrdU was added to cell media for 2 h, bringing incubation time to 24 h. Cells were next fixed with FixDenat solution at RT for 30 min. Anti-BrdU antibody dilution solution was added for 90 min at RT, in the dark. Cells were washed 3 x with washing buffer. Substrate solution was added to the cells and the absorbance at 370 nm was measured with Nanoquant Tecan Infinite® m200 Pro.

6.2.11 MTT Assay

A549 cells were seeded in 6-well plates and transfected as described in 6.2.3. The MTT assay kit protocol was followed. Briefly, MTT labelling reagent was added to the cells and cells were incubated in a humidified atmosphere containing 5 % CO_2 for 4 h. Next, solubilisation reagent was added to the cells for overnight incubation in humidified atmosphere containing 5 % CO_2. Absorbance was measured at 550 nm.

6.2.12 Primary mouse lung Alveolar epithelial type II cell isolation

Primary mouse lung Alveolar epithelial type II (ATII) cell isolation was performed as described previously (Alejandre-Alcazar et al. 2007). The ATII cells were cultured in DMEM supplemented with 10 % FCS (v/v) with 100 $U.ml^{-1}$ penicillin and 100 $\mu g.ml^{-1}$ streptomycin on air/liquid interface in a humidified 5 % (v/v) CO_2 atmosphere for three days following isolation.

7 Results

7.1 Expression of members of the Tgf-β pathway in late lung development in the mouse.

The expression of components of the Tgf-β signalling pathway is dynamically regulated throughout late lung development in the mouse (Alejandre-Alcazar et al. 2008), suggesting the involvement of the Tgf-β pathway as a driver of lung morphogenesis. The expression of *Tgfbr3* in mouse lung homogenates was profiled during late lung development at P3, P5 and P7. The steady-state levels of *Tgfbr3* peaked significantly at P5 (Fig. 10), the time-point that coincides with the peak of secondary septation and at P7, the expression of *Tgfbr3* returned to the levels from P3 (Fig. 10).

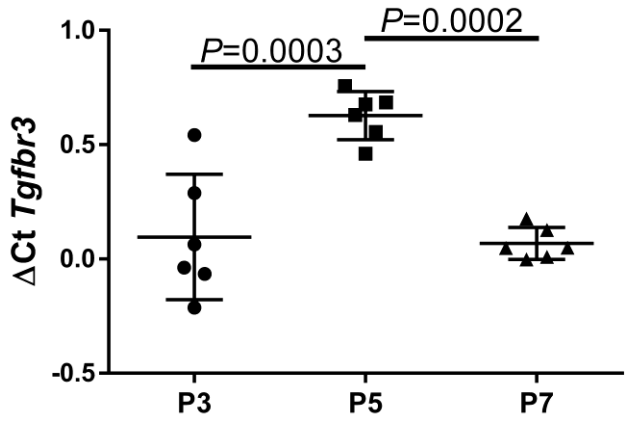

Figure 10| The expression of Tgfbr3 peaks at post-natal day 5 in late lung development.

The expression of Tgfbr3 in whole mouse lung homogenate peaked at post-natal day (P)5. Values represent mean ΔCt ± SD (n=6 mice per group). The ΔCt values were compared by one-way ANOVA with Tukey's *post hoc* test.

To determine the expression level of signalling and accessory receptors of the Tgf-β pathway in different lung cellular constituents, a FACS-based experiment was performed to separate lung mesenchymal (Fig. 11 *A*), Pecam$^+$ (Fig. 11 *B*), Epcam$^+$ (Fig. 11 C) and CD45$^+$ (Fig. 11 *D*) cell populations in mouse lung cell suspensions from lungs harvested at P7. Following gating for Pecam$^+$, Epcam$^+$ and CD45$^+$ populations, the remaining lung cells were regarded as a mesenchymal population,

and, indeed these cell populations revealed to express appreciable levels of the *Acta2* and *Myh11* genes, compared to other cell-type markers (Fig. 11 *A*).

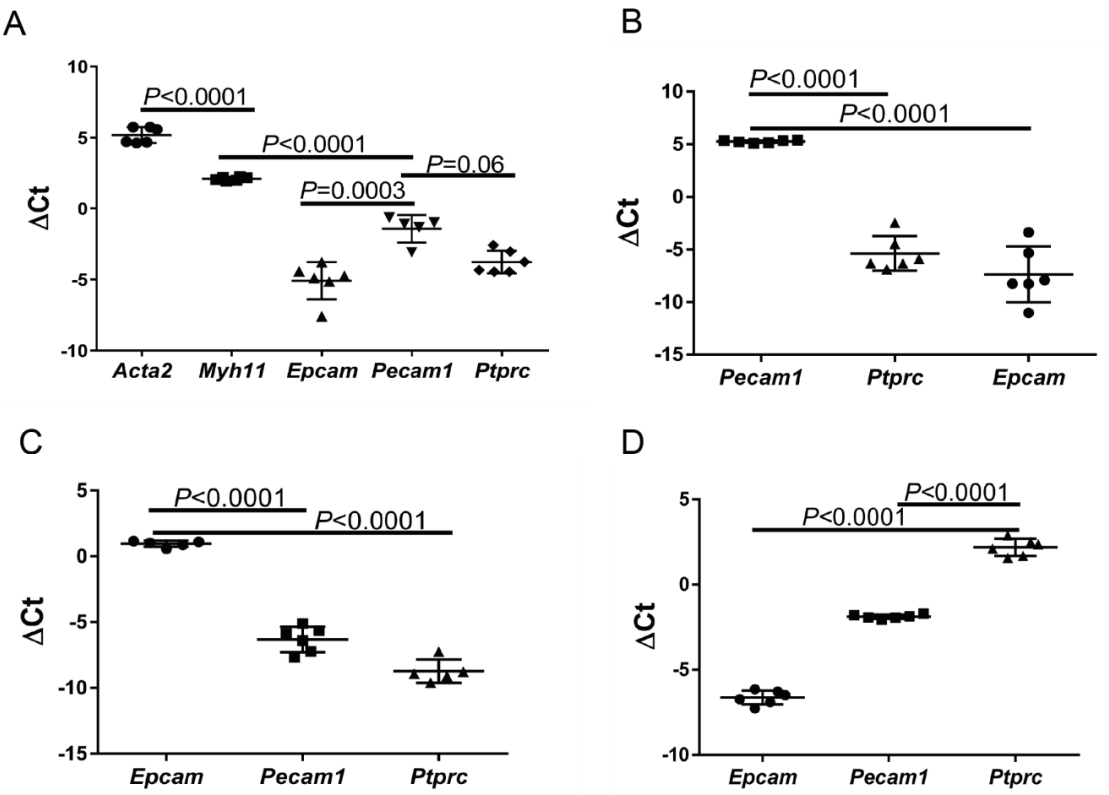

Figure 11 | Expression of cellular markers in fluorescence activated cell sorted cell populations from mouse pup lung suspension at post-natal day 7.

Fluorescence-activated cell sorting (FACS) was performed for (*A*) the mesenchymal population, (*B*) CD31$^+$ (Pecam$^+$) cells, (*C*) CD326$^+$ (Epcam$^+$) cells, and (*D*) CD45$^+$ (PTPRC$^+$) cells, assessed by qRT-PCR, values reflect mean ΔCt ± SD (n=6 mice per group), a one-way ANOVA with Tukey's *post hoc* test was performed to compare differences.

Following marker characterisation of sorted cell populations, the expression profile of Tgf-β pathway receptors was assessed by RT-qPCR. The expression of *Tgfbr1* did not differ significantly between different sorted lung cell-types at P7 (Fig. 12 *A*) whereas the expression of *Tgfbr2* was highest in CD31$^+$ cells (Pecam$^+$) (Fig. 12 *B*). *Tgfbr3* was found to be most highly expressed in the mesenchymal population (Fig. 12 *C*), followed by second highest expression in the endothelial, Pecam$^+$ population. *Acvrl1* and the *Eng* were the most highly expressed in CD31$^+$ cells, and the appreciable levels of expression were noted in the mesenchymal population (Fig. 12 *D* and *E*).

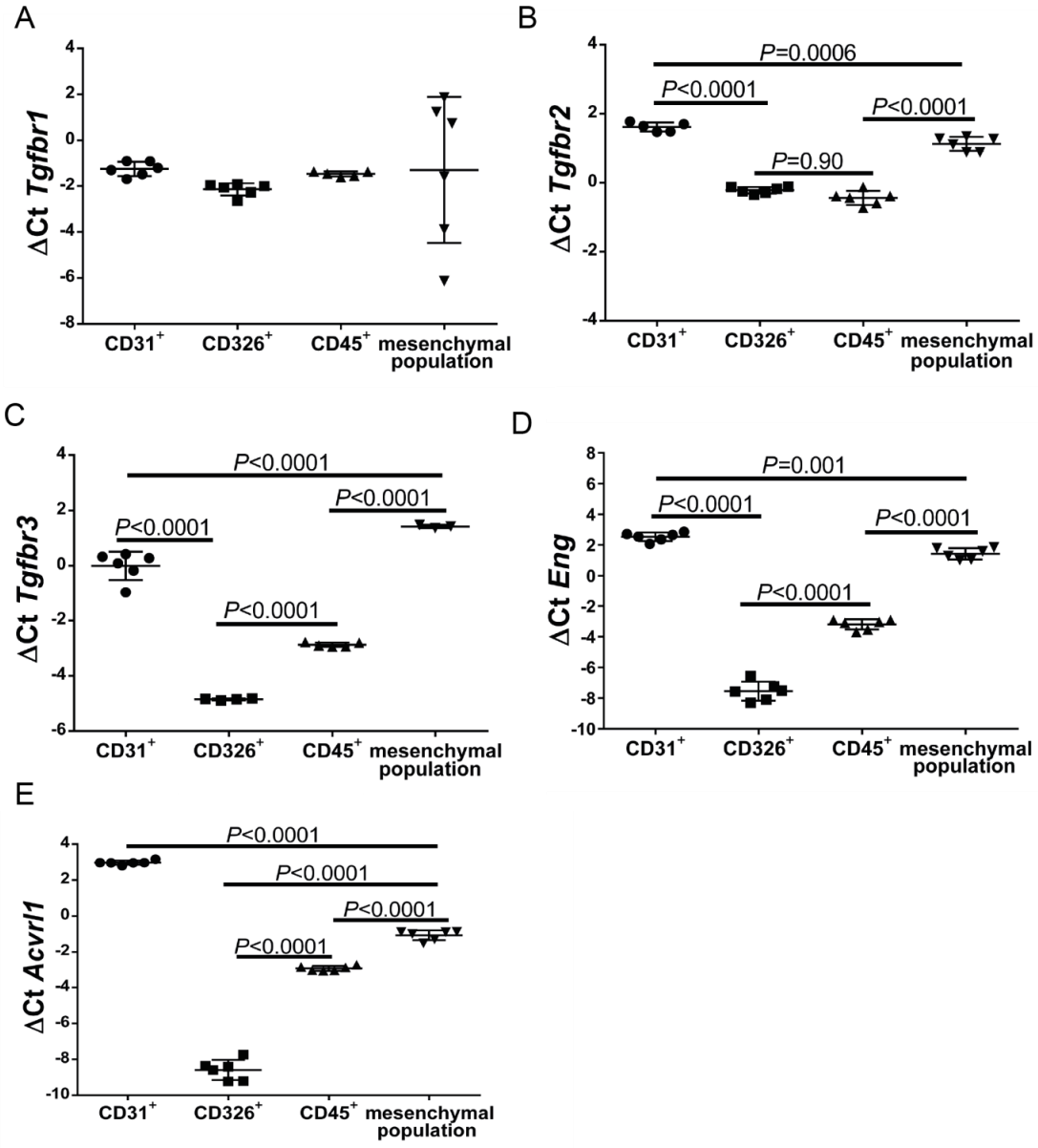

Figure 12| Expression profile of components of the Tgf-β pathway in different mouse lung cell-types.

The mRNA expression of components of the Tgf-β pathway in different mouse lung cell-types was assessed at post-natal day (P)7 for (*A*) *Tgfbr1*, (*B*) *Tgfbr2*, (*C*) *Tgfbr3*, and (*D*) *Eng*, (*E*) *Acvrl1* genes by qRT-PCR. Data reflect mean ΔCt ± SD (n=6 mice per group), comparisons between groups were performed by one-way ANOVA with Tukey's *post hoc* test.

7.2 Tgfbr3 regulates migration and proliferation of primary mouse lung fibroblasts.

Since Tgfbr3 was mostly expressed in the lung mesenchyme at P7, the role of Tgfbr3 was investigated in primary mouse lung fibroblasts, as this is the key cell-type of the lung mesenchymal compartment. The endogenous levels of Tgfbr3 protein were reduced with small interfering RNA (siRNA) in primary mouse lung fibroblasts. Following a 24 h incubation and successful Tgfbr3 knockdown, assessed by western blot (Fig. 13 *A*), healing of wound in the monolayers of primary lung fibroblasts was significantly increased, and this effect was independent of stimulation with Tgf-β1 ligand (Fig. 13 *D*). This reveals Tgfbr3 regulates migration of primary lung fibroblasts via the mechanisms of action that are independent of canonical Tgf-β-driven Smad signalling pathway. The effect of Tgfbr3 knockdown on primary lung fibroblast proliferation was assessed using a BrdU proliferation assay. The BrdU incorporation and proliferation of cells was significantly increased following the knockdown of Tgfbr3 in primary mouse lung fibroblasts (Fig. 14).

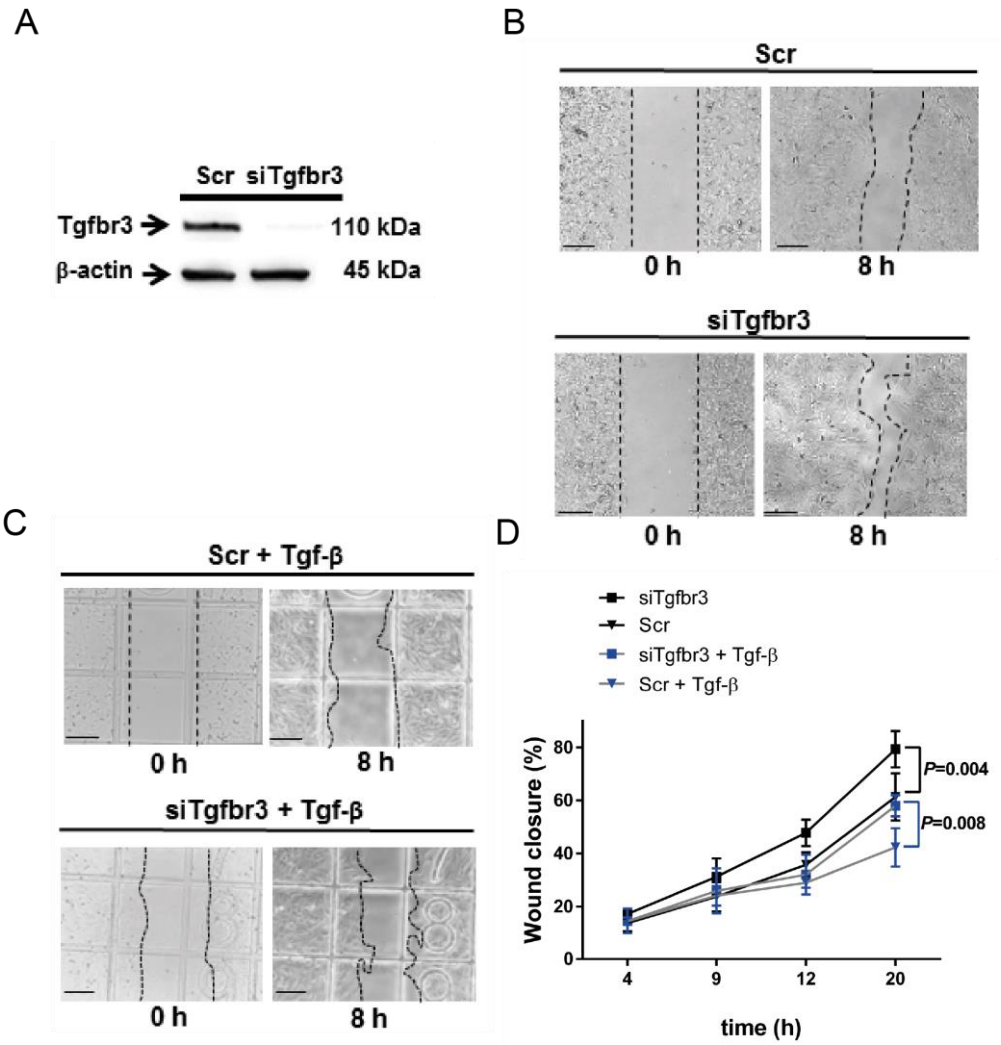

Figure 13| Increase in migration of primary mouse lung fibroblasts following knockdown of Tgfbr3.

(*A*) Western blot of proteins treated either with scrambled control (Scr) or siRNA to Tgfbr3 (siTgfbr3) revealed knockdown of Tgfbr3 expression. (*B*) Representative images of the wound created in primary mouse lung fibroblast monolayer that was treated either with Scr or siTgfbr3. (*C*) Representative images of wound created in primary mouse lung fibroblast monolayer treated either with Scr or siTgfbr3, both treatment groups were stimulated with 2 ng.ml^{-1} of Tgf-β. (*D*) Quantification of wound closure following knockdown of Tgfbr3 compared to Scr (black lines), following knockdown of Tgfbr3 with Tgf-β ligand 2 ng.ml^{-1} compared to Scr with Tgf-β ligand 2 ng.ml^{-1} (blue lines). Data reflect mean ± SD. Comparisons between groups were performed by one-way ANOVA with Tukey's *post hoc* test (n=4 chambers per group); scale bar represents 250 μm. Quantification of wound closure performed with the ImageJ tool.

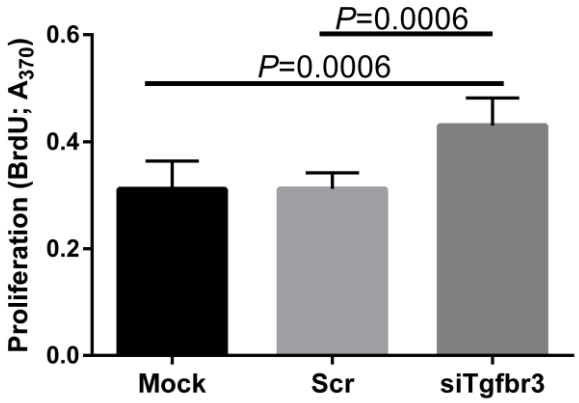

Figure 14 | Increase in proliferation of primary mouse lung fibroblasts following knockdown of Tgfbr3.

Primary mouse lung fibroblast increased incorporation of 5-bromo-2'-deoxyuridine (BrdU) following siRNA-mediated knockdown of Tgfbr3. Absorbance measured at 370 nm. Data reflect mean ± SD (n=8 wells per group). Comparisons between groups were performed by one-way ANOVA with Tukey's *post hoc* test.

7.3 Study of downstream signalling mechanisms of Tgfbr3

Since the effects of Tgfbr3 on primary mouse lung fibroblast properties were demonstrated to be independent of stimulation of Tgf-β ligand, to assess potential non-Tgf-β related downstream signalling mechanisms, a whole-genome microarray was performed previously in the laboratory where gene expression was assessed in human pulmonary artery smooth muscle cells (hPASMC) following 48 h siRNA-mediated knockdown of Tgfbr3. The microarray data have been deposited in the NCBI Gene Expression Omnibus and can be retrieved under accession number GSE92481. Extensive changes to transcriptome were noted (Table 5); including upregulation of expression of 868 genes, including Wnt, FGF, heparan sulfate and ECM members; and downregulation of expression of 768 genes, including signalling members within BMP, FGF, Wnt, heparan sulfate and ECM organisation pathways. Fig. 15 *A* presents the absolute fold change of example genes that were upregulated: limb bud and heart (*LBH*), integrin alpha-D (*ITGAD*) and metallothionein 1X (*MT1X*).

Table 5 | Changes in gene expression abundance following 48 h siRNA mediated knockdown of Tgfbr3 compared with Scr in human pulmonary artery smooth muscle cells, identified by whole genome microarray.

No	*P* (corr)	Difference (fold-change)	Gene Symbol	Full name
a) Most decreased in abundance mRNA transcripts				
1	0,0002	-2,65	*OSCP1*	Organic Solute Carrier Partner 1
2	0,0002	-3,37	*EI24*	Etoposide-induced protein 2.4
3	0,0006	-2,93	*CDK6*	Cyclin Dependent Kinase 6
4	0,0006	-2,80	*INSIG1*	Insulin Induced Gene 1
5	0,0006	-2,43	*MTMR9*	Myotubularin Related Protein 9
6	0,0007	-3,39	*ADAMTS9*	ADAM Metallopeptidase With Thrombospondin Type 1
7	0,0007	-3,20	*CYP2S1*	Cytochrome P450 Family 2 Subfamily S Member 1
8	0,0007	-2,79	*ABCA1*	ATP-Binding Cassette, Sub-Family A Member 1
9	0,0007	-2,19	*TDG*	Thymine-DNA glycosylase
10	0,0009	-2,04	*C5orf41*	CREB3 Regulatory Factor
11	0,0009	-3,51	*CSF3*	Colony Stimulating Factor 3
12	0,0009	-2,71	*TNFAIP2*	Tumor Necrosis Factor Alpha-Induced Protein 2
13	0,0009	-2,69	*NUPL1*	Nucleoporin p58/p45
14	0,0009	-2,04	*HMGA2*	High Mobility Group AT-Hook 2
15	0,0009	-3,09	*CXCL12*	C-X-C Motif Chemokine Ligand 12
16	0,001	-2,11	*KDR*	Kinase Insert Domain Receptor

No	*P* (corr)	Difference (fold-change)	Gene Symbol	Full name
b) Most increased in abundance mRNA transcripts				
1	0,0003	2,43	*ILF3*	Interleukin Enhancer Binding Factor 3
2	0,0004	3,48	*YWHAH*	14-3-3 Protein Eta
3	0,0004	2,40	*TMEM50B*	Transmembrane Protein 50B
4	0,0006	2,99	*EMP2*	Epithelial Membrane Protein 2
5	0,0006	2,24	*TACC2*	Transforming Acidic Coiled-Coil Containing Protein 2
6	0,0007	2,71	*SAR1B*	Secretion Associated Ras Related GTPase 1B
7	0,0007	2,64	*IL6ST*	Interleukin 6 Signal Transducer
8	0,0007	2,20	*AP1S3*	Adaptor Related Protein Complex 1 Subunit Sigma 3
9	0,0007	2,28	*IL10RB*	Interleukin 10 Receptor Subunit Beta
10	0,0007	2,10	*KLF2*	Kruppel Like Factor 2
11	0,0008	3,57	*DISC1*	Disrupted in schizophrenia 1
12	0,0008	3,24	*NUDT15*	Nudix hydrolase 15
13	0,0008	2,47	*ROD1*	Polypyrimidine tract-binding protein 3
14	0,0009	5,44	*DSP*	Desmoplakin
15	0,0009	3,16	*SEMA4F*	Semaphorin-4F
16	0,0009	2,86	*TLN1*	Talin-1

Abbreviations: no, numerical rank; *P* (corr), corrected *P*-value.

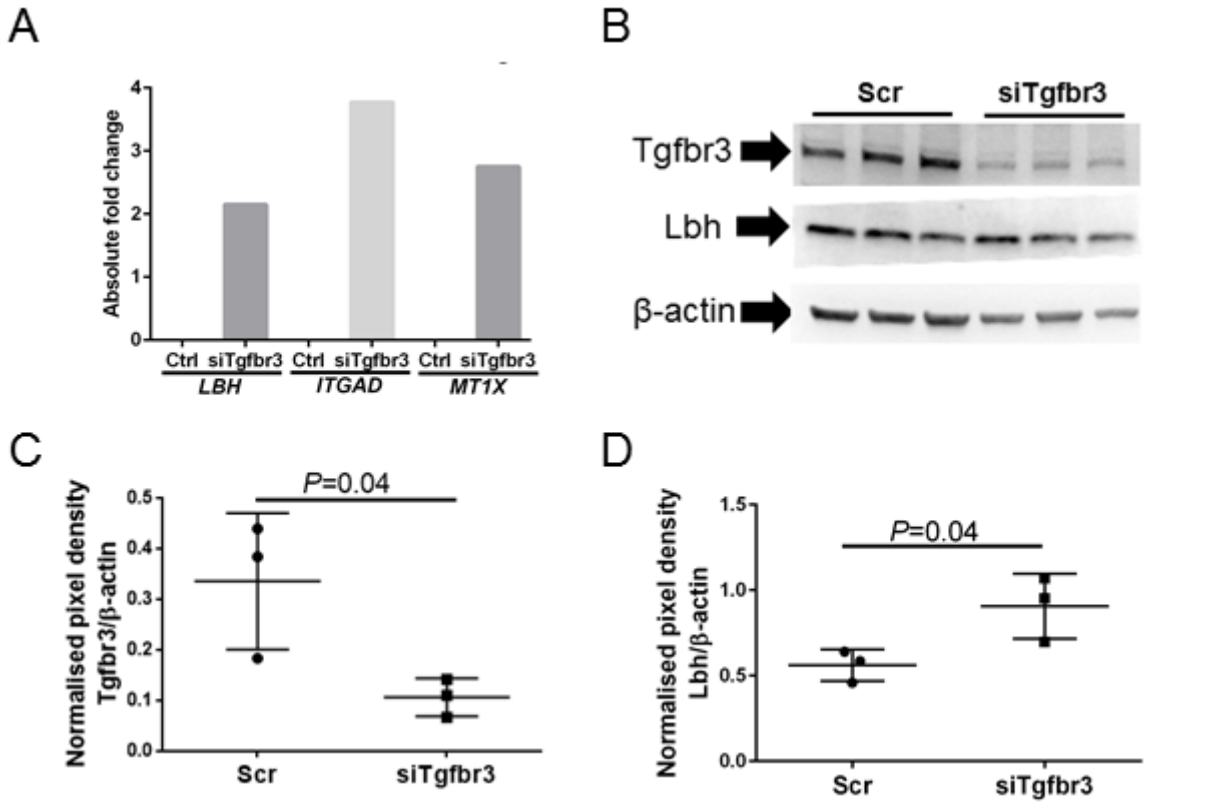

Figure 15 | Knockdown of Tgfbr3 *in vitro* results in an increase in the expression of Lbh.

(*A*) Example of genomic changes following 48-h knockdown of Tgfbr3 in human pulmonary artery smooth muscle cells (hPASMC). (*B*) Western blot reveals following siRNA-mediated knockdown of Tgfbr3 in primary mouse lung fibroblasts there is an increase in expression of Lbh. (*C, D*) Quantification of the original Tgfbr3 and Lbh immunoblot bands from *B* by densitometry normalised to the band of β-actin analysed for the same sample. Differences were assessed by unpaired Student's *t*-test; data reflect mean ± SD (n=3 wells per group).

Lbh is a co-transcription factor involved in the alveolarisation of mammary glands with a described role in basal stem cell maintenance, whereas the role of Lbh in lung development was not investigated. It was confirmed in primary mouse lung fibroblasts, that following siRNA-mediated knockdown of Tgfbr3, the expression of Lbh increases on the protein level (Fig. 15 *B-D*). To further assess the role of *Lbh* gene on the functions of primary mouse lung fibroblasts Lbh was knocked-down with siRNA, assessed by a western blot (Fig. 16 *A*). Healing of wound in fibroblast monolayers was significantly decreased following knockdown of Lbh (Fig. 16 *B* and *C*), and this effect was independent of stimulation with Tgf-β1 ligand (Fig. 16 *D* and

E). Assessment of proliferation of primary mouse lung fibroblasts revealed a significant decrease in proliferation after knockdown of Lbh (Fig. 17).

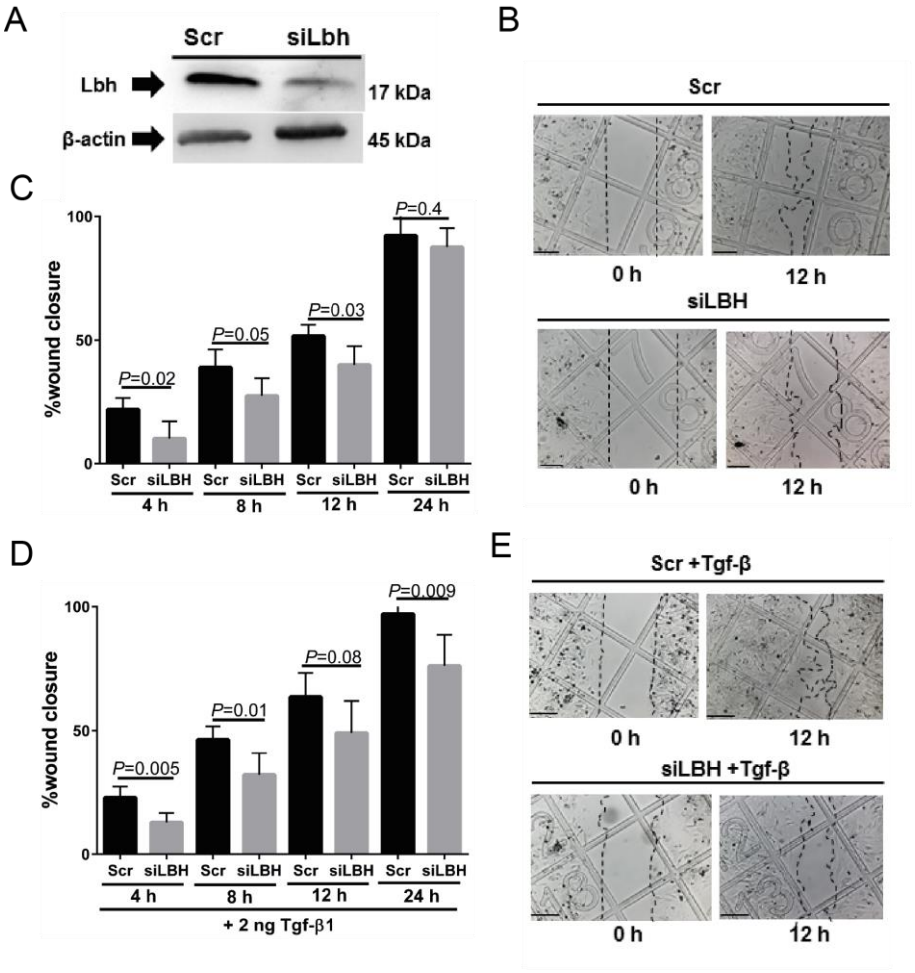

Figure 16 | Knockdown of Lbh attenuates primary mouse lung fibroblast migration in a wound healing assay.

(*A*) Western blot validating siRNA-mediated Lbh knockdown in primary mouse lung fibroblasts. (*B*) Representative images of the wound healing of primary mouse lung fibroblast monolayer following knockdown of Lbh compared to scrambled (Scr) Control. (*C*) Quantification of wound healing following siRNA-mediated knockdown of Lbh demonstrated a decrease in primary mouse lung fibroblast migration. (*D*) Quantification of a decrease in migration in wound healing following knockdown of Lbh and addition of 2 ng.ml^{-1} of Tgf-β1 ligand. (*E*) Representative images of the wound healing assay are quantified in *C*. Scale bar represents 250 µm; Comparisons between groups were performed by one-way ANOVA with Tukey's *post hoc* test. Data reflect mean ± SD (n=4 chambers per group). Quantification of wound closure performed with the ImageJ tool.

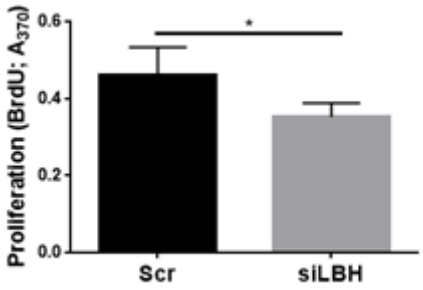

Figure 17 | Proliferation of primary mouse lung fibroblasts decreases following knockdown of Lbh.

Mouse primary lung fibroblasts demonstrated a decrease in 5-bromo-2'-deoxyuridine (BrdU) incorporation following treatment with siRNA to Lbh compared to scrambled (Scr) control. Differences were assessed by unpaired Student's *t*-test. Data reflect mean ± SD (n=8 wells per group).

7.4 Ablation of Tgfbr3 expression *in vivo* in cells with smooth muscle properties resulted in a decreased alveolarisation during late lung development.

To study the role of Tgfbr3 in post-natal lung development *in vivo*, a mouse strain with floxed exon 5 of *Tgfbr3* was employed. Application of tamoxifen to Tgfbr3$^{fl/fl}$ PDGFRα-CreER^{T2} mice and PDGFRα-CreER^{T2} mice at P1 and P2 resulted in the abrogation of Tgfbr3 expression assessed by a western blot from proteins from primary lung fibroblasts at P7 (Fig. 18 *B* and *C*), as well as by a decrease in *Tgfbr3* expression (Fig. 18 *F*). Gene expression analysis from FACS-sorted CD140a^{+} cells revealed a decrease in *Tgfbr3* expression (Fig. 18 *D*). The stereological analysis of plastic-embedded lung structure at P7 demonstrated a decrease in alveolarisation, reflected by 1.59 x 10^6 alveoli estimated in PDGFRα-CreER^{T2} mice compared to 1.18 x 10^6 alveoli in Tgfbr3$^{fl/fl}$ PDGFRα-CreER^{T2} mice (Fig. 19 *C*). Mean linear intercept (MLI) of distal airspaces was increased significantly from mean 47.25 ± 4.22 μm in PDGFRα-CreER^{T2} mice compared to 52.26 ± 2.04 μm in Tgfbr3$^{fl/fl}$ PDGFRα-CreER^{T2} mice. There was a significant decrease in the volume of septal walls in the lung, from 0.034 ± 0.01 cm^3 in PDGFRα-CreER^{T2} mice to 0.027 ± 0.00 cm^3 in Tgfbr3$^{fl/fl}$ PDGFRα-CreER^{T2} mice. There was no significant effect on the lung volume (Fig. 18 *A*), and septal thickness (Fig. 19 *D*). The Tgfbr3$^{fl/fl}$ PDGFRα-CreER^{T2} tamoxifen-treated mice display decreased thickness of all vessel walls (Fig. 19 *E*) and resistance vessels (Fig. 19 *F*). The expression of Lbh following the knockdown of *Tgfbr3* in Tgfbr3$^{fl/fl}$ PDGFRα-CreER^{T2} mouse tended towards downregulation by RT-qPCR from FACS-sorted cells at P7 (Fig. 18 *E*). Protein lysates from primary lung fibroblasts isolated from PDGFRα-CreER^{T2} and Tgfbr3$^{fl/fl}$ PDGFRα-CreER^{T2} mice at P7 revealed downregulation in Lbh expression in Tgfbr3$^{fl/fl}$ PDGFRα-CreER^{T2} lungs (Fig. 20 *A*).

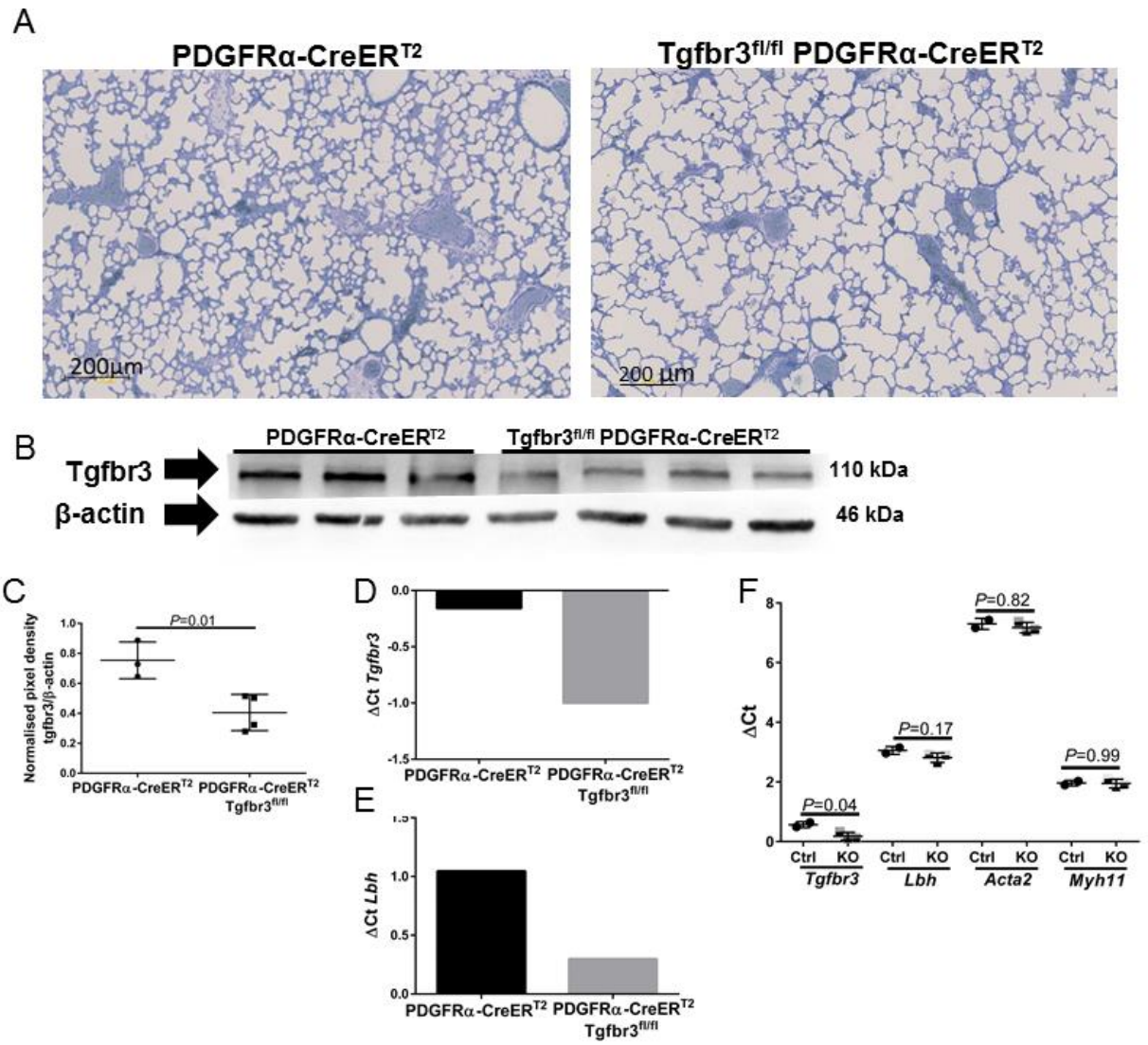

Figure 18| Ablation of Tgfbr3 in PDGFRα^{+} cells resulted in a decreased alveolarisation in mouse lungs.

(*A*) Representative images of plastic-embedded lungs from Tgfbr3$^{fl/fl}$ PDGFRα-CreER^{T2} and PDGFRα-CreER^{T2} tamoxifen-treated mice at P7. (*B*) Tgfbr3 expression in primary lung fibroblasts isolated from Tgfbr3$^{fl/fl}$ PDGFRα-CreER^{T2} and PDGFRα-CreER^{T2} tamoxifen-treated mice at P7. (*C*) Quantification by densitometry of western blots from *B*. Differences were assessed by unpaired Student's *t*-test. (*D*) RT-qPCR revealed a decrease in *Tgfbr3* expression PDGFRα^{+} fluorescence-activated cell sorted (FACS) cells from Tgfbr3$^{fl/fl}$ PDGFRα-CreER^{T2} tamoxifen-treated lungs (each bar represent pool of 4 lungs). (*E*) RT-qPCR revealed a decrease in *Lbh* expression in PDGFRα^{+} FACS-sorted cells from Tgfbr3$^{fl/fl}$ PDGFRα-CreER^{T2} tamoxifen-treated lungs (each bar represent pool of 4 lungs). (*F*) Gene expression in primary tamoxifen-treated mouse lung fibroblasts from Tgfbr3$^{fl/fl}$ PDGFRα-CreER^{T2} (KO) and PDGFRα-CreER^{T2} (Ctrl) mice at P7. Differences were assessed by unpaired Student's *t*-test. Data reflect mean ± SD (n=3 mice per group).

Gene assessment in primary lung fibroblasts isolated from Tgfbr3$^{fl/fl}$ PDGFRα-CreER^{T2} and PDGFRα-CreER^{T2} tamoxifen-treated mice at P7 revealed that expression of *Lbh* has a tendency to be downregulated but it is not significant (Fig. 18 *F*). The fibroblasts express appreciable levels of the *Acta2* and *Myh11* (Fig. 18 *F*), indicating myofibroblasts characteristics. The primary lung fibroblasts demonstrated increased expression of proliferating cell nuclear antigen (PCNA), fibronectin and β-catenin (Fig. 20 *B*). In *in vitro* set-up, siRNA-mediated knockdown of Tgfbr3 in primary mouse lung fibroblasts was demonstrated by western blot (Fig. 20 *C*), and increase in the expression of cellular fibronectin protein was noted (Fig. 20 *C*).

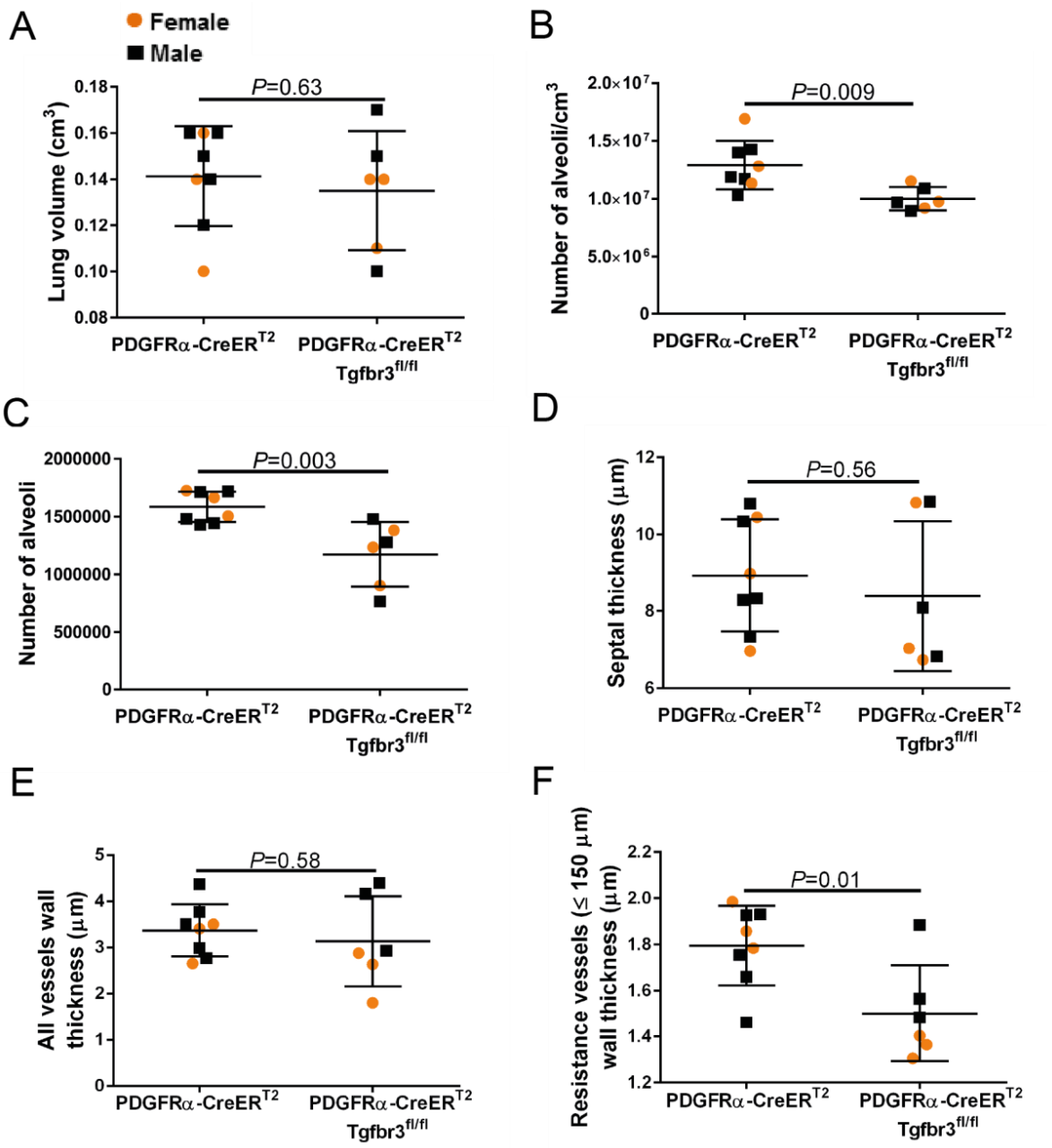

Figure 19| Stereological analysis of lungs from the tamoxifen-treated Tgfbr3$^{fl/fl}$ PDGFRα-CreER^{T2} and PDGFRα-CreER^{T2} mice.

Quantification of changes to the lung structure from Tgfbr3$^{fl/fl}$ PDGFRα-CreER^{T2} and PDGFRα-CreER^{T2} tamoxifen-treated mice for (*A*) lung volume, (*B*) alveoli density, (*C*) number of alveoli, (*D*) septal thickness, (*E*) wall thickness of all lung vessels, and (*F*) thickness of resistance vessel walls (diameter ≤ 150 µm). Differences were assessed by unpaired Student's *t*-test. Data reflect mean ± SD (n=6-8 lungs per group). The full list of stereological parameters assessed is provided in Table 6.

Table 6 | Structural parameters of lungs from Tgfbr3$^{fl/fl}$ PDGFRα-CreER^{T2} and PDGFRα-CreER^{T2} tamoxifen-treated mice.

Parameter			PDGFRα-CreER^{T2}			Tgfbr3$^{fl/fl}$ PDGFRα-CreER^{T2}		
			Mean ± SD			Mean ± SD		
***Vv* (par/lung) (%)**			84.69 ± 4.19			85.83 ± 4.22 (***P* = 0.62**)		
CE	CV	CE²/CV²	0.02	0.05	0.13	0.02	0.05	0.17
***Vv* (nonpar/lung) (%)**			15.31 ± 4.19			14.17 ± 4.22 (***P* = 0.08**)		
CE	CV	CE²/CV²	0.10	0.27	0.13	0.12	0.30	0.17
***Sv* (alv epi/par) (cm^{-}**			615.9 ± 33.98			581.0 ± 33.73 (***P* = 0.07**)		
CE	CV	CE²/CV²	0.01	0.05	0.13	0.02	0.05	0.17
***S* (alv epi, lung) (cm²)**			74.03 ± 9.26			63.46 ± 14.25 (***P* = 0.12**)		
CE	CV	CE²/CV²	0.04	0.13	0.13	0.09	0.22	0.17
***Vv* (alv air/ par) (%)**			72.52 ± 4.59			75.85 ± 4.33 (***P* = 0.21**)		
CE	CV	CE²/CV²	0.02	0.06	0.12	0.02	0.06	0.17
***V* (alv air, lung) (cm³)**			0.09 ± 0.02			0.09 ± 0.02 (***P* = 0.81**)		
CE	CV	CE²/CV²	0.07	0.20	0.12	0.09	0.21	0.17
***Vv* (sep/ par) (%)**			27.44 ± 4.60			24.15 ± 4.33 (***P* = 0.19**)		
CE	CV	CE²/CV²	0.06	0.17	0.13	0.07	0.18	0.17
***V* (sep, lung) (cm³)**			0.034 ± 0.01			0.027 ± 0.00 (***P* = 0.03**)		
CE	CV	CE²/CV²	0.06	0.17	0.12	0.05	0.12	0.17
MLI (μm)			47.25 ± 4.22			52.26 ± 2.04 (***P* = 0.02**)		
CE	CV	CE²/CV²	0.03	0.09	0.12	0.02	0.04	0.17

Values are presented as mean ± SD and *P*-values (n=6-8 lungs per group). Differences were assessed by unpaired Student's *t*-test. Abbreviations: alv air, alveolar air spaces; alv epi, alveolar epithelium; CE, coefficient of error; CV, coefficient of variation; MLI, mean linear intercept; non-par, non-parenchyma; par, parenchyma; sep, septum; s.d., standard deviation; S, surface area; SV, surface density; V, volume; V_V, volume density.

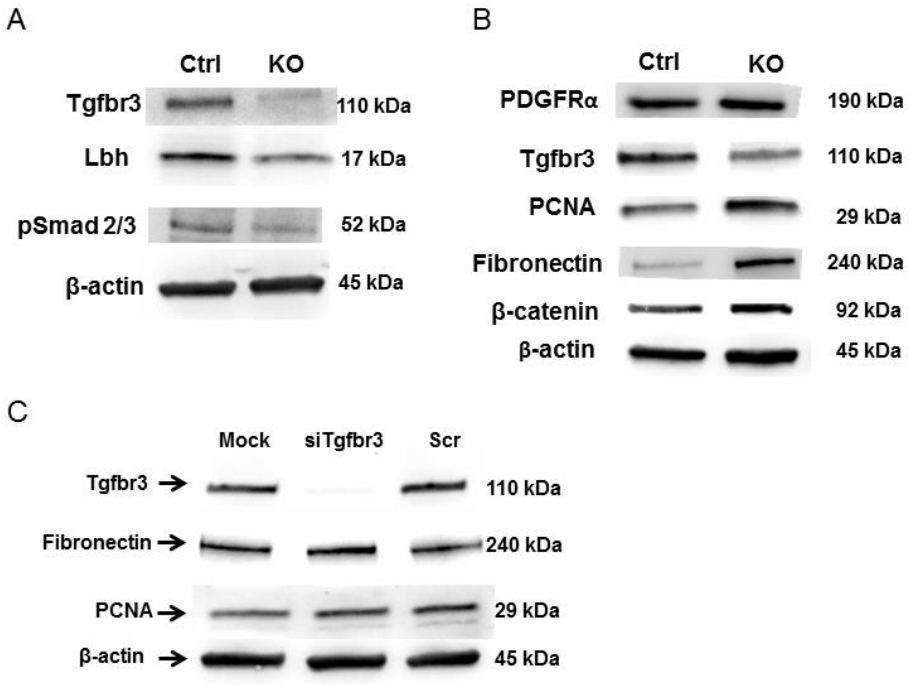

Figure 20| Protein expression following knockdown of Tgfbr3 *in vivo* and *in vitro* in primary mouse lung fibroblasts.

(*A*) Western blot for Tgfbr3, Lbh and pSmad2/3 from protein lysates from primary lung fibroblasts from PDGFRα-CreER^{T2} and Tgfbr3$^{fl/fl}$ PDGFRα-CreER^{T2} tamoxifen-treated mice at P7. (*B*) Western blot for PDGFRα, Tgfbr3, PCNA, fibronectin, β-catenin proteins from primary lung fibroblasts from PDGFRα-CreER^{T2} and Tgfbr3$^{fl/fl}$ PDGFRα-CreER^{T2} tamoxifen treated mice at P7. (*C*) Western blot following siRNA-mediated knockdown of Tgfbr3 in cultured primary mouse lung fibroblasts revealed changed to fibronectin expression.

Deletion of Tgfbr3 in SMMHC^{+} cells in the developing lung was tested by application of tamoxifen at P1 and P2 and stereological assessment of structure of the lungs at P7. The downregulation of Tgfbr3 was demonstrated by western blot from protein lysates extracted from primary PASMC isolated from tamoxifen-treated Tgfbr3$^{fl/fl}$ SMMHC-CreER^{T2} and SMMHC-CreER^{T2} mice (Fig. 21 *A*). Stereological analysis at P7 demonstrated a significant decrease in lung alveolarisation in Tgfbr3$^{fl/fl}$ SMMHC-CreER^{T2} mouse pups reflected by a decrease in alveoli number from 1.13 x 10^6 alveoli in SMMHC-CreER^{T2} pups compared to 0.8 x 10^6 alveoli in Tgfbr3$^{fl/fl}$ SMMHC-CreER^{T2} pups (Fig. 21 *E*). Tgfbr3$^{fl/fl}$ SMMHC-CreER^{T2} mice had an increased MLI of 52.26 μm compared to 47.25 μm in SMMHC-CreER^{T2} mice. Lung volume (Fig. 21 *C*), septal thickness (Fig. 21 *F*), and the thickness of the walls of the

vessels (Fig. 21 *G* and *H*) were not affected by the knockdown of Tgfbr3 from SMMHC^{+} cell-type.

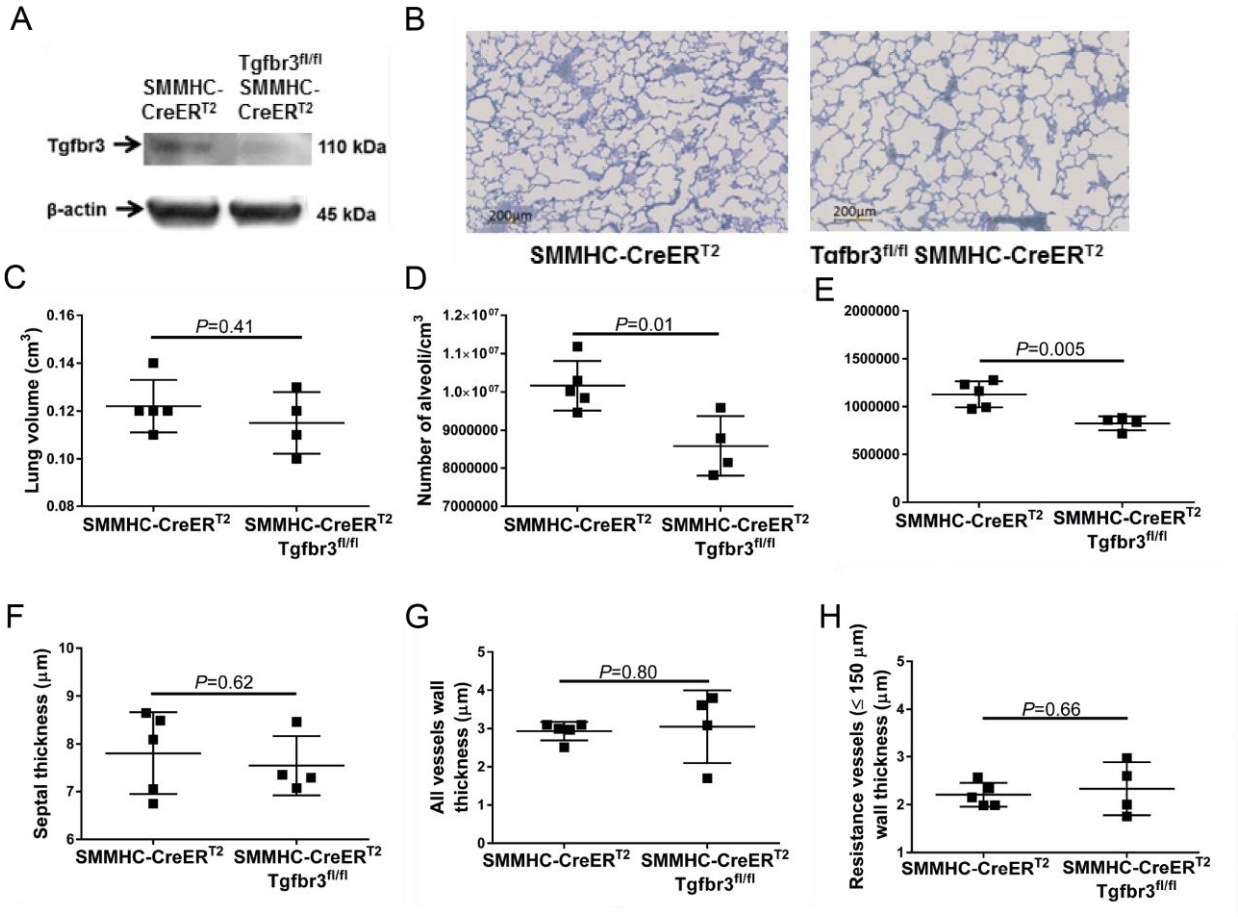

Figure 21| Ablation of Tgfbr3 in SMMHC^{+} cells resulted in a decreased alveolarisation.

(*A*) Changes in Tgfbr3 expression in pulmonary artery smooth muscle cells (PASMC) isolated from Tgfbr3$^{fl/fl}$ SMMHC-CreER^{T2} and SMMHC-CreER^{T2} tamoxifen-treated mice at post-natal day 7 (P7). (*B*) Representative images of plastic-embedded lungs morphometry in Tgfbr3$^{fl/fl}$ SMMHC-CreER^{T2} and SMMHC-CreER^{T2} mice. (*C*) Lungs volumes in Tgfbr3$^{fl/fl}$ SMMHC-CreER^{T2} and SMMHC-CreER^{T2} mice. *(D)* Tgfbr3$^{fl/fl}$ SMMHC-CreER^{T2} lungs display a decrease in alveoli density, and *(E)* number of alveoli. (*F*) Tgfbr3$^{fl/fl}$ SMMHC-CreER^{T2} lungs demonstrate no changes in mean septal thickness. (*G*) Stereological assessment of vessel wall thickness revealed no changes in all vessels and (*H*) resistance vessels (diameter ≤150 μm). Differences were assessed by unpaired Student's *t*-test. Data reflect mean ± SD (n=4-5 lungs per group). The full list of stereological parameters assessed is provided in Table 7.

Table 7 | Structural parameters of lungs from Tgfbr3$^{fl/fl}$ SMMHC-CreER^{T2} and SMMHC-CreER^{T2} tamoxifen-treated mice.

Parameter			SMMHC-CreER^{T2}			Tgfbr3$^{fl/fl}$ SMMHC-CreER^{T2}		
			Mean ± SD			Mean ± SD		
***Vv* (par/lung) (%)**			84.68 ± 4.19			85.83 ± 4.22 (***P* = 0.62**)		
CE	CV	CE²/CV	0.02	0.04	0.13	0.02	0.05	0.17
***Vv* (nonpar/lung) (%)**			15.31 ± 4.19			14.17 ± 4.22 (***P* = 0.62**)		
CE	CV	CE²/CV	0.02	0.05	0.17	0.12	0.29	0.17
***Sv* (alv epi/par) (cm^{-1})**			615.90 ± 32.09			580.90 ± 33.73 (***P* = 0.07**)		
CE	CV	CE²/CV	0.02	0.05	0.13	0.02	0.05	0.17
***S* (alv epi, lung) (cm²)**			74.03 ± 9.26			63.46 ± 14.25 (***P* = 0.12**)		
CE	CV	CE²/CV	0.04	0.13	0.12	0.09	0.22	0.17
***Vv* (alv air/ par) (%)**			72.52 ± 4.59			75.85 ± 4.33 (***P* = 0.19**)		
CE	CV	CE²/CV	0.02	0.06	0.12	0.05	0.05	0.17
***V* (alv air, lung) (cm³)**			0.09 ± 0.02			0.08 ± 0.02 (***P* = 0.81**)		
CE	CV	CE²/CV	0.07	0.20	0.12	0.09	0.21	0.17
***Vv* (sep/ par (%)**			27.44 ± 4.60			24.15 ± 4.33 (***P* = 0.20**)		
CE	CV	CE²/CV	0.06	0.17	0.13	0.07	0.18	0.17
***V* (sep, lung) (cm³)**			0.03 ± 0.01			0.027 ± 0.00 (***P* = 0.03**)		
CE	CV	CE²/CV	0.12	0.25	0.20	0.05	0.12	0.17
MLI (μm)			47.25 ± 4.22			52.26 ± 2.05 (***P* = 0.02**)		
CE	CV	CE²/CV	0.03	0.09	0.12	0.02	0.04	0.17

Values are presented as mean ± SD and *P*-values (n=4-5 lungs per group). Differences were assessed by unpaired Student's *t*-test. Abbreviations: alv air, alveolar air spaces; alv epi, alveolar epithelium; CE, coefficient of error; CV, coefficient of variation; MLI, mean linear intercept; non-par, non-parenchyma; par, parenchyma; sep, septum; s.d., standard deviation; S, surface area; SV, surface density; V, volume; V_V, volume density.

7.5 Ablation of Tgfbr3 *in vivo* from Tie2^{+} cells resulted in a decreased septal thickness during late lung development.

To investigate the role of Tgfbr3 in endothelial cells during late lung development, Tgfbr3$^{fl/fl}$ Tie2-CreER^{T2} and Tie2-CreER^{T2} mice were employed. To delete Tgfbr3 from Tie2^{+} cells throughout post-natal late lung development, tamoxifen was applied at P1 and P2 and *Tgfbr3* gene knockdown was confirmed with RT-qPCR from FACS-sorted Tie^{+} cells isolated from tamoxifen-treated Tgfbr3$^{fl/fl}$ Tie2-CreER^{T2} and Tie2-CreER^{T2} mice at P7 (Fig. 22 *A*). The stereological analysis revealed no changes to lungs volume, alveoli density or alveoli number (Fig. 22 *C-E*). The altered phenotype of Tgfbr3$^{fl/fl}$ Tie2-CreER^{T2} mice include significantly decreased septal thickness (Fig. 22 *F*), from 11.28 ± 1.5 μm in Tie2-CreER^{T2} pups vs 9.00 ± 1μm in Tgfbr3$^{fl/fl}$ Tie2-CreER^{T2} pups. Also a reduction in all vessel wall thickness (Fig. 22 *G*) and resistance vessel wall thickness (Fig. 22 *H*) were noted. Analysis by flow cytometry revealed a significant decrease in abundance of Tie2^{+} cells in the Tgfbr3$^{fl/fl}$ Tie2-CreER^{T2} lungs compared to Tie2-CreER^{T2} lungs (Fig. 23 *A* and *B*). Recently published RNA-seq study by Delaughter et al. from epicardial cells isolated from global Tgfbr3 KO embryos at E11.5 revealed genomic pathway changes that converged on the transcription factor NFκB (DeLaughter et al. 2016). In Tgfbr3$^{fl/fl}$ Tie2-CreER^{T2} tamoxifen-treated mice at P7 the significant downregulation of *Nfkb1* expression was also noted (Fig. 24 *E*). Components of Tgf-β pathway such as *Smad2* and *Smad9* (Fig. 24 *B-C*) were not affected in tamoxifen-treated Tgfbr3$^{fl/fl}$ Tie2-CreER^{T2} pups in contrast to the study by DeLaughter et al., suggesting the observed phenotype in the post-natal lung development is independent of the Smad signalling.

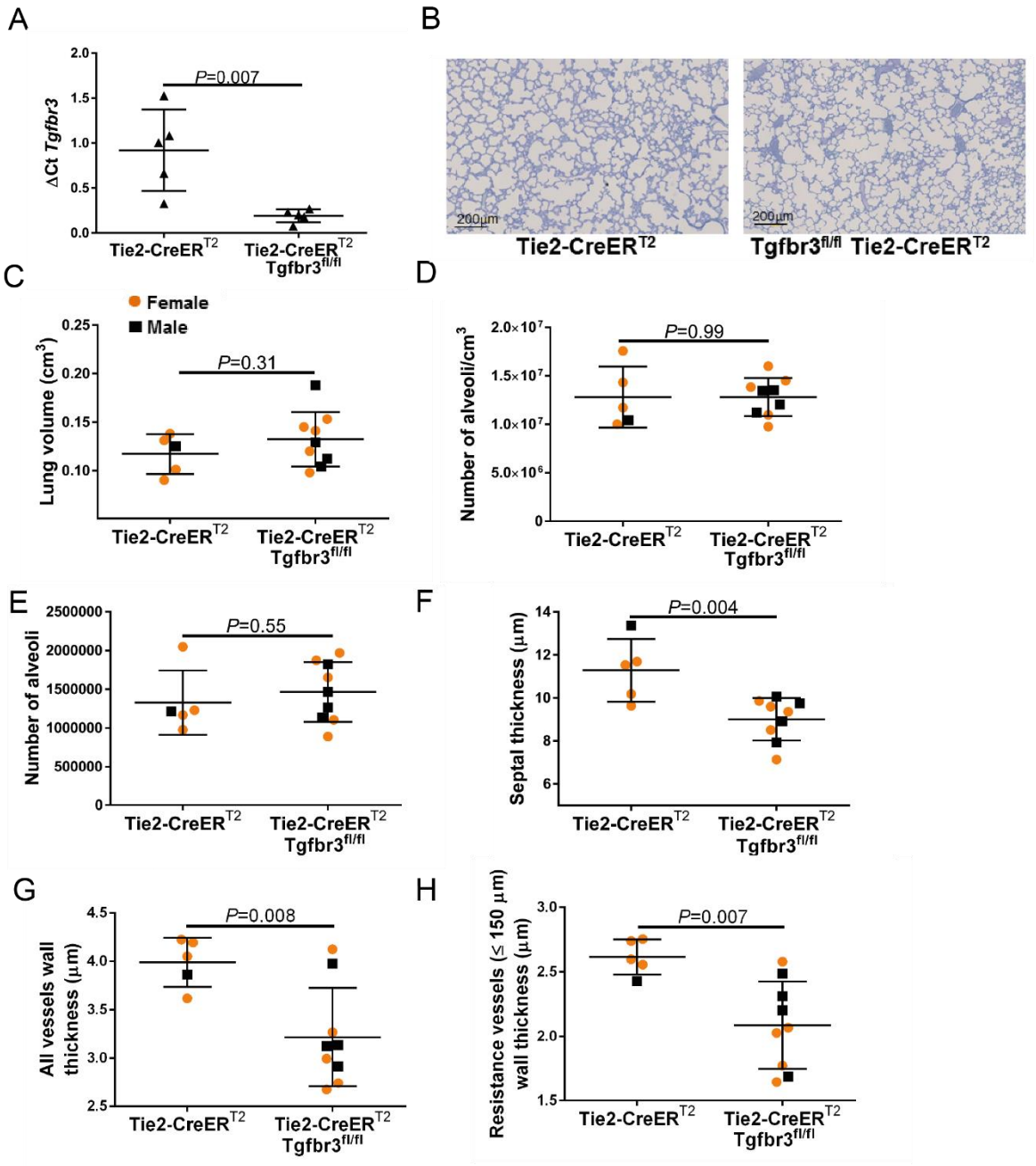

Figure 22 | Ablation of Tgfbr3 in Tie2$^+$ cells resulted in a decreased septal thickness.

(*A*) RT-qPCR results from FACS-sorted Tie2$^+$ cells from Tie2-CreER^{T2} and Tgfbr3$^{fl/fl}$ Tie2CreER^{T2} tamoxifen-treated lungs revealed downregulation of *Tgfbr3* (*B*) Representative images of lungs from plastic-embedded Tgfbr3$^{fl/fl}$ Tie2-CreER^{T2} and Tie2-CreER^{T2} mouse pups. (*C*) Estimation of lung volume. (*D*) Stereological assessment of mouse lung alveoli density, (*E*) number of alveoli, (*F*) and septal thickness. (*G*) Stereological assessment of vessel wall thickness reveal changes to wall thickness of all vessels, (*H*) and resistance vessels (diameter ≤ 150 µm) wall thickness. Differences were assessed by unpaired Student's *t*-test. Data reflect mean ± SD (n=5-9 lungs per group). The full list of stereological parameters assessed is provided in Table 8.

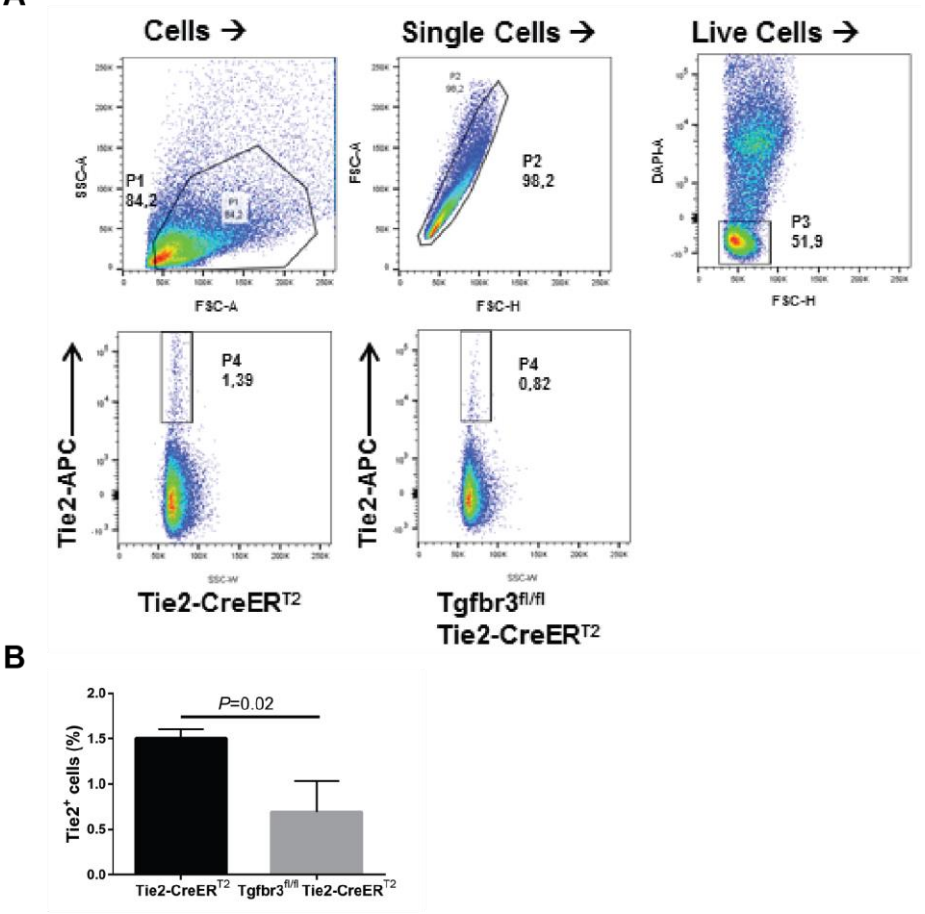

Figure 23 | Lungs from tamoxifen-treated Tgfbr3$^{fl/fl}$ Tie2-CreER^{T2} mice demonstrate a decreased abundance in Tie2^{+} cell-type population.

(*A*) Scatter plots demonstrate gating settings employed for the analysis of Tie2-CreER^{T2} and Tgfbr3$^{fl/fl}$ Tie2-CreER^{T2} lungs. (*B*) Quantification of Tie2^{+} cell-types in Tie2-CreER^{T2} and Tgfbr3$^{fl/fl}$ Tie2-CreER^{T2} whole lungs cell suspension. Differences were assessed by unpaired Student's *t*-test. Data reflect mean ± SD (n=3 lungs per group).

Table 8 | Structural parameters from stereological analysis of lungs from Tgfbr3$^{fl/fl}$ Tie2-CreER^{T2} and Tie2-CreER^{T2} tamoxifen-treated mice.

Parameter			Tie2-CreER^{T2}			Tgfbr3$^{fl/fl}$ Tie2-CreER^{T2}		
			Mean ± SD			Mean ± SD		
***Vv* (par/lung) (%)**			88.17 ± 3.87			86.28 ± 4.23 (***P* = 0.43**)		
CE	CV	CE²/CV²	0.02	0.25	0.00	0.02	0.25	0.00
***Vv* (nonpar/lung) (%)**			11.83 ± 3.87			13.72 ± 4.124 (***P* = 0.43**)		
CE	CV	CE²/CV²	0.15	0.25	0.34	0.10	0.25	0.17
***Sv* (alv epi/par) (cm^{-1})**			629.80 ± 97.32			724.10 ± 68.92 (***P* = 0.05**)		
CE	CV	CE²/CV²	0.07	0.25	0.08	0.03	0.25	0.06
***S* (alv epi, lung) (cm²)**			65.79 ± 17.96			81.83 ± 14.75 (***P* = 0.10**)		
CE	CV	CE²/CV²	0.12	0.25	0.23	0.06	0.25	0.06
***Vv* (alv air/ par) (%)**			64.93 ± 3.59			67.20 ± 5.93 (***P* = 0.45**)		
CE	CV	CE²/CV²	0.02	0.25	0.01	0.03	0.35	0.01
***V* (alv air, lung) (cm³)**			0.07 ± 0.01			0.08 ± 0.02 (***P* = 0.37**)		
CE	CV	CE²/CV²	0.08	0.25	0.11	0.09	0.25	0.13
***Vv* (sep/ par) (%)**			35.07 ± 3.50			32.80 ± 5.93 (***P* = 0.45**)		
CE	CV	CE²/CV²	0.05	0.13	0.11	0.06	0.13	0.21
***V* (sep, lung) (cm³)**			0.037 ± 0.01			0.037 ± 0.01 (***P* = 0.99**)		
CE	CV	CE²/CV²	0.10	0.13	0.60	0.06	0.13	0.24
MLI (µm)			42.33 ± 9.06			37.69 ± 6.88 (***P* = 0.30**)		
CE	CV	CE²/CV²	0.10	0.13	0.52	0.06	0.13	0.21

Values are presented as mean ± SD and *P*-values (n=5-9 lungs per group). Differences were assessed by unpaired Student's *t*-test. Abbreviations: alv air, alveolar air spaces; alv epi, alveolar epithelium; CE, coefficient of error; CV, coefficient of variation; MLI, mean linear intercept; non-par, non-parenchyma; par, parenchyma; sep, septum; s.d., standard deviation; S, surface area; S_V, surface density; V, volume; V_V, volume density.

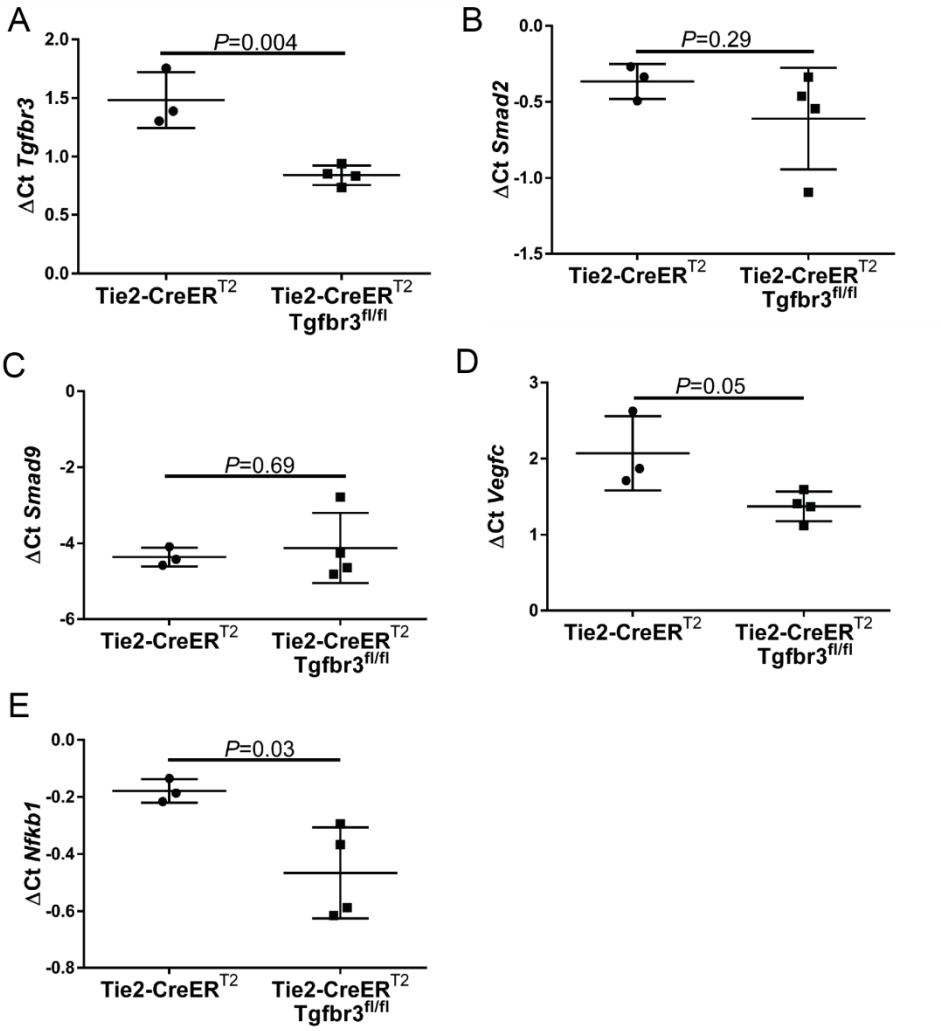

Figure 24| Changes in gene expression in Tie2^{+} cells from tamoxifen-treated Tgfbr3$^{fl/fl}$ Tie2-CreER^{T2} and Tie2-CreER^{T2} mouse lungs.

Gene expression changes were assessed for (*A*) *Tgfbr3*, (*B*) *Smad2*, (*C*) *Smad9*, (*D*) *Vegfc*, and (*E*) *Nfkb1* by RT-qPCR in fluorescence activated cells sorted (FACS) Tie2^{+} cells from Tie2-CreER^{T2} and Tgfbr3$^{fl/fl}$ Tie2-CreER^{T2} lungs. Differences were compared by unpaired Student's *t*-test. Data reflect mean ΔCt ± SD (n=3-4 lungs per group).

7.6 Global knockout of Lbh results in an increased septal thickness.

The expression of Lbh increased following 48 h siRNA-mediated knockdown of Tgfbr3 in microarray in hPASMC (Fig. 15 *A*), and also the expression of Lbh protein was increased following 48 h siRNA-mediated knockdown of Tgfbr3 in primary mouse lung fibroblasts (Fig. 15 *B*). To investigate the effect of Lbh in late lung development, stereological analysis was performed on the global Lbh KO mouse lungs at P7. Whole lung homogenates from mice homozygous for Lbh KO allele revealed complete abrogation of Lbh protein expression (Fig 25 *B*). The volume of Lbh KO lungs was significantly decreased, from 0.18 ± 0.04 cm^3 in Wt mice vs 0.15 ± 0.02 cm^3 in Lbh KO mice (Fig. 25 *C*). Septal thickness was significantly increased from 8.34 ± 1.34 μm in Wt mice vs 10.44 ± 1.59 μm in Lbh KO mice (Fig. 25 *D*). There were no significant changes to the alveoli density (Fig. 25 *E*) and the alveoli number was decreased in Lbh KO lungs, i.e. 1.32 x 10^6 ± 0.20 alveoli in Lbh KO vs 1.77 x 10^6 alveoli in Wt mice (Fig. 25 *F*). Epithelial surface area of the lungs, as well as alveolar airspaces volumes were both significantly decreased in Lbh KO mice (Table 9). The expression of Lbh was assessed in hyperoxia model of developmental disease, BPD, which characterises with thickened septa. It was revealed that the expression of Lbh in primary ATII cells from mouse pups was downregulated (Fig. 26 *G*). To further analyse the role of Lbh in epithelium, Lbh was knockdown using siRNA in A549 cell line. Following knockdown it was revealed that proliferation of A549 cells was increased assessed by BrdU incorporation (Fig. 26 *B*), and by MTT incorporation (Fig. 26 *C*). There were no changes to the viability of A549 cells, reflected by unaltered number of cells negative for trypan blue staining (Fig. 26 *D*). The wound closure created in A549 monolayers was increased following the reduction in Lbh expression (Fig. 26 *E* and *F*).

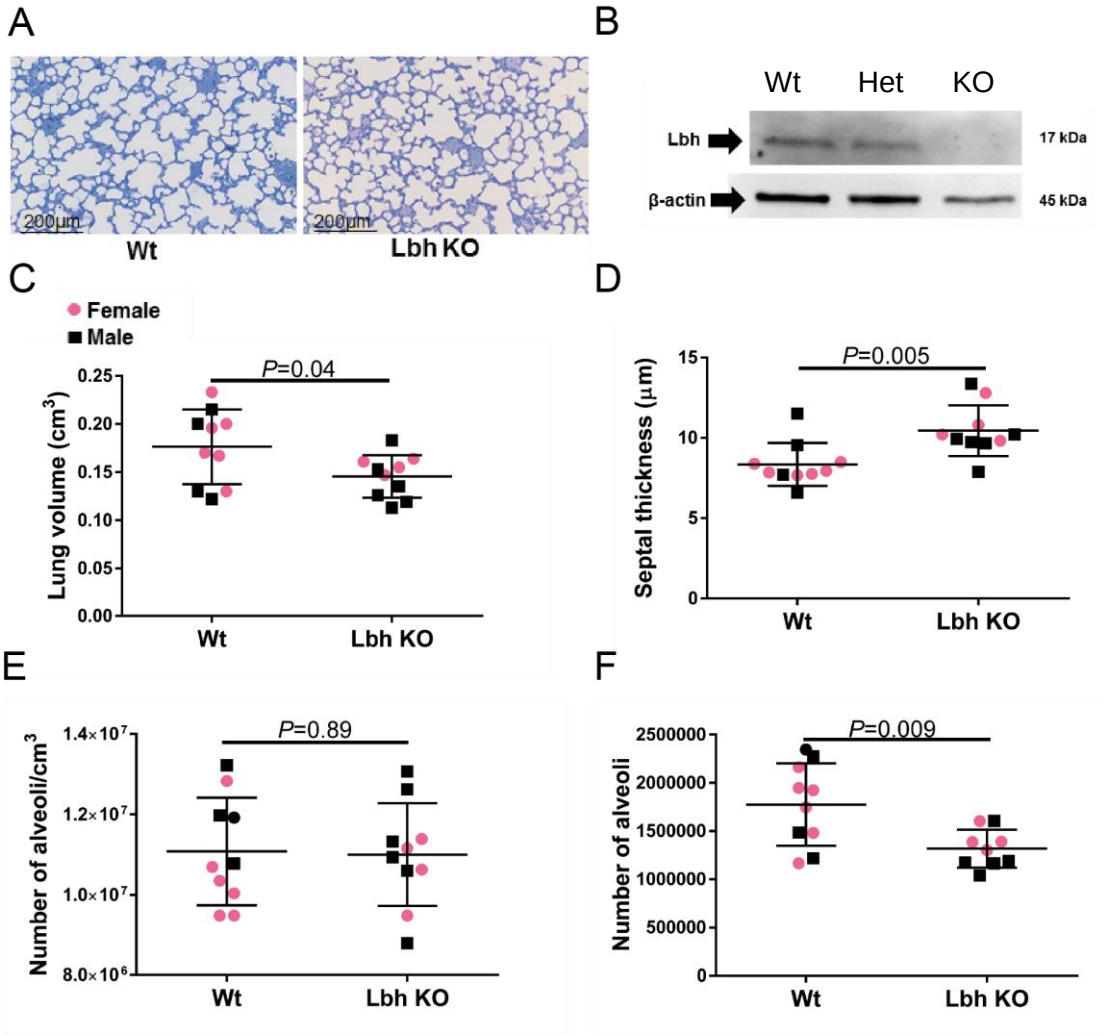

Figure 25 | Stereological analysis of lungs from Lbh knockout mouse pups revealed an increase in septal thickness.

(*A*) Representative images from plastic-embedded wild-type (Wt) and Lbh knockout (KO) lungs. (*B*) Lbh expression in whole lung protein homogenate in Wt mouse, mouse heterozygous (Het) for Lbh KO allele, and mouse homozygous (-/-) for Lbh KO allele (*C*) Lungs volume in Wt and Lbh KO mice. Stereological assessment of (*D*) septal thickness; (*E*) alveoli density; and (*F*) number of alveoli in Wt and Lbh KO mice. The full list of stereological parameters assessed is provided in Table 9. Unpaired Student's *t*-test was used for data comparison. Data reflect mean ± SD (n=9-10 lungs per group).

Table 9 | Stereological parameters from analysis of Lbh KO and Wt mouse lung structure at post-natal day 7.

Parameter			Wt			Lbh KO		
			Mean ± SD			Mean ± SD		
***Vv* (par/lung) (%)**			91.11 ± 2.90			87.40 ± 3.56 (***P* = 0.02**)		
CE	CV	CE^2/CV^2	0.01	0.03	0.10	0.01	0.04	0.10
***Vv* (nonpar/lung) (%)**			8.89 ± 2.90			12.60 ± 3.56 (***P* = 0.02**)		
CE	CV	CE^2/CV^2	0.10	0.33	0.10	0.09	0.22	0.17
***Sv* (alv epi/par) (cm^{-1})**			751 ± 48.39			728 ± 80.92 (***P* = 0.45**)		
CE	CV	CE^2/CV^2	0.20	0.06	0.10	0.04	0.11	0.10
***S* (alv epi, lung) (cm^2)**			119.3 ± 21.30			87.95 ± 13.60 (***P* = 0.002**)		
CE	CV	CE^2/CV^2	0.06	0.18	0.10	0.05	0.15	0.11
***Vv* (alv air/ par) (%)**			68.46 ± 5.48			62.43 ± 3.67 (***P* = 0.01**)		
CE	0.08	0.10	0.03	0.08	0.10	0.02	0.06	0.10
***V* (alv air, lung) (cm^3)**			0.11 ± 0.02			0.08 ± 0.02 (***P* = 0.005**)		
CE	CV	CE^2/CV^2	0.07	0.22	0.10	0.07	0.21	0.10
***V* (sep, lung) (cm^3)**			0.05 ± 0.02			0.05 ± 0.01 (***P* = 0.54**)		
CE	CV	CE^2/CV^2	0.10	0.31	0.10	0.04	0.12	0.10
MLI (μm)			36.77 ± 4.32			34.73 ± 4.65 (***P* = 0.32**)		
CE	CV	CE^2/CV^2	0.04	0.12	0.10	0.04	0.14	0.10

Values are presented as mean ± SD, and *P*-values (n=10 lungs per group). Unpaired Student's *t*-test was applied for data comparison. Abbreviations: alv air, alveolar air spaces; alv epi, alveolar epithelium; CE, coefficient of error; CV, coefficient of variation; Lbh, limb bud and heart; MLI, mean linear intercept; non-par, non-parenchyma; par, parenchyma; sep, septum; s.d., standard deviation; S, surface area; SV, surface density; V, volume; VV, volume density; Wt, wild-type.

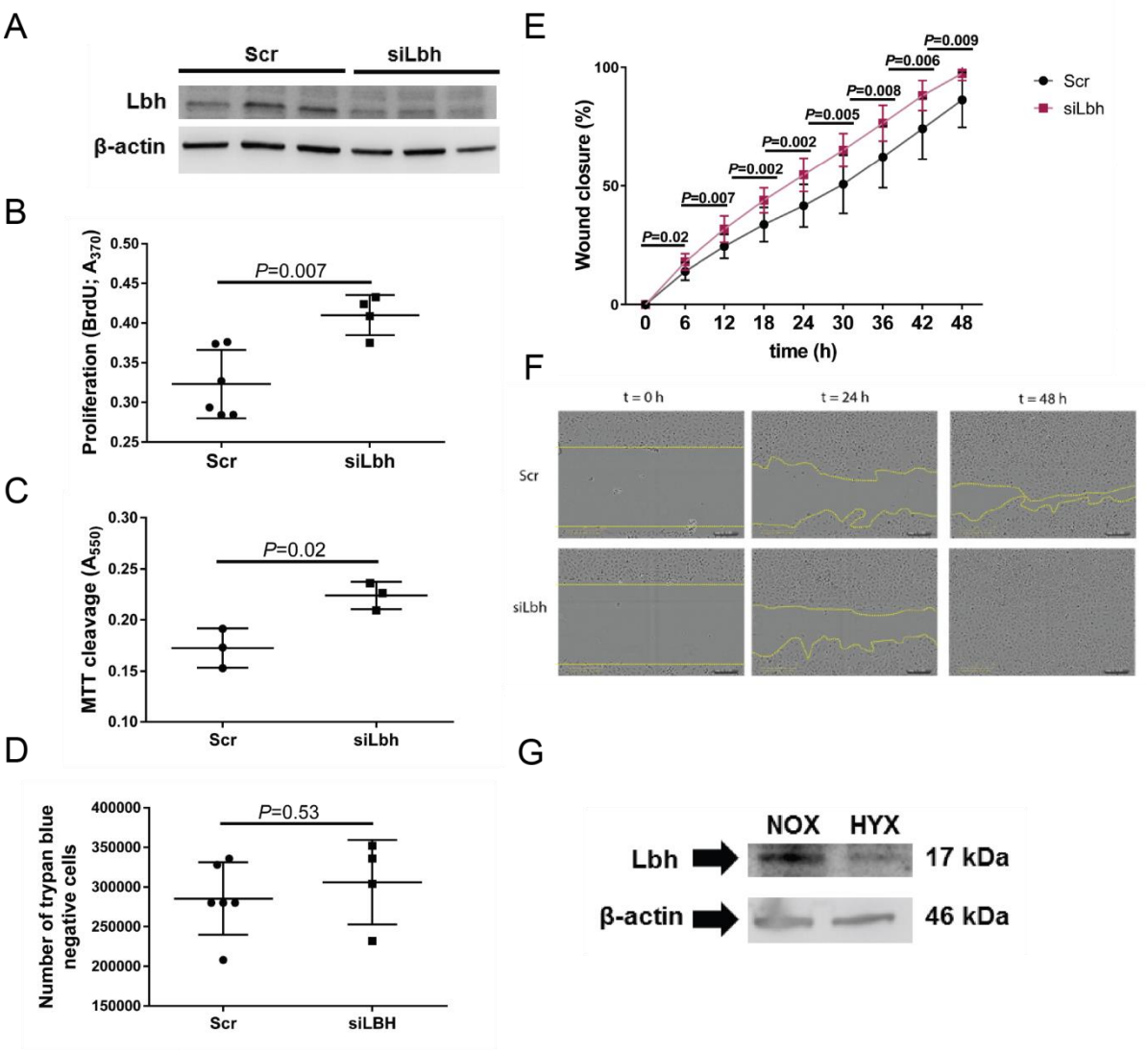

Figure 26 | The impact of siRNA-mediated knockdown of Lbh in A549 cells.

(*A*) Western blot presenting siRNA-mediated knockdown of Lbh from A549 cells. (*B*) BrdU incorporation in A549 cells increased following knockdown of Lbh. Unpaired Student's *t*-test was used for data comparison. Data reflect mean ± SD (n=4-6 wells per group). (*C*) MTT cleavage increased following knockdown of Lbh. Data reflect mean ± SD (n=3 wells per group). (*D*) Viability of A549 cells assessed by trypan blue staining following knockdown of Lbh. Unpaired Student's *t*-test was used for data comparison. Data reflect mean ± SD (n=4-6 wells per group). (*E*) Wound closure increased following knockdown of Lbh (n=8 wells per group). Unpaired Student's *t*-test was used for data comparison. Data reflect mean ± SD (n=8 wells per group). (*F*) Representative images of wounds created in A549 monolayers quantified in *E*. (*G*) Western blot representing expression of Lbh in primary lung ATII cells from mouse pup lungs at post-natal day (P)14 in normoxic (21% O_2) (NOX) and hyperoxic (85% O_2) (HYX) conditions.

8 Discussion

Mouse lungs in the first weeks of post-natal life continue to undergo development and re-modelling with a dynamic alveolarisation stage involving secondary septation and the thinning of the septal walls to establish a large surface area for gas exchange (Pozarska et al. 2017). Alveolarisation is facilitated by concerted cross-signalling between different cell types, and controlled by growth factor signalling such as Tgf-β pathway (Wu and Hill 2009). Lung development in the mouse has been demonstrated to be regulated by the Tgf-β signalling pathway components (Alejandre-Alcazar et al. 2008) and disruptions to the Tgf-β pathway can result in BPD, a disease of impaired alveolarisation (Oak and Hilgendorff 2017). Tgfbr3 is a highly expressed accessory receptor of Tgf-β pathway with no intracellular signalling kinase activity, but it was documented to undergo phosphorylation at the CD and interact with intracellular binding partners such as β arrestin 2. The expression of *Tgfbr3* was profiled in the whole lungs homogenates of Wt mice at P3, P5 and P7. The significant upregulation of *Tgfbr3* at P5, a time-point that coincides with the peak of secondary septation, reveals that the expression of *Tgfbr3* is dynamically regulated during late lung development. The expression of *Tgfbr3* was demonstrated to be significantly highest in the mesenchymal, expressing high levels of αSMA and SMMHC FACS-sorted cell population from the mouse lungs at P7. The siRNA-mediated depletion of Tgfbr3 from primary mouse lung fibroblasts resulted in an increase in proliferation and migration that was independent of stimulation with Tgf-β1 ligand, which suggests that Tgfbr3 regulates properties of fibroblasts by the mechanisms of action that are independent of Tgf-β signalling pathway.

Tgfbr3 plays a role in post-natal mouse lung alveolarisation by regulation of PDGFRα$^+$ fibroblasts and SMMHC$^+$ cell properties

PDGFRα$^+$ fibroblasts regulate process of secondary septation and reside at the tips of secondary septa (Ntokou et al. 2015; Bostrom et al. 1996), forming alveolar ring muscles. PDGFRα$^+$ fibroblasts secrete ECM components, such as elastin and fibronectin, which serve as scaffold for alveolarisation (Bostrom et al. 1996). Mouse strain carrying floxed exon 5 of Tgfbr3 was employed to knockdown Tgfbr3 at the day of birth with the application of tamoxifen using PDGFRα-CreER^{T2} conditional driver. The tamoxifen-injected Tgfbr3$^{fl/fl}$ PDGFRα-CreER^{T2} mouse pups display altered lung structure reflected by a decreased alveoli density, alveoli number and an increased MLI, parameter that acts as a surrogate for the alveolar diameter, assessed by design-based stereology of plastic embedded lungs at P7. These results indicate key role for Tgfbr3 in regulation of PDGFRα$^+$ fibroblasts during post-natal lung development, secondary septation, ECM protein deposition and remodelling. PDGFRα$^+$ in post-natal lung development was revealed to dynamically co-localise with number of different cellular markers (Ntokou et al. 2015). To this end, by injection of tamoxifen to Tgfbr3$^{fl/fl}$ PDGFRα-CreER^{T2} mice, *Tgfbr3* was conditionally ablated from PDGFRα$^+$ fibroblasts, and also from proportion of CD73$^+$, adipose differentiation-related protein (ADRP)$^+$ and CD146$^+$ cell-type populations. PDGFRα is a receptor for platelet-derived growth factor (PDGF)-A which is also expressed by the epithelial cells facilitating the mesenchymal-epithelial communication. Deleting Tgfbr3 from PDGFRα$^+$ cells could therefore disrupt the process of paracrine signalling between different lung cell-types and EMT in the developing lung, however, the contribution of EMT to the post-natal lung development has not yet been largely studied.

The primary mouse lung fibroblasts from tamoxifen-treated Tgfbr3$^{fl/fl}$ PDGFRα-CreER^{T2} pups at P7 were positive for PDGFRα and displayed increased expression of PCNA suggesting that disrupted alveolarisation may result from impaired motility of PDGFRα$^+$ fibroblasts, alteration to the progression of the cell cycle and/or chromatin remodelling. Disturbances to ECM turnover and remodelling were noted with the increase in cellular fibronectin expression in Tgfbr3$^{fl/fl}$ PDGFRα CreER^{T2} lungs. Furthermore, Tgfbr3$^{fl/fl}$ PDGFRα-CreER^{T2} fibroblasts display an increase in β-catenin expression, which is the main intracellular effector of Wnt pathway, and can be induced by TGF-β1 ligand, that regulates cell proliferation,

differentiation and fate determination. TGF-β1 was documented to induce β-catenin resulting in the increased fibronectin expression in pulmonary fibroblasts (Baarsma et al. 2011), and it would be interesting to study further the role of Tgfbr3 in this signalling axis. Changes in the Tgf-β pathway included decreased pSmad2/3 expression, which might result from the absence of Tgfbr3 to form heterotetrameric complexes with the Tgf-β signalling receptors and therefore transmit Tgf-β2 signal to Tgfbr2.

The tamoxifen-induced conditional knockout Tgfbr3$^{fl/fl}$ SMMHC-CreER^{T2} at the day of birth resulted in a decreased alveoli density, alveoli number, increased MLI assessed at P7. The employed SMMHC-CreER^{T2} cellular driver in this study targeted SMMHC^{+} cells, and the pool of myofibroblasts positive for SMMHC, encompassing some proportion of cells expressing PDGFRα^{+}, population targeted with PDGFRα-CreER^{T2} driver. Whether the cell population double-positive for SMMHC and PDGFRα or the cell population singly-positive for SMMHC were responsible for the loss of alveoli in study with SMMHC-CreER^{T2} driver would require further investigation. Vascular development was assessed by design-based stereology and it was revealed that Tgfbr3$^{fl/fl}$ PDGFRα-CreER^{T2} mice display reduced vessel thickness whereas no changes were noted to the vessel wall thickness of Tgfbr3$^{fl/fl}$ SMMHC-CreER^{T2} mice pups.

General caveat when employing Cre recombinase-expressing mice strains include off-target Cre expression leading to the false interpretation of the resulting phenotypes. The effectiveness and specificity of given Cre recombinase mouse strain could be investigated with its cross to the reporter mouse lines such as ROSAmT/mG that would label targeted cell-types.

Taken together these data demonstrate that Tgfbr3 is an essential homeostatic component of PDGFRα^{+} fibroblasts with smooth muscle cell characteristics and SMMHC^{+} cell-types to regulate secondary septation. Knockdown of Tgfbr3 expression results in disruption to the normal alveoli development and alterations to molecular signalling in the lung in the main developmental pathways.

Tgfbr3 controls lung development by regulation of properties of Tie2^{+} cells

High expression levels of *Tgfbr3* were observed in the Pecam^{+} endothelial cell population in mouse lungs at P7. Data generated previously in the laboratory revealed that following siRNA-mediated knockdown of Tgfbr3 from human pulmonary artery endothelial cells (hPAEC), there was a decrease in tube formation and migration of hPAEC. Tgfbr3 tamoxifen-induced conditional knockdown *in vivo* on the day of pup birth from Tie2^{+} cells resulted in a reduction in septal thickness of the lung, thickness of walls of all lung vessels and resistance vessels, assessed by stereological counting. Decrease in angiogenesis in tamoxifen-treated Tgfbr3$^{fl/fl}$ Tie2-CreER^{T2} was further demonstrated by FACS-based sorting of Tie2^{+} cells from tamoxifen-treated Tgfbr3$^{fl/fl}$ Tie2-CreER^{T2} and Tie2-CreER^{T2} mice lungs, which revealed a significant reduction in abundance in Tie2^{+} cells. It was demonstrated previously that reduction in Tie2^{+} cells results in a severe disruptions to the microvascular development in developing mice (Suri et al. 1996). Tie2^{+} cells are highly positive for Pecam at P7, confirming their endothelial phenotype; however, it was reported that 84 % of embryonic hematopoietic progenitors, T cells, monocytes, granulocytes, and B cells are Tie2^{+} (Tang et al. 2010); other non-endothelial cells expressing Tie2 include fibroblasts (Uchida et al. 2000), smooth muscle cells (Dewachter et al. 2006), mural cells (Metheny-Barlow et al. 2004) and mural precursor cells (Iurlaro et al. 2003). Recombination of Tie2-CreER^{T2} in non-endothelial cells could be potentially responsible for the observed reduction is septal thickness in tamoxifen-treated Tgfbr3$^{fl/fl}$ Tie2-CreER^{T2} mice. Recent RNA-seq analysis performed from immortalised Tgfbr3$^{-/-}$ epicardial cells isolated from global Tgfbr3 knockout embryos at E11.5 and stimulated with either Tgf-β1, Tgf-β2, or BMP-2 ligands revealed NF-κB as a focal gene of altered signalling pathways assessed by Gene Ontology (DeLaughter et al. 2016). FACS sorting of Tie2^{+} cells from tamoxifen-treated Tgfbr3$^{fl/fl}$ Tie2-CreER^{T2} and Tie2-CreER^{T2} lungs demonstrated a significant decrease in the expression of *Nfkb1* transcription factor in Tgfbr3$^{fl/fl}$ Tie2-CreER^{T2} mice. NFκB1 is documented to be crucial for the proliferation of the neonatal pulmonary endothelial cells (Iosef et al. 2012), to contain 'shear stress' response element in its promoter region, where lung stretching was able to upregulate NFκB1 expression (Schwartz et al. 1996). Global inhibition of NFκB1 with BAY inhibitor led to stunted alveolarisation, angiogenesis, and a decrease in Pecam^{+}

cells in the neonatal lung (Iosef et al. 2012). Tgfbr3 was reported previously to negatively regulate NFκB1 expression in MCF10A breast epithelial and MDA-MB-231 breast cancer cells lines via signalling through adaptor protein β-arrestin 2 (You, How, and Blobe 2009). Findings of this study present and confirm direct relation of Tgfbr3 and NFκB1 *in vivo* in the endothelial cells of the developing lung, and that the altered lung structure in tamoxifen-treated Tgfbr3$^{fl/fl}$ Tie2-CreER^{T2} mouse pups could be mediated at least in part through disruption in NFκB1 expression, which presents a mode of Tgfbr3 to regulate post-natal lung angiogenesis and development.

Relation between Tgfbr3 and Lbh expression

Whole genome microarray was performed previously in the laboratory in hPASMC following siRNA-mediated knockdown of Tgfbr3, indicating transcription factor Lbh, as a downstream signalling candidate. Lbh was reported to be a Wnt-responsive co-transcription factor involved in mammary gland alveolarisation, stem cell expansion of the mammary gland and the maintenance of epithelial basal lineage (Lindley et al. 2015), whereas its role in lung development was not described. Following siRNA-induced Lbh knockdown, proliferation and migration of primary mouse lung fibroblasts decreased significantly, effects that were independent of stimulation with Tgf-β1 ligand. Following knockdown of Tgfbr3 in the primary mouse lung fibroblasts, the expression of Lbh increased, both on mRNA and protein level. In contrast, FACS sorting of PDGFRα^{+} cells from tamoxifen-treated Tgfbr3$^{fl/fl}$ PDGFRα-CreER^{T2} mouse pups at P7 demonstrated a tendency for Lbh expression to be downregulated. Primary mouse lung fibroblasts from tamoxifen-treated Tgfbr3$^{fl/fl}$ PDGFRα-CreER^{T2} pups at P7 revealed a decreased Lbh protein expression. The difference between effects on Lbh expression from *in vitro* and *in vivo* set-ups might be due to the effect of transfection reagents such as Scr control on gene expression, culture conditions, the indirect signalling relationship, variability in gene expression between neonatal and adult cells, and the higher complexity of the *in vivo* system. The stereological analysis of global Lbh KO mice displayed a significant increase in septal wall thickness and a decrease in surface area of the lungs, suggesting a potential role for Lbh in maintenance of mesenchyme or epithelial cell homeostasis *in vivo* in the developing lung. To further investigate the role of Lbh in lung epithelium, Lbh was knockdown with siRNA in A549 cell line. Following the reduction of the endogenous levels of Lbh, A549 cells demonstrated a significant increase in healing

of wound created in the cellular monolayers and in proliferation assessed by BrdU incorporation and MTT cleavage, with no effect on the viability of A549 cells. To this end, downregulation of Lbh protein expression was noted in primary mouse lung ATII cells in a mouse model of BPD, a condition characterised by thickened septal walls.

Other genomic changes from the microarray performed following the knockdown of Tgfbr3 were validated *in vivo* such as changes to Wnt pathway and components of ECM revealing common signalling mechanisms directed by Tgfbr3 in *in vitro* cell culture set-up and during normal lung development *in vivo*. Loss of alveoli and pathological enlargement of the alveolar spaces is present in emphysema, COPD and BPD, and data presented in this study suggests that Tgfbr3 is a key molecule required for alveolarisation and vascular development during late lung development.

9 References

Alejandre-Alcazar, M. A., G. Kwapiszewska, I. Reiss, O. V. Amarie, L. M. Marsh, J. Sevilla-Perez, M. Wygrecka, B. Eul, S. Kobrich, M. Hesse, R. T. Schermuly, W. Seeger, O. Eickelberg, and R. E. Morty. 2007. 'Hyperoxia modulates TGF-beta/BMP signaling in a mouse model of bronchopulmonary dysplasia', *Am J Physiol Lung Cell Mol Physiol*, 292: L537-49.

Alejandre-Alcazar, M. A., M. Michiels-Corsten, A. G. Vicencio, I. Reiss, J. Ryu, R. R. de Krijger, G. G. Haddad, D. Tibboel, W. Seeger, O. Eickelberg, and R. E. Morty. 2008. 'TGF-beta signaling is dynamically regulated during the alveolarization of rodent and human lungs', *Dev Dyn*, 237: 259-69.

Baarsma, H. A., A. I. Spanjer, G. Haitsma, L. H. Engelbertink, H. Meurs, M. R. Jonker, W. Timens, D. S. Postma, H. A. Kerstjens, and R. Gosens. 2011. 'Activation of WNT/beta-catenin signaling in pulmonary fibroblasts by TGF-beta(1) is increased in chronic obstructive pulmonary disease', *PLoS One*, 6: e25450.

Bishop, J. R., M. Schuksz, and J. D. Esko. 2007. 'Heparan sulphate proteoglycans fine-tune mammalian physiology', *Nature*, 446: 1030-7.

Blair, C. R., J. B. Stone, and R. G. Wells. 2011. 'The type III TGF-beta receptor betaglycan transmembrane-cytoplasmic domain fragment is stable after ectodomain cleavage and is a substrate of the intramembrane protease gamma-secretase', *Biochim Biophys Acta*, 1813: 332-9.

Bostrom, H., K. Willetts, M. Pekny, P. Leveen, P. Lindahl, H. Hedstrand, M. Pekna, M. Hellstrom, S. Gebre-Medhin, M. Schalling, M. Nilsson, S. Kurland, J. Tornell, J. K. Heath, and C. Betsholtz.

1996. 'PDGF-A signaling is a critical event in lung alveolar myofibroblast development and alveogenesis', *Cell*, 85: 863-73.

Branchfield, K., R. Li, V. Lungova, J. M. Verheyden, D. McCulley, and X. Sun. 2016. 'A three-dimensional study of alveologenesis in mouse lung', *Dev Biol*, 409: 429-41.

Chen, W., K. C. Kirkbride, T. How, C. D. Nelson, J. Mo, J. P. Frederick, X. F. Wang, R. J. Lefkowitz, and G. C. Blobe. 2003. 'Beta-arrestin 2 mediates endocytosis of type III TGF-beta receptor and down-regulation of its signaling', *Science*, 301: 1394-7.

Copland, I., and M. Post. 2004. 'Lung development and fetal lung growth', *Paediatr Respir Rev*, 5 Suppl A: S259-64.

DeLaughter, D. M., C. R. Clark, D. C. Christodoulou, C. E. Seidman, H. S. Baldwin, J. G. Seidman, and J. V. Barnett. 2016. 'Transcriptional Profiling of Cultured, Embryonic Epicardial Cells Identifies Novel Genes and Signaling Pathways Regulated by TGFbetaR3 In Vitro', *PLoS One*, 11: e0159710.

Dewachter, L., S. Adnot, E. Fadel, M. Humbert, B. Maitre, A. M. Barlier-Mur, G. Simonneau, M. Hamon, R. Naeije, and S. Eddahibi. 2006. 'Angiopoietin/Tie2 pathway influences smooth muscle hyperplasia in idiopathic pulmonary hypertension', *Am J Respir Crit Care Med*, 174: 1025-33.

Fehl, J., A. Pozarska, C. Nardiello, P. Rath, D. E. Surate Solaligue, I. Vadasz, K. Mayer, S. Herold, W. Seeger, and R. E. Morty. 2019. 'Control Interventions Can Impact Alveolarization and the Transcriptome in Developing Mouse Lungs', *Anat Rec (Hoboken)*, 302: 346-63.

Gao, Y., and J. U. Raj. 2010. 'Regulation of the pulmonary circulation in the fetus and newborn', *Physiol Rev*, 90: 1291-335.

Gatza, C. E., S. Y. Oh, and G. C. Blobe. 2010. 'Roles for the type III TGF-beta receptor in human cancer', *Cell Signal*, 22: 1163-74.

Geraci, M. W., M. Moore, T. Gesell, M. E. Yeager, L. Alger, H. Golpon, B. Gao, J. E. Loyd, R. M. Tuder, and N. F. Voelkel. 2001. 'Gene expression patterns in the lungs of patients with primary pulmonary hypertension: a gene microarray analysis', *Circ Res*, 88: 555-62.

Golpon, H. A., C. D. Coldren, M. R. Zamora, G. P. Cosgrove, M. D. Moore, R. M. Tuder, M. W. Geraci, and N. F. Voelkel. 2004. 'Emphysema lung tissue gene expression profiling', *Am J Respir Cell Mol Biol*, 31: 595-600.

Groeneveld, M. E., N. Bogunovic, R. J. P. Musters, G. J. Tangelder, G. Pals, W. Wisselink, D. Micha, and K. K. Yeung. 2018. 'Betaglycan (TGFBR3) up-regulation correlates with increased TGF-beta signaling in Marfan patient fibroblasts in vitro', *Cardiovasc Pathol*, 32: 44-49.

Grzenda, A., J. Shannon, J. Fisher, and M. S. Arkovitz. 2013. 'Timing and expression of the angiopoietin-1-Tie-2 pathway in murine lung development and congenital diaphragmatic hernia', *Dis Model Mech*, 6: 106-14.

He, K., X. Yan, N. Li, S. Dang, L. Xu, B. Zhao, Z. Li, Z. Lv, X. Fang, Y. Zhang, and Y. G. Chen. 2015. 'Internalization of the TGF-beta type I receptor into caveolin-1 and EEA1 double-positive early endosomes', *Cell Res*, 25: 738-52.

He, L., M. Vanlandewijck, M. A. Mae, J. Andrae, K. Ando, F. Del Gaudio, K. Nahar, T. Lebouvier, B. Lavina, L. Gouveia, Y. Sun, E. Raschperger, A. Segerstolpe, J. Liu, S. Gustafsson, M. Rasanen, Y. Zarb, N. Mochizuki, A. Keller, U. Lendahl, and C. Betsholtz. 2018. 'Single-cell RNA sequencing of mouse brain and lung vascular and vessel-associated cell types', *Sci Data*, 5: 180160.

Hempel, N., T. How, S. J. Cooper, T. R. Green, M. Dong, J. A. Copland, C. G. Wood, and G. C. Blobe. 2008. 'Expression of the type III TGF-beta receptor is negatively regulated by TGF-beta', *Carcinogenesis*, 29: 905-12.

Henen, M. A., P. Mahlawat, C. Zwieb, R. B. Kodali, C. S. Hinck, R. D. Hanna, T. C. Krzysiak, U. Ilangovan, K. E. Cano, G. Hinck, M. Vonberg, M. McCabe, and A. P. Hinck. 2018. 'TGF-beta2 uses the concave surface of its extended finger region to bind betaglycan's ZP domain via three residues specific to TGF-beta and Inhibin-alpha', *J Biol Chem*.

Herriges, M., and E. E. Morrisey. 2014. 'Lung development: orchestrating the generation and regeneration of a complex organ', *Development*, 141: 502-13.

Hersh, C. P., N. N. Hansel, K. C. Barnes, D. A. Lomas, S. G. Pillai, H. O. Coxson, R. A. Mathias, N. M. Rafaels, R. A. Wise, J. E. Connett, B. J. Klanderman, F. L. Jacobson, R. Gill, A. A. Litonjua, D. Sparrow, J. J. Reilly, E. K. Silverman, and Icgn Investigators. 2009. 'Transforming growth factor-beta receptor-3 is associated with pulmonary emphysema', *Am J Respir Cell Mol Biol*, 41: 324-31.

Hislop, A. A. 2002. 'Airway and blood vessel interaction during lung development', *J Anat*, 201: 325-34.

Hooper, S. B., and R. Harding. 1995. 'Fetal lung liquid: a major determinant of the growth and functional development of the fetal lung', *Clin Exp Pharmacol Physiol*, 22: 235-47.

Hooper, S. B., G. R. Polglase, and C. C. Roehr. 2015. 'Cardiopulmonary changes with aeration of the newborn lung', *Paediatr Respir Rev*, 16: 147-50.

Hsia, C. C., D. M. Hyde, M. Ochs, E. R. Weibel, and Ats Ers Joint Task Force on Quantitative Assessment of Lung Structure. 2010. 'An official research policy statement of the American Thoracic Society/European Respiratory Society: standards for quantitative assessment of lung structure', *Am J Respir Crit Care Med*, 181: 394-418.

'http://betsholtzlab.org/VascularSingleCells/database.html'.

Huang, J. J., A. L. Corona, B. P. Dunn, E. M. Cai, J. N. Prakken, and G. C. Blobe. 2019. 'Increased type III TGF-beta receptor shedding decreases tumorigenesis through induction of epithelial-to-mesenchymal transition', *Oncogene*, 38: 3402-14.

Iosef, C., T. P. Alastalo, Y. Hou, C. Chen, E. S. Adams, S. C. Lyu, D. N. Cornfield, and C. M. Alvira. 2012. 'Inhibiting NF-kappaB in the developing lung disrupts angiogenesis and alveolarization', *Am J Physiol Lung Cell Mol Physiol*, 302: L1023-36.

Iurlaro, M., M. Scatena, W. H. Zhu, E. Fogel, S. L. Wieting, and R. F. Nicosia. 2003. 'Rat aorta-derived mural precursor cells express the Tie2 receptor and respond directly to stimulation by angiopoietins', *J Cell Sci*, 116: 3635-43.

Jones, M. R., S. Dilai, A. Lingampally, C. M. Chao, S. Danopoulos, G. Carraro, R. Mukhametshina, J. Wilhelm, E. Baumgart-Vogt, D. Al Alam, C. Chen, P. Minoo, J. S. Zhang, and S. Bellusci. 2018. 'A Comprehensive Analysis of Fibroblast Growth Factor Receptor 2b Signaling on Epithelial Tip Progenitor Cells During Early Mouse Lung Branching Morphogenesis', *Front Genet*, 9: 746.

Judge, S. M., R. L. Nosacka, D. Delitto, M. H. Gerber, M. E. Cameron, J. G. Trevino, and A. R. Judge. 2018. 'Skeletal Muscle Fibrosis in Pancreatic Cancer Patients with Respect to Survival', *JNCI Cancer Spectr*, 2: pky043.

Kicheva, A., and M. Gonzalez-Gaitan. 2008. 'The Decapentaplegic morphogen gradient: a precise definition', *Curr Opin Cell Biol*, 20: 137-43.

Kirkbride, K. C., T. A. Townsend, M. W. Bruinsma, J. V. Barnett, and G. C. Blobe. 2008. 'Bone morphogenetic proteins signal through the transforming growth factor-beta type III receptor', *J Biol Chem*, 283: 7628-37.

Knust, J., M. Ochs, H. J. Gundersen, and J. R. Nyengaard. 2009. 'Stereological estimates of alveolar number and size and capillary length and surface area in mice lungs', *Anat Rec (Hoboken)*, 292: 113-22.

Kovacs, J. J., M. R. Hara, C. L. Davenport, J. Kim, and R. J. Lefkowitz. 2009. 'Arrestin development: emerging roles for beta-arrestins in developmental signaling pathways', *Dev Cell*, 17: 443-58.

Kubiczkova, L., L. Sedlarikova, R. Hajek, and S. Sevcikova. 2012. 'TGF-beta - an excellent servant but a bad master', *J Transl Med*, 10: 183.

Kugler, M. C., A. L. Joyner, C. A. Loomis, and J. S. Munger. 2015. 'Sonic hedgehog signaling in the lung. From development to disease', *Am J Respir Cell Mol Biol*, 52: 1-13.

Lau, M., A. Masood, M. Yi, R. Belcastro, J. Li, and A. K. Tanswell. 2011. 'Long-term failure of alveologenesis after an early short-term exposure to a PDGF-receptor antagonist', *Am J Physiol Lung Cell Mol Physiol*, 300: L534-47.

Lefkowitz, R. J., and S. K. Shenoy. 2005. 'Transduction of receptor signals by beta-arrestins', *Science*, 308: 512-7.

Lek, M., K. J. Karczewski, E. V. Minikel, K. E. Samocha, E. Banks, T. Fennell, A. H. O'Donnell-Luria, J. S. Ware, A. J. Hill, B. B. Cummings, T. Tukiainen, D. P. Birnbaum, J. A. Kosmicki, L. E. Duncan, K. Estrada, F. Zhao, J. Zou, E. Pierce-Hoffman, J. Berghout, D. N. Cooper, N. Deflaux, M. DePristo, R. Do, J. Flannick, M. Fromer, L. Gauthier, J. Goldstein, N. Gupta, D. Howrigan, A. Kiezun, M. I. Kurki, A. L. Moonshine, P. Natarajan, L. Orozco, G. M. Peloso, R. Poplin, M. A. Rivas, V. Ruano-Rubio, S. A. Rose, D. M. Ruderfer, K. Shakir, P. D. Stenson, C. Stevens, B. P. Thomas, G. Tiao, M. T. Tusie-Luna, B. Weisburd, H. H. Won, D. Yu, D. M. Altshuler, D. Ardissino, M. Boehnke, J. Danesh, S. Donnelly, R. Elosua, J. C. Florez, S. B. Gabriel, G. Getz, S. J. Glatt, C. M. Hultman, S. Kathiresan, M. Laakso, S. McCarroll, M. I. McCarthy, D. McGovern, R. McPherson, B. M. Neale, A. Palotie, S. M. Purcell, D. Saleheen, J. M. Scharf, P. Sklar, P. F. Sullivan, J. Tuomilehto, M. T. Tsuang, H. C. Watkins, J. G. Wilson, M. J. Daly, D. G. MacArthur, and Consortium Exome Aggregation. 2016. 'Analysis of protein-coding genetic variation in 60,706 humans', *Nature*, 536: 285-91.

Li, R., K. Bernau, N. Sandbo, J. Gu, S. Preissl, and X. Sun. 2018. 'Pdgfra marks a cellular lineage with distinct contributions to myofibroblasts in lung maturation and injury response', *Elife*, 7.

Lin, S. J., Y. Hu, J. Zhu, T. K. Woodruff, and T. S. Jardetzky. 2011. 'Structure of betaglycan zona pellucida (ZP)-C domain provides insights into ZP-mediated protein polymerization and TGF-beta binding', *Proc Natl Acad Sci U S A*, 108: 5232-6.

Lindley, L. E., K. M. Curtis, A. Sanchez-Mejias, M. E. Rieger, D. J. Robbins, and K. J. Briegel. 2015. 'The WNT-controlled transcriptional regulator LBH is required for mammary stem cell expansion and maintenance of the basal lineage', *Development*, 142: 893-904.

Liu, M., A. K. Tanswell, and M. Post. 1999. 'Mechanical force-induced signal transduction in lung cells', *Am J Physiol*, 277: L667-83.

Liu, T., and X. H. Feng. 2010. 'Regulation of TGF-beta signalling by protein phosphatases', *Biochem J*, 430: 191-8.

Lopez-Casillas, F., J. L. Wrana, and J. Massague. 1993. 'Betaglycan presents ligand to the TGF beta signaling receptor', *Cell*, 73: 1435-44.

Metheny-Barlow, L. J., S. Tian, A. J. Hayes, and L. Y. Li. 2004. 'Direct chemotactic action of angiopoietin-1 on mesenchymal cells in the presence of VEGF', *Microvasc Res*, 68: 221-30.

Miano, J. M., P. Cserjesi, K. L. Ligon, M. Periasamy, and E. N. Olson. 1994. 'Smooth muscle myosin heavy chain exclusively marks the smooth muscle lineage during mouse embryogenesis', *Circ Res*, 75: 803-12.

Mythreye, K., and G. C. Blobe. 2009. 'The type III TGF-beta receptor regulates epithelial and cancer cell migration through beta-arrestin2-mediated activation of Cdc42', *Proc Natl Acad Sci U S A*, 106: 8221-6.

Mythreye, K., E. H. Knelson, C. E. Gatza, M. L. Gatza, and G. C. Blobe. 2013. 'TbetaRIII/beta-arrestin2 regulates integrin alpha5beta1 trafficking, function, and localization in epithelial cells', *Oncogene*, 32: 1416-27.

Nakamura, K. T., and P. B. McCray, Jr. 2000. 'Fetal airway smooth-muscle contractility and lung development. A player in the band or just someone in the audience?', *Am J Respir Cell Mol Biol*, 23: 3-6.

Nardiello, C., and R. E. Morty. 2016. 'MicroRNA in late lung development and bronchopulmonary dysplasia: the need to demonstrate causality', *Mol Cell Pediatr*, 3: 19.

Ntokou, A., F. Klein, D. Dontireddy, S. Becker, S. Bellusci, W. D. Richardson, M. Szibor, T. Braun, R. E. Morty, W. Seeger, R. Voswinckel, and K. Ahlbrecht. 2015. 'Characterization of the platelet-derived growth factor receptor-alpha-positive cell lineage during murine late lung development', *Am J Physiol Lung Cell Mol Physiol*, 309: L942-58.

Oak, P., and A. Hilgendorff. 2017. 'The BPD trio? Interaction of dysregulated PDGF, VEGF, and TGF signaling in neonatal chronic lung disease', *Mol Cell Pediatr*, 4: 11.

Pozarska, A., and R. E. Morty. 2017. 'A Tale of Two Endoglins: How Does Tail-Less Soluble Endoglin Deregulate Lung Development?', *Am J Respir Cell Mol Biol*, 57: 388-90.

Pozarska, A., J. A. Rodriguez-Castillo, D. E. Surate Solaligue, A. Ntokou, P. Rath, I. Mizikova, A. Madurga, K. Mayer, I. Vadasz, S. Herold, K. Ahlbrecht, W. Seeger, and R. E. Morty. 2017. 'Stereological monitoring of mouse lung alveolarization from the early postnatal period to adulthood', *Am J Physiol Lung Cell Mol Physiol*, 312: L882-L95.

Rautureau, Y., S. C. Coelho, J. C. Fraulob-Aquino, K. G. Huo, A. Rehman, S. Offermanns, P. Paradis, and E. L. Schiffrin. 2015. 'Inducible human endothelin-1 overexpression in endothelium raises blood pressure via endothelin type A receptors', *Hypertension*, 66: 347-55.

Ray, B. N., N. Y. Lee, T. How, and G. C. Blobe. 2010. 'ALK5 phosphorylation of the endoglin cytoplasmic domain regulates Smad1/5/8 signaling and endothelial cell migration', *Carcinogenesis*, 31: 435-41.

Reinhard, C., B. Meyer, H. Fuchs, T. Stoeger, G. Eder, F. Ruschendorf, J. Heyder, P. Nurnberg, M. H. de Angelis, and H. Schulz. 2005. 'Genomewide linkage analysis identifies novel genetic Loci for lung function in mice', *Am J Respir Crit Care Med*, 171: 880-8.

Risau, W. 1997. 'Mechanisms of angiogenesis', *Nature*, 386: 671-4.

Rivers, L. E., K. M. Young, M. Rizzi, F. Jamen, K. Psachoulia, A. Wade, N. Kessaris, and W. D. Richardson. 2008. 'PDGFRA/NG2 glia generate myelinating oligodendrocytes and piriform projection neurons in adult mice', *Nat Neurosci*, 11: 1392-401.

Ruiz-Camp, J., J. Quantius, E. Lignelli, P. F. Arndt, F. Palumbo, C. Nardiello, D. E. Surate Solaligue, E. Sakkas, I. Mizikova, J. A. Rodriguez-Castillo, I. Vadasz, W. D. Richardson, K. Ahlbrecht, S.

Herold, W. Seeger, and R. E. Morty. 2019. 'Targeting miR-34a/Pdgfra interactions partially corrects alveologenesis in experimental bronchopulmonary dysplasia', *EMBO Mol Med*, 11.

Santiago-Sim, T., S. Mathew-Joseph, H. Pannu, D. M. Milewicz, C. E. Seidman, J. G. Seidman, and D. H. Kim. 2009. 'Sequencing of TGF-beta pathway genes in familial cases of intracranial aneurysm', *Stroke*, 40: 1604-11.

Schittny, J. C. 2017. 'Development of the lung', *Cell Tissue Res*, 367: 427-44.

Schittny, J. C., S. I. Mund, and M. Stampanoni. 2008. 'Evidence and structural mechanism for late lung alveolarization', *Am J Physiol Lung Cell Mol Physiol*, 294: L246-54.

Schwartz, M. D., E. E. Moore, F. A. Moore, R. Shenkar, P. Moine, J. B. Haenel, and E. Abraham. 1996. 'Nuclear factor-kappa B is activated in alveolar macrophages from patients with acute respiratory distress syndrome', *Crit Care Med*, 24: 1285-92.

Silva, D. M., C. Nardiello, A. Pozarska, and R. E. Morty. 2015. 'Recent advances in the mechanisms of lung alveolarization and the pathogenesis of bronchopulmonary dysplasia', *Am J Physiol Lung Cell Mol Physiol*, 309: L1239-72.

Skarnes, W. C., B. Rosen, A. P. West, M. Koutsourakis, W. Bushell, V. Iyer, A. O. Mujica, M. Thomas, J. Harrow, T. Cox, D. Jackson, J. Severin, P. Biggs, J. Fu, M. Nefedov, P. J. de Jong, A. F. Stewart, and A. Bradley. 2011. 'A conditional knockout resource for the genome-wide study of mouse gene function', *Nature*, 474: 337-42.

Somashekar, S. T., I. Sammour, J. Huang, J. Dominguez-Bendala, R. Pastori, S. Alvarez-Cubela, E. Torres, S. Wu, and K. C. Young. 2017. 'Intra-Amniotic Soluble Endoglin Impairs Lung Development in Neonatal Rats', *Am J Respir Cell Mol Biol*, 57: 468-76.

Sriram, G., J. Y. Tan, I. Islam, A. J. Rufaihah, and T. Cao. 2015. 'Efficient differentiation of human embryonic stem cells to arterial and venous endothelial cells under feeder- and serum-free conditions', *Stem Cell Res Ther*, 6: 261.

Stenvers, K. L., M. L. Tursky, K. W. Harder, N. Kountouri, S. Amatayakul-Chantler, D. Grail, C. Small, R. A. Weinberg, A. M. Sizeland, and H. J. Zhu. 2003. 'Heart and liver defects and reduced transforming growth factor beta2 sensitivity in transforming growth factor beta type III receptor-deficient embryos', *Mol Cell Biol*, 23: 4371-85.

Sticchi, E., R. De Cario, A. Magi, S. Giglio, A. Provenzano, S. Nistri, G. Pepe, and B. Giusti. 2018. 'Bicuspid Aortic Valve: Role of Multiple Gene Variants in Influencing the Clinical Phenotype', *Biomed Res Int*, 2018: 8386123.

Suri, C., P. F. Jones, S. Patan, S. Bartunkova, P. C. Maisonpierre, S. Davis, T. N. Sato, and G. D. Yancopoulos. 1996. 'Requisite role of angiopoietin-1, a ligand for the TIE2 receptor, during embryonic angiogenesis', *Cell*, 87: 1171-80.

Tang, Y., A. Harrington, X. Yang, R. E. Friesel, and L. Liaw. 2010. 'The contribution of the Tie2+ lineage to primitive and definitive hematopoietic cells', *Genesis*, 48: 563-7.

Uchida, T., M. Nakashima, Y. Hirota, Y. Miyazaki, T. Tsukazaki, and H. Shindo. 2000. 'Immunohistochemical localisation of protein tyrosine kinase receptors Tie-1 and Tie-2 in synovial tissue of rheumatoid arthritis: correlation with angiogenesis and synovial proliferation', *Ann Rheum Dis*, 59: 607-14.

Vanlandewijck, M., L. He, M. A. Mae, J. Andrae, K. Ando, F. Del Gaudio, K. Nahar, T. Lebouvier, B. Lavina, L. Gouveia, Y. Sun, E. Raschperger, M. Rasanen, Y. Zarb, N. Mochizuki, A. Keller, U. Lendahl, and C. Betsholtz. 2018. 'A molecular atlas of cell types and zonation in the brain vasculature', *Nature*, 554: 475-80.

Wiater, E., C. A. Harrison, K. A. Lewis, P. C. Gray, and W. W. Vale. 2006. 'Identification of distinct inhibin and transforming growth factor beta-binding sites on betaglycan: functional separation of betaglycan co-receptor actions', *J Biol Chem*, 281: 17011-22.

Wirth, A., Z. Benyo, M. Lukasova, B. Leutgeb, N. Wettschureck, S. Gorbey, P. Orsy, B. Horvath, C. Maser-Gluth, E. Greiner, B. Lemmer, G. Schutz, J. S. Gutkind, and S. Offermanns. 2008. 'G12-G13-LARG-mediated signaling in vascular smooth muscle is required for salt-induced hypertension', *Nat Med*, 14: 64-8.

Wu, M. Y., and C. S. Hill. 2009. 'Tgf-beta superfamily signaling in embryonic development and homeostasis', *Dev Cell*, 16: 329-43.

You, H. J., T. How, and G. C. Blobe. 2009. 'The type III transforming growth factor-beta receptor negatively regulates nuclear factor kappa B signaling through its interaction with beta-arrestin2', *Carcinogenesis*, 30: 1281-7.

Zhang, Y. E. 2017. 'Non-Smad Signaling Pathways of the TGF-beta Family', *Cold Spring Harb Perspect Biol*, 9.


WILLIAM G. KERCKHOFF
HERZFORSCHUNGSINSTITUT